CLONING AND EXPRESSION OF ORGANIC CATION TRANSPORTERS (ORCT AND ORCT2) FROM THE FRUIT FLY DROSOPHILA MELANOGASTER MEIGEN

by

Brieanne Joelle Matier

B.Sc., The University of British Columbia, 2009

A THESIS SUBMITTED IN PARTIAL FULFILLMENT OF
THE REQUIREMENTS FOR THE DEGREE OF

MASTER OF SCIENCE

in

The College of Graduate Studies

(Biology)

THE UNIVERSITY OF BRITISH COLUMBIA

(Okanagan)

December 2011

Abstract

Organic cations include endogenous metabolites, and xenobiotics (drugs, pesticides, environmental toxins), that must be effectively eliminated in order for organisms to survive. The midgut and Malpighian tubules of insects have been shown to play a role in the active transport of organic cations. Two putative organic cation transporters (OCTs) were cloned from adult *Drosophila melanogaster*. Phylogenetic analysis indicated that these OCTs exist in an insect specific clade separate and equally divergent from identified vertebrate OCT isoforms. Gene expression patterns for these *D. melanogaster* transporters were determined using quantitative real time polymerase chain reaction (qPCR). *D. melanogaster* genes were found to be differentially distributed across the Malpighian tubules and the midgut. The isolated ORCT protein was transiently expressed in Sf9 insect cell lines. Preliminary experiments indicated successful expression of ORCT, visualized through Western blotting. A complete understanding of the molecular structure, tissue expression, and physiological characterization of these organic cation transporters may hold promise for the formulation of more effective and environmentally benign insecticides, and may provide insights into the evolutionary origin of OCTs themselves.

Preface

As required by the UBC Animal Care Committee, I had successfully completed the Canadian Council on Animal Care (CCAC) National Institutional Animal User Training prior to beginning my research.

All research presented in Chapter 2 was conduced solely by the author, under the supervision of Dr. Mark Rheault at the University of British Columbia – Okanagan.

Research presented in Chapter 3 was conducted with collaboration from the Insect Pathology laboratory at Pacific Agri-Research Center (PARC), Summerland, B.C. with Mrs. Nadia Sokal, and under the direction of Dr. David Theilmann and Dr. Mark Rheault. I was responsible for the creation of all *orct* constructs and for the creation and isolation of positive *orct*-p2ZOPe2 constructs for transient cell line expression. All transfections, infections and Western blotting were performed together at PARC.

Figures 1.1 (Maddrell, 1981), 1.2 (Ianowski and O'Donnell, 2004), and 1.3 (Dow, 2009) were reproduced in this thesis with permission from the Journal of Experimental Biology. Figure 1.4 (Wright and Dantzler, 2004) did not require permission and was reproduced from The American Physiological Society through Copywright Clearance Center Inc.

Table of Contents

Abstract ..... **ii**

Preface ..... **iii**

Table of Contents ..... **iv**

List of Tables ..... **vi**

List of Figures ..... **vii**

List of Abbreviations ..... **ix**

Acknowledgements ..... **xiii**

Dedication ..... **xv**

Chapter 1 General Introduction **1**

1.1 Organization of the Insect Excretory System 1
1.2 Fluid and Ion Secretion by Malpighian Tubules 2
1.3 Models of Inorganic Ion Secretion by Insect Malpighian Tubules 3
1.4 Secretion of Organic Cations 5
1.5 Overview of Organic Cation Transport by Vertebrate Renal Tubules 6
1.6 Molecular Identification of Vertebrate Organic Cation Transporters 9
1.7 Transport of Organic Cations in Insects 10
1.8 Heterologous Protein Expression as a Tool to Study Organic Cation Transport Pathways 13
1.9 Research Purpose 17

Chapter 2 Cloning and mRNA Expression of *orct* and *orct2* **25**

2.1 Synopsis 25
2.2 Materials and Methods 26
2.2.1 Insect Rearing 26
2.2.2 RNA Extraction and Reverse Transcription 26
2.2.3 Primer Design 28
2.2.4 Primer Optimization 30
2.2.5 Cloning of Full Length cDNA Encoding *orct* and *orct2* 32
2.2.6 *orct* and *orct2* Sequence Analysis 34
2.2.7 Phylogeny of Organic Cation Transporters 35
2.2.8 Quantitative Real-Time Polymerase Chain Reaction 36
2.2.9 Data Analysis 37
2.3 Results 39
2.3.1 Sequence and Structural Features 39
2.3.2 Alignments and Phylogenetic Relationships 42

2.3.3 Gene Expression Analysis of *orct* and *orct2* Using Quantitative Real-Time Polymerase Chain Reaction 43
2.4 Summary 45

Chapter 3 Expression of the ORCT Protein in Insect Cell Lines 75

3.1 Synopsis 75
3.2 Materials and Methods 77
3.2.1 Insect Rearing 77
3.2.2 RNA Extraction and Reverse Transcription 77
3.2.3 Primer Design 77
3.2.4 Amplification and Preparation of Amplicons 78
3.2.5 Cloning into p2ZOPe2 79
3.2.6 Cloning into p*Ac*Bac 81
3.2.7 Transfection and Collection of Budded Virus 84
3.2.8 Infection 85
3.2.9 Protein Preparation and Sodium Dodecyl Sulfate Polyacrylamide Gel Electrophoresis 86
3.2.10 Coomassie Staining and Western Blotting 87
3.2.11 Selection for Stable Expressing Polyclonal Cell Line 88
3.3 Results 88
3.3.1 Proof of Method 88
3.3.2 Transfection Results 89
3.3.3 Infection Results 90
3.4 Summary 91

Chapter 4 Discussion 100

4.1 General Discussion 100
4.2 Molecular Identification of Organic Cation Transporters in *D. melanogaster* 101
4.3 Heterologous Protein Expression in Insect Sf9 Cells 105
4.4 Relative mRNA Expression of *orct* and *orct2* 108
4.5 Future Studies 110

References 113

Appendix 1: qPCR Normalization Using Multiple Reference Genes 129

List of Tables

Table 1.1 Tissue localization of vertebrate organic cation transporters 19

Table 2.1 Cloning primers 47

Table 2.2 Quantitative real-time PCR primers 48

Table 2.3 Sequencing primers 49

Table 2.4 Protein sequences for alignments 50

Table 2.5 Sequence analysis for *orct* showing nucleotide substitutions 51

Table 2.6 Sequence analysis for *orct2* showing nucleotide substitutions 52

Table 2.7 Sequence identity shared between organic cation transporter-like representative proteins 53

Table 3.1 Expression primers 93

List of Figures

Figure 1.1 Structure of the insect alimentary and excretory systems 20

Figure 1.2 Physiology of inorganic cation secretion in *D. melanogaster* 21

Figure 1.3 Physiology of the secretion of inorganic anions in *D. melanogaster*..... 22

Figure 1.4 Schematic representation of organic cation transport in renal cells of vertebrates..... 23

Figure 1.5 Schematic of the proposed transport mechanism for organic cations in *D. melanogaster*..... 24

Figure 2.1 Representative RNA gel..... 54

Figure 2.2 Sample MELT curve analysis for *orct*..... 55

Figure 2.3 Sample plate schematic for temperature and primer concentration optimization using quantitative real-time PCR..... 56

Figure 2.4 Optimal annealing temperatures for quantitative real-time PCR primers..... 57

Figure 2.5 Sample plate schematic for determination of primer set efficiency..... 58

Figure 2.6 Efficiency curves..... 59

Figure 2.7 Sample schematic for a quantitative real-time PCR experimental plate.. 60

Figure 2.8 Annotated protein sequence of ORCT..... 61

Figure 2.9 Schematic representation of the predicted secondary structure of ORCT62

Figure 2.10 Annotated protein sequence of ORCT2 63

Figure 2.11 Schematic representation of the predicted secondary structure of ORCT2 64

Figure 2.12 Alignment of representative vertebrate organic cation transporters and organic cation transporter orthologs with sequences from

D. melanogaster 65

Figure 2.13 Hydrophobicity plots of ORCT and ORCT2 with representative vertebrate oganic cation transporter orthologs 66

Figure 2.14 Alignment of representative insect organic cation transporter-like orthologs 67

Figure 2.15 Hydrophobicity plots of ORCT and ORCT2 with representative insect organic cation transporter-like orthologs 68

Figure 2.16 Phylogenetic analysis of representative organic cation transporter-like orthologs from the major facilitator superfamily 69

Figure 2.17 Reference gene stability analysis 70

Figure 2.18 Tissue distribution profiles of *orct* and *orct2* 71

Figure 2.19 Comparative expression of *orct* and *orct2* within *D. melanogaster* tissues 72

Figure 2.20 Relative expression of *orct* mRNA following exposure to tetraethylammonium after 1 and 15 generations 73

Figure 2.21 Relative expression of *orct2* mRNA following exposure to tetraethylammonium after 1 and 15 generations 74

Figure 3.1 Schematic diagram showing constructs and cloning into p2ZOPe2 94

Figure 3.2 Schematic diagram showing constructs and cloning into p*Ac*Bac 95

Figure 3.3 Images of Sf9 cells following transfection with pE28-GFP 96

Figure 3.4 Results of transfection with p2ZOPe2 constructs 97

Figure 3.5 Results of transfection with p*Ac*Bac constructs 98

Figure 3.6 Results of infection with budded virus constructs 99

List of Abbreviations

aa	amino acid
*Ac*MNPV	*Autographa californica* multicapsid nuclear polyhedrosis virus
actin 42A	actin 42A gene, *D. melanogaster*, reference gene
ANOVA	analysis of variance, statistical test
apical	the cell membrane bordering the lumen
bacmid	a shuttle vector that can be propagated in both *E. coli* and insect cells
basolateral	the cell membrane bordering the haemolymph or blood
bmon14272	*Autographa californica* Multicapsid Nucleopolyhedro virus bacmid
BLAST	Basic Local Alignment Search Tool
BV	budded virus
cDNA	complimentary DNA
ColE1	replication origin
Cq	quantification cycle
Ct	threshold cycle
ctl	control, undigested circular plasmid
Da	Dalton, atomic mass unit
DDAB	dimethyldioctadecyl-ammonium bromide
DEPC	diethylpyrocarbonate
DH10β	*E. coli* cell strain
DOPE	L-alpha- phosphatidylethanolamine dioleoyl
E	efficiency
EM7	bacterial promoter
FBS	fetal bovine serum

FLIPT	fly-like putative transporter
gapdh-1	glyceraldehyde 3-phosphate dehydrogenase, *D. melanogaster*, reference gene
GFP	green fluorescent protein
goi	gene of interest
HA-tag	human influenza hemagglutinin amino acid sequence (YPY DVP DYA)
heterologous	from a different species, transplant between species
hpi	hours post infection
hpt	hours post transfection
ie2	immediate early promoter from *Orgyia pseudotsugata*
JM109	*E. coli* cell strain
J_{MAX}	maximum flux
Kc1	a cell line from the dipteran *Drosophila melanogaster*
Km	concentration of substrate that will give half-maximal velocity of transport capability
LB	Luria-Bertani media/agar
MATE	multi drug and toxin extrusion transporter
MDR	multi-drug resistant protein
MFS	major facilitator superfamily
mRNA	messenger RNA
MT	Malpighian tubule
NAPS	Nucleic Acid Protein Service Unit
NCBI	National Center for Biotechnology Information
NHE	sodium/proton exchanger

NMN	N-methylnicotinamide
NRQ	normalized relative quantity
NRT	no reverse transcription control
NTC	no template control
OAT	organic anion transporter
OB	occlusion body
OC	organic cation
OCT	organic cation transporter
OCTN	organic cation/carnitine transporter
ODV	occlusion derived virus
*Op*MNPV	*Orgyia pseudotsugata* multicapsid nuclear polyhedrosis virus
orct	organic cation transporter-like, *D. melanogaster*, gene of interest
orct2	organic cation transporter-like 2, *D. melanogaster*, gene of interest
ORF	open reading frame
p2ZOPe2	a plasmid
p*Ac*Bac	recombinant plasmid
pE38-GFP	a plasmid with a green fluorescent protein construct
pFastBac-1™	a plasmid
pGEM®-T Easy	a plasmid
pmon7124	transfer plasmid
PBS	phosphate buffered saline
PCR	polymerase chain reaction
PKA	cAMP dependant protein kinase
PKC	protein kinase C

qPCR	quantitative real time polymerase chain reaction
ref	reference gene
rp49	ribosomal protein 49, *D. melanogaster*, reference gene
SDS-PAGE	sodium dodecyl sulfate polyacrylamide gel electrophoresis
SEM	standard error of the mean
Sf9	a cell line from the lepidopteran *Spodoptera frugiperda*
SL2	a cell line from the dipteran *Drosophila melanogaster*
SLC22A	solute carrier superfamily 22A
SMART	Simple Modular Architecture Research Tool
SNP	single nucleotide polymorphism
TEA	tetraethylammonium
TEMED	tetramethylethylenediamine , N,N,N',N'-tetramethyl- ethane-1,2-diamine
Tm	annealing temperature
TMD	transmembrane domain
Tn7	transposition site
V-ATPase	vacuolar type H^+-ATPase

Acknowledgements

It is with the deepest appreciation I would like to extend my thanks to the faculty, staff and students at the Okanagan campus of UBC for making my many years here an unforgettable and rewarding experience. It is the atmosphere of the campus and the ongoing support of everyone that I have had the pleasure of working that have made these years so memorable.

I find it hard to put into words my unending gratitude to my supervisor Dr. Mark Rheault for granting me the opportunity to learn from him. Through his guidance I have learned more about myself and what I am capable of over anything I would have expected. His unwavering confidence in my ability and his respect pushed me to exceed all of my own expectations and has raised my confidence and abilities to new heights.

Thank you to all members of my committee; Dr. Scott Reid, Dr. Michael Russello and Dr. Andis Klegeris for your feedback, support and respect. It has been a pleasure working with you and learning from you.

Thank you to my collaborators for help with this and other projects, Mrs. Nadia Sokal and Dr. David Theilmann (PARC); Miss Sarah Chahine (McMaster University, Hamilton, ON); and Miss Jesmila Marusalin and Dr. Andrew Donini (York University, Toronto, ON).

Special thanks should be given to Lukman (Rony) Sarker and Zerihun Demissie for their friendship, support, positive thinking and knowledge – I could not have made it through without you. Thank you Kevin Duncan and Patrick Bobyn for your patience and help developing techniques for our lab and for always inspiring great music on long dissection days. Thank you also to my current lab mate Matt Glover for your understanding during my writing months.

Thank you to the Natural Sciences and Engineering Research Council of Canada (NSERC), the Canadian Foundation for Innovation (CFI), the Canadian Society of Zoologists (CSZ) and the Association of Professional Biologists of British Columbia (APB) for granting the funding to complete and share this research.

Finally to my family – you are my drive, my inspiration, my strength, my support, my world, and even though I'm sure you can only wonder at what I have been doing for the last two years, I am so grateful everyday that we could go through it together. Mom, Dad, Matt, you are my best friends and I love you.

To Joy and family

Chapter 1 General Introduction

1.1 Organization of the Insect Excretory System

The excretory system in the majority of insects consists of the Malpighian tubules (MTs) and the hindgut, working in concert with other areas of the alimentary system (i.e. midgut) and respiratory system (i.e. anal papillae) to maintain osmotic balance. Malpighian tubules, which are analogous to vertebrate renal tissue, are present in all known insects except Springtails (order Collembola), Bristle-tails (order Diplura), Coneheads (order Protura), and Stylops (order Strepsiptera) (Phillips, 1981). The number of MTs found between species is variable and ranges from 2 in coccids to more than 250 in locusts (Phillips, 1981). Malpighian tubules are variable in length and can range from 2 – 70 mm (Phillips, 1981). Although MTs of insects show variability in number and length, their overall morphology is relatively well conserved. Malpighian tubules are blind-ended and in the majority of insects open to the alimentary system at the junction of the midgut and hindgut (Figure 1.1). Malpighian tubules are composed of a single layer of squamous epithelial cells. Two to five cells make up a tubule in cross-section (Phillips, 1981). Insects such as *Rhodnius prolixus* or *Locusta migratoria* have tubules are composed of a single cell type, while other insects such as the dipterans *D. melanogaster* and *Aedes aegypti* have tubules composed of both principal cells and a different , secondary, cell type, called stellate cells (Dow, 2009). Ultrastructural studies have revealed that tubules have membrane structures consistent with transporting epithelia. Electron micrographs of tubules show that the apical and basal membranes are highly folded. The total surface area of a tubule is ~20 times greater than that of the vertebrate glomeruli per unit body weight (Phillips, 1981). In *R. prolixus*, it has been calculated that the apical side of the cell is increased 150-fold due to the presence of microvilli and that the surface area of the basal side of the cell is increased by a factor of 40

due to the extensive infolding of the membrane (O'Donnell and Maddrell, 1983). The increases in surface area as a result of this folding are presumed to be necessary for the incorporation of membrane-bound proteins that are utilized for transport of inorganic and organic ions in MTs. Based on cell dimensions, the width of the intercellular spaces and the extensive membrane infolding the ratio of the area of the membrane to the intercellular cleft has been calculated to be 120 000:1 (Phillips, 1981). Given the high value of this ratio it has been suggested that the dominant route for fluid and ion transport in *R. prolixus* MTs is transcellular rather than paracellular (O'Donnell and Maddrell, 1983).

1.2 Fluid and Ion Secretion by Malpighian Tubules

Malpighian tubules, which are analogous to the proximal segments of the vertebrate renal tubule, are responsible for the secretion of primary urine, waste products and toxins, while the hindgut is responsible for downstream reabsorption of water from the primary urine and can be considered functionally analogous to the collecting duct of the vertebrate renal tubule (Phillips *et al*., 1981). Malpighian tubules and the hindgut acting in concert comprise the insect functional kidney. In contrast to the vertebrate kidney where urine is formed through hydrostatic filtration of the plasma at the glomerulus, production of primary urine in insects occurs by a secretory process driven by the active transport of ions into the tubule lumen, and a consequent flow of osmotically obliged water (O'Donnell and Maddrell, 1983; Dow *et al*., 1994). Secreted fluid is nearly iso-osmotic or slightly hyper-osmotic to the haemolymph of the insect. The rates of fluid secretion by tubules can be extremely high. Fully stimulated MTs of *R. prolixus* or *D. melanogaster* can secrete a volume of near iso-osmotic fluid equivalent to each cells own intracellular volume every 10-15 seconds (Maddrell, 1991; Dow *et al*., 1994).

1.3 Models of Inorganic Ion Secretion by Insect Malpighian Tubules

The physiology of inorganic ion transport by the MTs has been investigated in a number of insect species. Current models propose that cations are transported through a transcellular pathway (O'Donnell and Maddrell, 1983), but differing pathways for inorganic anion transport have been described in tubules from different insect species. Inorganic anion transport may involve paracellular pathways or transcellular pathways, through the same cell type as cations or through a different cell type (Beyenbach, 2003; O'Donnell *et al*., 2003; O'Donnell *et al*., 1998).

Figure 1.2 shows the current models of inorganic ion transport for the MTs of *D. melanogaster*. Early models of fluid secretion by insect MTs suggested that an apical alkali cation pump was responsible for energizing ion transport (Wieczorek *et al*., 1986; Harvey *et al*., 1983). It is now widely accepted that the apical cation pump is in fact comprised of two separate transporters, a ouabain insensitive vacuolar-type H^+-ATPase (V-ATPase) (Schweikl *et al*., 1989) that can be inhibited by bafilomycin A_1 (Bertram *et al*., 1991; Bowman *et al*., 1988), coupled to an amiloride sensitive alkali cation/H^+ exchanger (Wieczorek *et al*., 1991). The V-ATPase maintains an electrochemical proton derived gradient, which makes the lumen side of the membrane positive relative to the intracellular side of the apical membrane. This electrochemical gradient provides the driving force for the secondary facilitated transport of alkali cations from the cell to lumen through the alkali cation/H^+ antiporter (Wieczorek *et al.,* 1991). Recent studies by Rheault *et al*. (2007) have provided molecular evidence that the previously proposed Weiczoreck alkali cation/H^+ antiporter is in fact a member of the cation/proton antiporter family of transport proteins designated NHE (sodium/proton exchanger).

Mechanisms of inorganic cation movement across the apical membrane in different insect species have been extensively studied and the mechanisms have been found to be similar across insect species. However, there has been much debate as to the transporters responsible for the entry of inorganic cations across the basolateral membrane between different insect species. Early models have proposed separate entry pathways for K^+ and Na^+ in phytophagous insects such as *D. melanogaster*. The first of these early models suggested that K^+ transport across the basolateral membrane of the principal cells occurs through K^+ channels (Dow *et al.,* 1994; O'Donnell *et al*., 1996). A recent study by Evans *et al*. (2005) has provided evidence that a low-affinity class of inward rectifying K^+ channels may play a minor role in fluid secretion by unstimulated MTs but a more significant role in MTs in which fluid secretion has been stimulated by diuretic factors. A second model proposed by Linton and O'Donnell (1999) suggests that K^+ crosses the basolateral membrane through both the Na^+/K^+-ATPase and a K^+:Cl^- co-transporter. More recently a study by Ianowski and O'Donnell (2004), in which basolateral electrochemical potentials were calculated, has ruled out both of these suggested routes of K^+ basolateral entry for unstimulated tubules. Instead a bumetanide sensitive Na^+:K^+:2Cl^- co-transporter was shown to be responsible for inorganic cation entry, with most of the Na^+ that enters the cells being recycled back to the haemolymph via a basolateral Na^+/K^+-ATPase. The routes of transepithelial Cl^- transport are shown in Figure 1.2 and Figure 1.3. Studies by O'Donnell *et al*. (1996, 1998) have indicated that transepithelial Cl^- transport in *D. melanogaster* is mediated by passive movement down a favorable electrochemical gradient for Cl^- through stellate cells, possibly mediated by chloride channels. However, Ianowski and O'Donnell (2004) have shown that Cl^- enters across the basolateral membrane of the principal cells of *D. melanogaster* MTs via the Na^+:K^+:2Cl^- co-transporter. While a small portion of this Cl^- is recycled back across the

basolateral membrane the majority must exit across the apical membrane by a yet undefined or characterized apical pathway. Alternatively, in another dipteran, the yellow fever mosquito, *A. aegypti*, there is evidence to suggest that transepithelial Cl^- transport is mediated via a paracellular pathway (Pannabecker *et al*., 1993).

1.4 Secretion of Organic Cations

Renal secretion of organic ions plays a critical role in limiting an organism's susceptibility to the effects of toxic compounds of both exogenous and endogenous origin. Secretion of organic cations (OCs) has been demonstrated in the renal tissues of a number of mammalian and non-mammalian vertebrates (Miller and Holohan, 1987; Burg and Weller, 1969; Hawk and Dantzler, 1984, Dantzler, 1989; Rennick, 1981), and in several invertebrate species (Miller and Holliday, 1987; Maddrell and Gardiner, 1976). Insects have evolved a number of defensive mechanisms to cope with the accumulation of toxic substances in their haemolymph and tissues including detoxification by metabolic enzymes (Li *et al.,* 2002, 2007) and through elimination across insect MTs and gut (O'Donnell *et al.,* 2003). Organic cations include xenobiotics such as environmental pollutants, plant defensins, animal toxins and pharmacological drugs (Dresser *et al.,* 1999). In addition, both endogenous and exogenous compounds have the potential of being metabolized into OCs. All OCs share a common hydrophobic carbon backbone (Meijer *et al.,* 1990) giving each molecule a certain level of hydrophobicity. As well, all OCs posses a positively charged amine group at physiological pH 7 (Meijer *et al.,* 1990) implicating carrier mediated transport in the excretion of these compounds. Type I OCs such as tetraethylammonium (TEA), and N-methylnicotinamide (NMN) are typically monovalent and have a molecular weight <400 g mol^{-1}. Type II OCs such as vinblastin and vecuronium are typically

polyvalent with a molecular weight >500 g mol^{-1} (Meijer *et al.,* 1990). It is generally accepted that the principal function of transport processes associated with the movement of OCs is clearing the body of xenobiotic compounds (Pritchard and Miller, 1993; Wright and Dantzler, 2004).

Much of what is known about OC renal secretion and the mechanisms involved has been derived from experimental work on vertebrate renal tissue over the past 30 years. Thus, it is appropriate to begin our discussion of the mechanisms potentially involved in MT OC transport by discussing models of vertebrate renal transport.

1.5 Overview of Organic Cation Transport by Vertebrate Renal Tubules

Renal excretion of OCs was first demonstrated in vertebrate tissue almost 65 years ago (Sperber, 1947; Rennick *et al.,* 1947). Since then, further studies have shown that excretion of a wide range of OCs is a common characteristic of vertebrate and invertebrate renal tissues (Miller and Holliday, 1987; Boom *et al.,* 1992; Hawk and Dantzler, 1984; McKinney *et al.,* 1981; Wright *et al.,* 2004). In 1993 Pritchard and Miller reviewed the physiological evidence for the "classical" OC transport pathway in vertebrates. This pathway involved carrier-mediated potential-driven uptake of OCs through a single pathway at the basolateral membrane, intracellular sequestration of the OCs, and luminal exit through an OC/ H^+ exchanger or by a multi-drug resistance transport protein (MDR). Incorporation of more recent physiological and molecular evidence suggested that this classical model is an oversimplification of the OC transport pathways. More extensive reviews by Wright and Dantzler (2004) and Wright (2005) incorporating available evidence indicated that there are multiple OC transporters with differential expression and affinities

for a broad range of type I and type II OCs at both the basolateral and apical membranes of renal cells.

Figure 1.4 shows the complement of transporters proposed by Wright and Dantzler in 2004 for the transepithelial transport of OCs in the vertebrate renal proximal tubule. Basolateral entry of Type I OCs involves one or more electrogenic facilitated diffusion mechanisms driven by the inside-negative basolateral membrane potential (Smith *et al*., 1988; Busch *et al*., 1996). The transporters responsible have been cloned and characterized in vertebrates and labeled as organic cation transporters (OCT1, OCT2, OCT3). Evidence for potential-driven facilitated diffusion at the basolateral membrane of an intact epithelium comes from the study of proximal tubules of two species of marine teleost fish, namely the southern flounder and the killifish (Smith *et al.,* 1988). Smith *et al.* (1988) found that treatments that depolarize the basolateral membrane (high K^+, Ba^{+2}) inhibit OC uptake, while treatments that hyperpolarize the basolateral membrane (low K^+) stimulate uptake. Smith *et al.* (1988) also found that the addition of OCs such as TEA or darstine (mepiperphenidol) to the bathing medium reversibly depolarizes the basolateral membrane potential. Two-electrode voltage clamp studies of *Xenopus laevis* oocytes in which an organic cation transporter 1 (OCT1) from the rat is expressed demonstrated inwardly directed currents upon exposure to TEA (Busch *et al.,* 1996). Furthermore, uptake of radiolabeled TEA by oocytes expressing rat OCT1 is inhibited by depolarization of the membrane potential (Grüdemann *et al*., 1994). Thus data from both intact renal tissue and from isolated protein expression studies with oocytes provide support for an electrogenic facilitated diffusion transporter, which is dependent on membrane potential for the uptake of OCs across the basolateral membrane.

Type II OCs cross the basolateral membrane due to their larger size and degree of hydrophobicity through simple diffusion, providing an additional, potential driven pathway for basolateral OC entry.

Some OCs may be sequestered into organelles, however the loading capacity and trafficking of OCs by organelles is unknown (Sweet and Pritchard, 1999).

Transport across the apical membrane is driven by proton exchange maintained by a proposed NHE (Wright and Dantzler, 2004). Studies using isolated apical membrane vesicles show evidence that acidification of vesicles can stimulate OC uptake (Dantzler *et al*., 1991; McKinney and Kunnemann,, 1985; Ott *et al*., 1991). Furthermore luminal perfusion of intact proximal tubules with an acidifying solution also supports the concept of an apical electrogenic OC/ H^+ exchanger (Dantzler *et al*., 1989; McKinney, 1984). The first molecular candidate for the apical transport protein was an organic cation/carnitine transporter (OCTN) (Tamai *et al.,* 1997). However, due to the low kidney expression and low affinity of OCTN for TEA, new candidate proteins for the apical transporter have been proposed: multi drug and toxin extrusion (MATE) transporter 1 (Otsuka *et al.,* 2005) and MATE2 (Masuda *et al.,* 2006). These transporters exchange TEA and other OCs at the apical membrane for a proton, and have expression profiles consistent with other renal transporters (Zhang *et al.,* 2007). MDR or p-glycoprotein transporters may transport larger or more hydrophobic type I OCs, however their contribution to OC transport has not been quantified (Buss and Callaghan, 2007).

An ATP-dependent MDR mediates exit of type II OCs across the luminal membrane. Expression of MDR in the apical membrane of the vertebrate renal proximal tubule cells suggests that these transporters likely play a role in the secretion of at least some OCs. Studies by Miller (1995) have shown that teleost renal proximal tubules actively secrete the

fluorescent anthracycline daunomycin into their lumen, and this transport could be reduced by known p-glycoprotein substrates such as cyclosporin A, and the known p-glycoprotein inhibitors verapamil and vanadate. In addition, there is evidence that the teleost renal proximal tubules can actively secrete the fluorescent analogues of cyclosporin (Schramm *et al*., 1995) and rapamycin (Miller *et al*., 1997).

1.6 Molecular Identification of Vertebrate Organic Cation Transporters

Organic cation transporters belong to the solute carrier superfamily 22A (SLC22A), which also includes OCTNs and organic anion transporters (OATs) (Wright and Dantzler, 2004). Three isoforms of OCTs have been identified in humans, rats and mice, and orthologs of these isoforms have been identified in other species. The first OCT to be cloned in vertebrates (OCT1) was from a rat kidney cDNA library (Grundemann *et al.,*1994). The cDNA transcript encodes a 556-amino acid (aa) sequence with 12 predicted trans membrane domains (TMDs). The predicted topology is that both the amino and carboxyl termini of the peptide chain are located intracellularly and when inserted into the membrane, the peptide forms a large extracellular loop between TMD1 and TMD2 and a large intracellular loop between TMD6 and TMD7. Since the discovery of OCT1 in rat, two other transporters have been cloned and characterized that share identity with OCT1, named OCT2 (Okuda *et al.,* 1996; Gorboulev *et al.,* 1997) and OCT3 (Kekuda *et al.,* 1998). Physiological studies in *X. laevis* oocytes with isolated OCT transporters show a large inward current associated with high concentrations of TEA in the bath (Dresser *et al.,*2001). Thus it is believed that these transporters are localized to the basolateral membrane.

Table 1.1 summarizes the tissue localization of vertebrate OCTs and OCTNs. All of the known vertebrate OCT isoforms and orthologs exist in the kidneys and most are present

in the liver. Expression of these transporters is consistent with the expression of proteins responsible for the elimination of toxic compounds. All of the OCTs are present at the basolateral membrane (Wright and Dantzler, 2004; Dresser *et al*., 2001).

1.7 Transport of Organic Cations in Insects

Although mechanisms of inorganic cation transport in insect MTs and their regulatory control have been extensively studied and reviewed (Dow and Davies, 2001; O'Donnell and Spring, 2000), it has not been until very recently that physiological evidence has emerged elucidating the mechanisms underlying the transport of OCs by the MTs of insects (Rheault and O'Donnell, 2004; Rheault *et al.*, 2005; 2006; Bijelic and O'Donnell, 2005; Bijelic *et al*., 2005). Nijhout (1975) provided the first evidence for the transport of OCs across insect MTs from *Manduca sexta*. In this study the MTs transported the cationic dyes methyl green and methylene blue. Subsequently MTs of *R. prolixus* were shown to secrete the basic, cationic dyes methyl green and methylene blue as well (Maddrell and Gardiner, 1976). Tubules of the larvae of *Chironomous* have been shown to rapidly concentrate the dye neutral red (Salkind, 1930), while the tubules of *Blatta orientalis*, *Forficula auricularia*, and *Carasius morosus* cannot (Lison, 1938). All historical observations of basic dye transport by MTs were purely qualitative. Attempts were not made in these studies to quantify the transport of these dyes by the MTs. However, it is of interest that all of these basic dyes contain a positively charged amine nitrogen at physiological pH and are thus candidate substrates for the OC transport pathway.

It has been observed that, in addition to the transport of basic dyes, insect MTs also actively secrete the plant alkaloid nicotine (Maddrell and Gardiner, 1976) and the p-glycoprotein substrate vinblastine (Gaertner *et al*., 1998). The possibility that nicotine

transport in insect MTs is mediated by a p-glycoprotein-like mechanism has been suggested by the observations that verapamil, a known p-glycoprotein inhibitor, blocks the transport of nicotine, while nicotine interferes with the transport of vinblastine by the isolated MTs from larval *M. sexta* (Gaertner *et al*., 1998). A recent study by Leader and O'Donnell (2005) has shown that p-glycoprotein may play a role in the secretion of daunorubicin by insect MTs due to the fact that verapamil also inhibits transepithelial transport of daunorubicin. In polarized mammalian epithelia, OCs cross the basolateral membrane through passive diffusion or by facilitated diffusion (Wright and Dantzler, 2004). P-glycoprotein is expressed only at the apical membrane where it is proposed to actively transport OCs out of the cell (Wright and Dantzler, 2004). Thus, p-glycoprotein is a potential candidate for an apical but not basolateral route of OC transport in insect MTs. Further evidence, which suggests that p-glycoprotein is not involved in basolateral OC uptake by insect MTs, comes from studies using the fluorescent p-glycoprotein substrate daunomycin on the MTs of larval *M. sexta* (Gaertner and Morris, 1999). In this study, although the MTs quickly took up daunomycin, uptake could not be blocked by verapamil or nicotine, indicating that uptake at the basolateral membrane does not involve a p-glycoprotein-like mechanism.

A number of recent studies have provided physiological evidence for the transport of the prototypical type I OC, TEA, by insect MTs and extrarenal tissues. Rheault and O'Donnell (2004) used newly developed TEA ion selective microelectrodes to show that TEA was transported from bathing medium across the MT epithelia into the lumen along the length of the main, lower and ureter segments of the MTs. The posterior midgut displayed TEA secretion rates similar to the MT main segment. The analysis of secreted fluids showed a nearly 12-fold increase in TEA concentration in the secreted fluid when compared to bathing medium. This observation combined with measurements of a positive

potential in lumen of MTs provides support for an active transporter mechanism (Rheault and O'Donnell, 2004).

Tetraethylammonium is a positively charged OC at physiological pH. Thus its movement from the haemolymph across the basolateral membrane is opposed by the hydrophobic lipid bilayer of the cell and as such necessitates some form of facilitated transport. Rheault *et al.* (2005) provided the first evidence for an electrogenic, carrier-mediated basolateral transport mechanism for OCs in insect MTs. Briefly they showed that TEA transport was metabolically dependent, was dependent on membrane potential and could be inhibited by the addition of a number of type I OCs (Rheault *et al*., 2005). Transport of TEA across isolated MTs was saturable indicating a transcellular carrier mediated pathway.

Pharmacological studies on *D. melanogaster* MTs with type I and type II OCs affected TEA transport in different ways. Verapamil, a type II OC, had no effect on transport of TEA, where as cimetidine, a type I OC, significantly decreased TEA influx. These findings led researchers to conclude that there may be different transport pathways for type I and type II OCs. Transport for type I OCs thus may be carrier mediated, shown through competition between cimetidine and TEA for transport (Rheault and O'Donnell, 2004).

In a comparative study of different insects, it was found that secretion of type I and type II OCs may occur through separate transporter-mediated pathways (Rheault *et al*., 2006). Of interest in this study was that blood-feeding insects such as *R. prolixus* and *A. aegypti* do not exhibit active transport of TEA across cells of the MTs. The current hypothesis is that these insects either secrete OCs in other parts of the body (i.e. the gut) or that a life history in which plant alkaloids and pesticides were not routinely ingested did not allow the development of OC transport proteins. In this study the transport of the p-

glycoprotein substrate, nicotine, was inhibited by verapamil, a p-glycoprotein inhibitor in insects such as *M. sexta*. However, in previous studies, verapamil had no effects on TEA transport. Currently, research suggests different modes of transport for type I OCs and other OC, plant alkaloids such as nicotine (Rheault *et al*., 2006). Based on evidence gathered surrounding the transport of OC in insects, a model for OC transport across the MTs of *D. melanogaster* has been proposed and is shown in figure 1.5.

Historically, studies on the transport of OCs across insect tissues have focused on whole body or whole tissue transport. Researchers have yet to study insect putative OCT genes in isolation to determine the contributions of individual proteins to overall tissue transport of OCs. Therefore, there exists a need for the development of an expression system that would be suitable for the expression of isolated insect proteins for functional studies.

1.8 Heterologous Protein Expression as a Tool to Study Organic Cation Transport Pathways

Heterologous protein expression systems are useful tools to produce high levels of foreign protein that can be used for both structural and functional analysis. More commonly used expression systems include *Escherichia coli*, yeast, baculovirus/insect cells, oocytes and mammalian cells (Brondyk, 2009). Choosing an appropriate system to express a foreign protein depends on the proteins characteristics, the characteristics of the expression system and the planned use of the protein for various physiological assays (Brondyk, 2009). Prokaryotic systems such as *E. coli* and yeast are generally simple and inexpensive, which explains their wide use and appeal (Midgett and Madden, 2007). Differences in protein glycosylation, membrane lipid composition and processing machinery needed to fold, assemble and stabilize eukaryotic proteins make these systems

less than ideal for eukaryotic protein expression (Midgett and Madden, 2007, Hegedus *et al.,* 1999). The use of a baculovirus is advantageous because protein production occurs in a eukaryotic system. Transfection of a baculovirus vector containing a foreign gene, into an insect cell line allows large amounts of protein production and correct post translational modifications of the protein, resulting in proper formation of the foreign proteins (Miller, 1988). It is known that three glycosylation pathways exist in insect cells that are dissimilar to comparable pathways in higher eukaryotes such as mammalian cells (Miller, 1997), making insect cell lines in combination with a baculovirus vector ideal for expression of an insect protein. Sf9 embryonic cell lines from the Fall armyworm (*Spodoptera frugiperda*) have been recently exploited to characterize a number of human and other vertebrate proteins using a baculovirus vector (Sarkade *et al.,* 1992, Hegedus *et al.,* 1999, Bakos *et al.,* 2000, Ozvegy *et al.,* 2001).

Baculoviruses have long been used as insect pest control agents to protect economically important crops due to the specific nature of baculovirus to infect only insect cells (Miller, 1997). More recently, it has been found that baculovirus genomes could be manipulated to express heterologous proteins at high levels, leading to the development of baculovirus expression vector systems (Smith *et al.,* 1983). A widely used baculovirus for expression research has been the alphabaculovirus *Autographa californica* multiple nucleopolyhedrovirus (*Ac*MNPV), which undergoes successful replication in Sf9, cells (Jehle *et al.,* 2006). *Ac*MNPV has a large double-stranded circular genome with 154 open reading frame (ORF) coding regions (Rormann, 2008). Alphabaculoviruses, including *Ac*MNPV, all produce budded virus (BV) and occlusion derived virus (ODV) over the course of their replication cycle (Jehle *et al.,* 2006). Occlusion derived viruses are produced embedded in a polyhedrin protein matrix that allows the virus to survive outside of the host as occlusion

bodies (OB) (Rohrmann, 2008). The virus is spread between hosts via ingestion of OB from a contaminated food source. The polyhedrin matrix is broken down within the midgut of the new host, releasing the viron to infect midgut cells (Rohrmann, 2008). Production of BV in the latter stages of infection allows the spread of systemic infection throughout the host (Rohrmann, 2008). In order to use a baculovirus expression vector, the foreign gene is first inserted into the virus and applied to an insect cell culture. Budded virus is produced following transfection of the cells and can be collected and subsequently used to infect insect cells for protein production (Miller, 1997).

The baculovirus system works by exploiting the polyhedrin gene, which is under the control of a strong late promoter, which results in high levels of polyhedrin protein production late in the viral replication cycle (Rohrmann, 1986). Therefore replacing the polyhedrin ORF with a foreign gene, would result in high levels of foreign gene expression with minimal effect on the production of BV (Smith *et al.,* 1983, Vialard *et al.,* 1990, Zuidema *et al.,* 1990). Due to the lack of polyhedrin production following foreign gene insertion, ODV are not produced, resulting in an inability of the virus to transmit to other insects; and because ODV are not formed, infected cells can be identified visually under a light microscope by the absence of OB (Smith *et al.,* 1983).

One method for the creation of recombinant *Ac*MNPV baculovirus is site-specific transposition in bacterial culture, described by Luckow *et al.* (1993). Transposition involves 1) a shuttle vector including the virus genome 2) a transfer plasmid including the foreign gene and 3) a helper plasmid encoding a transposase enzyme to allow transposition of the foreign gene into the virus genome. The shuttle vector, or bacmid, includes the *Ac*MNPV genome with 4 modifications within the polyhedrin locus. First a mini-F region was added which allowed viral replication in bacterial cells to simplify recombinant virus

construction. Second, two Tn7 bacterial transposition sites were added to allow insertion of the foreign gene from the transfer plasmid into the bacmid. Third, a kanamycin resistance gene was incorporated necessary for bacmid selection in bacteria on supplemented media. Fourth, the *lacZ* gene was added between the transposition target sites, which allowed blue white screening (Sambrook and Russell, 2001) due to insertional gene interruption. The transfer plasmid contains a gentamicin resistance gene for selection and a strong late polyhedrin promoter between the Tn7 transposition sites (Luckow *et al.,* 1993). The combination of the bacmid, transfer plasmid and helper plasmid in bacterial *E. coli* cells, allows site specific transposition of the foreign gene. The resulting recombinant bacmid, containing the foreign gene, was identified by kanamycin resistance, gentamicin resistance and the white color of the colony. The success of the baculovirus polyhedrin promoter at expressing heterologous proteins in Sf9 cells led to the development of numerous plasmid vectors that could be used for both transient and stable expression of a protein in insect cell lines (Pfeifer *et al.,* 1999; Pfeifer *et al.,* 2001; Dai *et al.,* 2005). One plasmid, p2ZOPe2, uses and immediate-early promoter (ie2) from the *Orgyia pseudotsugata* multicapsid nuclear polyhedrosis virus (*Op*MNPV) to transcribe heterologous cDNA sequences in insect cells. The plasmid is either degraded or integrated into the Sf9 genomic DNA by intracellular processes as soon as 48 hours post transfection (hpt)(Dai *et al*., 2005). This expression system thus reduces toxicity in Sf9 cells resulting from prolonged protein accumulation. Integration of the plasmid into the genomic DNA of the cells allows for the selection of stably expressing cell lines through the use of an antibiotic (Dai *et al.,* 2005). The zeocin selectable marker under the control of an EM7 bacterial promoter and the ColE1 origin allows for selection and rapid amplification of the plasmid in *E. coli*. A multiple cloning site containing a number of restriction sites just downstream of the ie2 promoter

allows insertion and transcription of the foreign cDNA for expression (Hededus *et al.,* 1998; Hegedus *et al.,* 1999; Theilmann and Stewart, 1992; Invitrogen InsectSelect™ System Manual, 2010).

1.9 Research Purpose

Mechanisms of inorganic cation transport across the MTs of insects, and the regulatory control governing the movements of these ions have been extensively studied and reviewed (Dow and Davies, 2001; O'Donnell and Spring, 2000); however it has not been until recently that physiological evidence has emerged describing the mechanism underlying the transport of OCs by insect MTs (Rheault and O'Donnell, 2004; Rheault *et al.,* 2005, 2006; Bijelic and O'Donnell, 2005). These studies have provided the first evidence for the transport of the prototypical type I OC, TEA by *D. melanogaster* tissues. Rheault and O'Donnell (2004), demonstrated TEA transport across the posterior midgut, as well as across the main and lower segments of the MTs using ion-selective microelectrodes. In 2005, Rheault *et al.* provided the first evidence for an electrogenic carrier-mediated basolateral organic cation transport mechanism in *D. melanogaster* MTs.

In 1997, a sequence transcript in the genomic DNA of *D. melanogaster* was discovered which showed a high degree of similarity to vertebrate OCT coding regions (Taylor *et al.,* 1997). The gene giving rise to this transcript has been named organic cation transporter-like (*orct*). Further annotations of the *D. melanogaster* genome (Hoskins *et al*., 2007) have revealed a second candidate gene *orct2*, which also showed high similarity to vertebrate OCTs.

This thesis describes the cloning of the candidate OCT-like genes *orct* and *orct2* from *D. melanogaster* for the first time. Using phylogenetic analysis I determined the sequence

identities to vertebrate OCT orthologs and predicted OCT-like orthologs from other insect species. Additionally this thesis describes the topology of the amino acid peptide chains of the ORCT and ORCT2 proteins. Furthermore, this thesis describes the mRNA expression profiles of *orct* and *orct2* across a number of *D. melanogaster* tissues and describes the changes in expression following exposure to TEA.

Synthesis of the proteins would be needed for functional assays in order to verify the hypothesis that these gene transcripts play a role in OC transport across *D. melanogaster* tissues.

I evaluated the ability of both a baculovirus vector and a plasmid vector to express ORCT in insect Sf9 cell lines for the purpose of future functional assays. In addition, a plasmid vector was used to create a polyclonal, stably expressing Sf9 cell line to be used in future work. Expression was assessed through western blotting following transfection with both vector systems and following infection with collected budded virus over a series of time points. Results of this study will lay the groundwork for researchers to choose an optimal expression vector for future physiological studies of ORCT and ORCT2.

Table 1.1 Tissue localization of vertebrate organic cation transporters. Information gathered from Wright and Dantzler (2004)[1] and Dresser *et al.*, (2001)[2]. Localization profiles summarized here are not exhaustive of the literature, and shows only the most common and highest expressing sites for a number of vertebrate species. Acronyms are defined as: BLM, basolateral membrane

Localization										
Type	Kidney	Liver	Nervous	Gut	Muscle	Heart	Fetal	Genital	Apical	BLM
OCT1	✓[1,2]	✓[1,2]	✓[2]	✓[1,2]	✓[2]		✓[2]			✓[1]
OCT2	✓[1,2]		✓[1,2]	✓[2]			✓[2]		✓[1]	✓[1]
OCT3	✓[1]	✓[1]	✓[1]	✓[1]	✓[1]			✓[1]		✓[1]
OCTN1	✓[1]					✓[1]	✓[1]	✓[1]	✓[1]	
OCTN2	✓[1]	✓[1]	✓[1]		✓[1]	✓[1]	✓[1]			

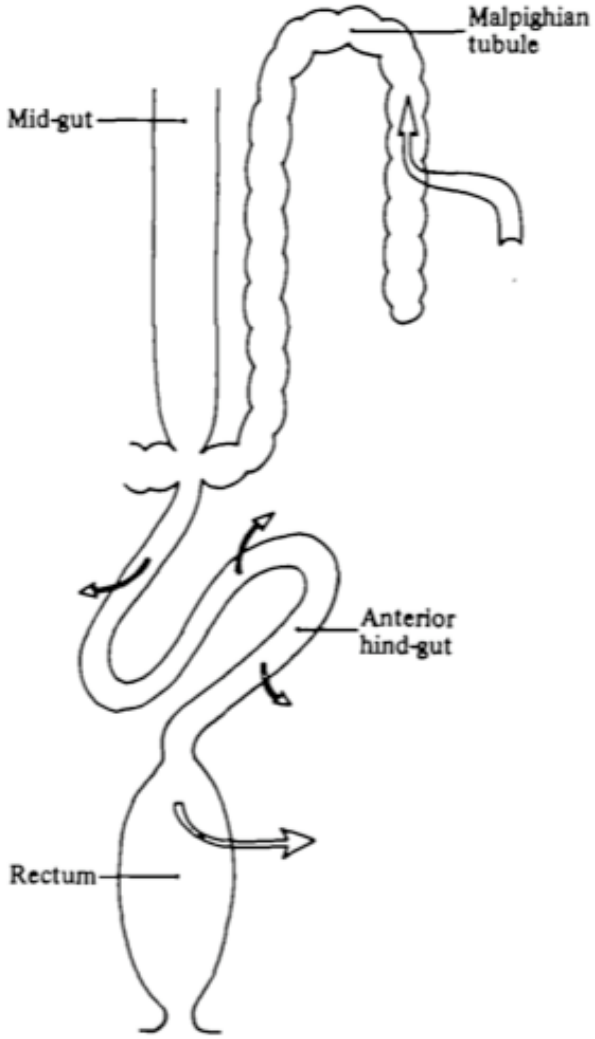

Figure 1.1 Structure of the insect alimentary and excretory system, showing branching of the Malpighian tubules from the junction between the midgut and hindgut. Reproduced from Maddrell (1981) with permission from the Journal of Experimental Biology.

Apical membrane

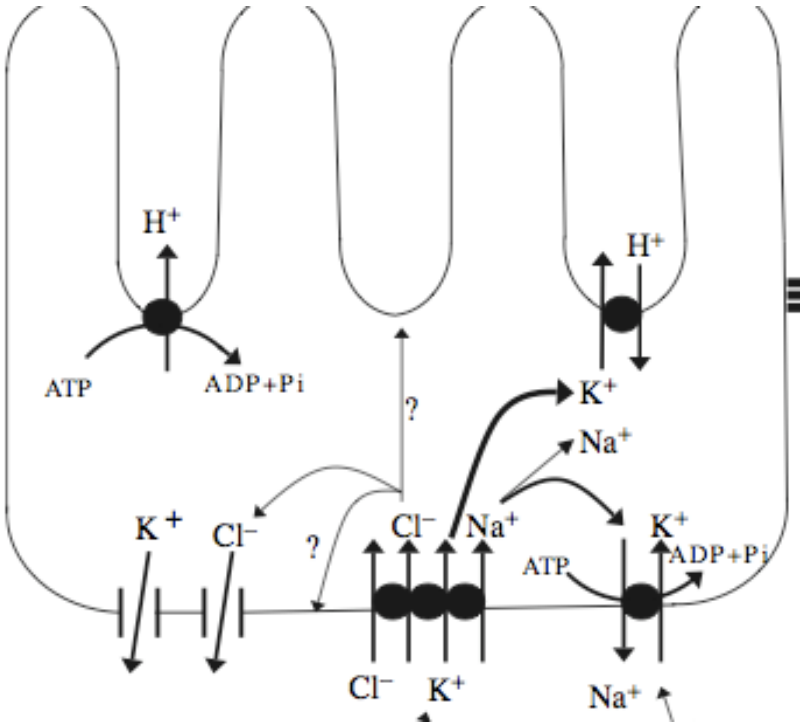

Basolateral membrane

Figure 1.2 Physiology of inorganic cation secretion from a principle cell of the MTs of *D. melanogaster*. Secretion of cations is coupled to the concentration gradient created through the action of an H^+ ATPase on the apical brush border membrane. Reproduced from Ianowski and O'Donnell (2004) with permission from the Journal of Experimental Biology.

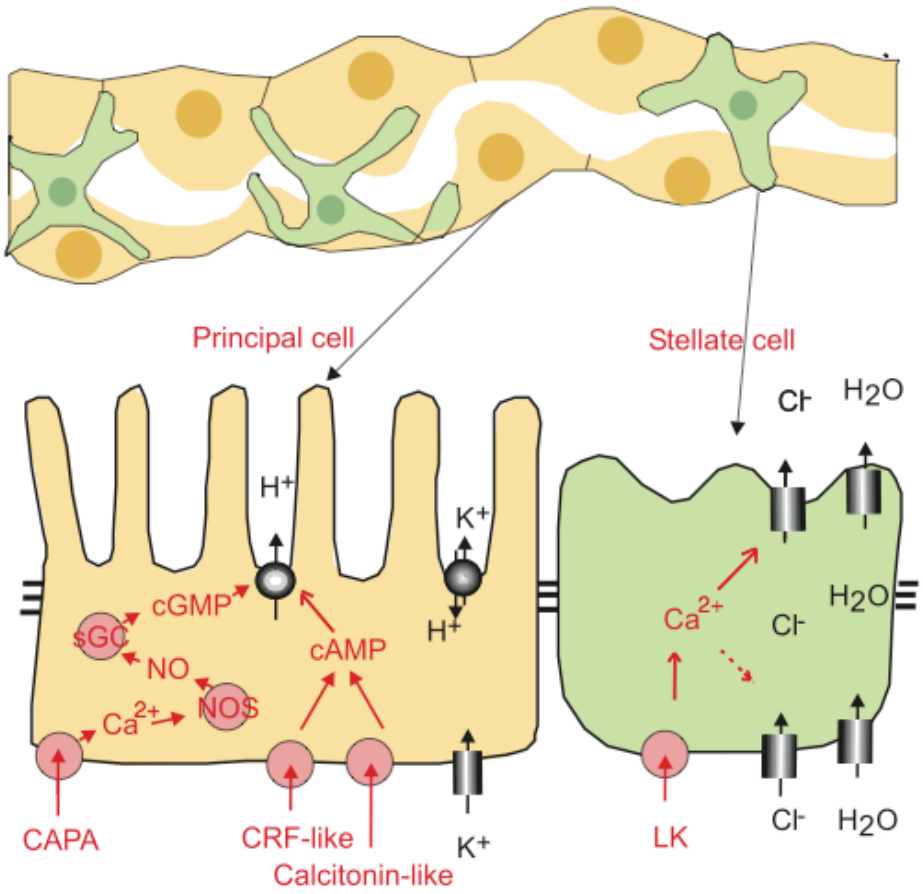

Figure 1.3 Physiology of the secretion of inorganic anions from the stellate cells (green) of the MTs of *D. melanogaster*. Reproduced from Dow (2009) with permission from the Journal of Experimental Biology. Schematic shows a segment of a whole MT (above) and the placement of the stellate cells and principle cells (yellow) within the complete MT. Abreviations on the figure are defined as follows: cGMP, cyclic guanosine monophosphate; cAMP, cyclic adenoside monophosphate; LK, leucokinin; CRF, corticotropin-releasing factor; CAPA, cardioacceleratory peptide; NOS, nitric oxide synthase; NO, nitric oxide; sGC, soluble guanylate cyclase.

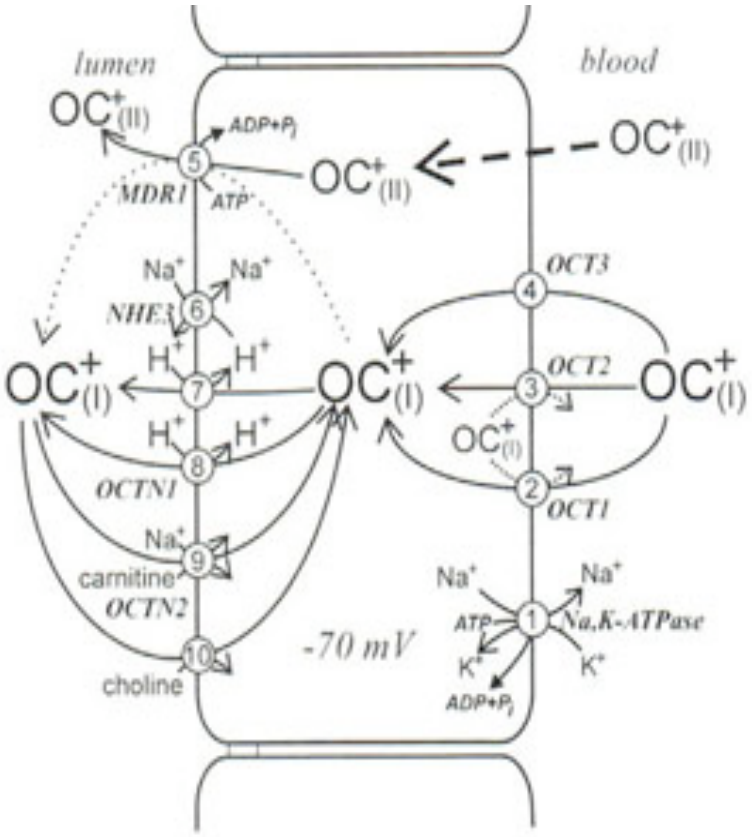

Figure 1.4 Schematic representation of organic cation transport in renal cells of vertebrates. Reproduced from Wright and Dantzler (2004). The 3 OCT isoforms are shown on the blood side of the cell. OCTN transporters are shown on the lumen side of the cell. Other transporters must be present in order to maintain electrochemical gradients necessary for driving OC transport. A Na^+/K^+ ATPase at the basolateral membrane moves Na^+ out of the cell creating a driving force for the exchange of Na^+ for OCs through OCTNs at the apical membrane. An NHE (Na^+/H^+ exchanger) at the apical membrane establishes a proton gradient that is used to drive the exchange of OCs for H^+ through apical transporters. Reproduced with permission from Copyright Clearance Inc.

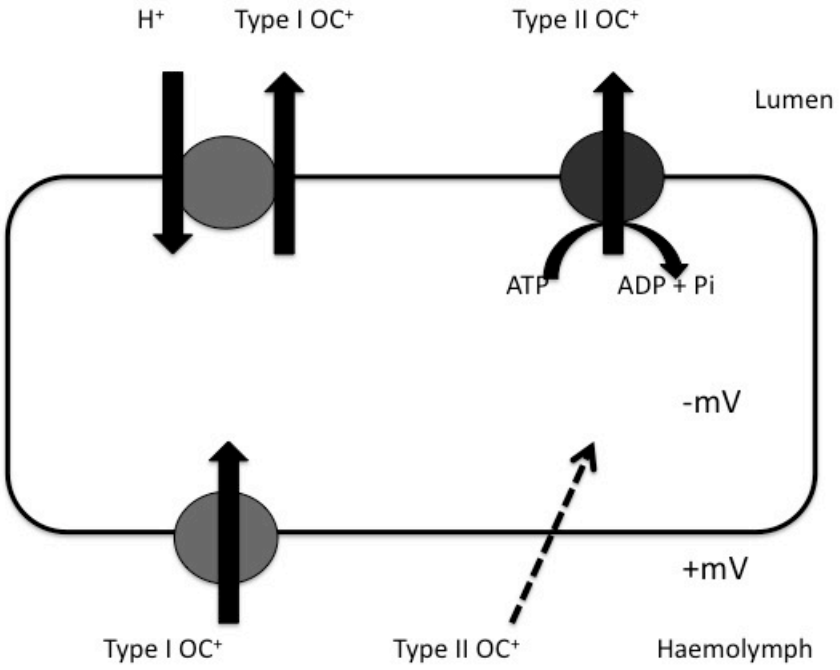

Figure 1.5 Schematic of the proposed transport mechanism for organic cations in *D. melanogaster*. Transport of type I OCs from the haemolymph across the cell membrane is mediated through a carrier protein. Type I OCs are transported across the cell membrane to the lumen through a, OC/ H^+ exchanger; where the proton gradient is maintained by a separate NHE (not shown). Transport of type II OCs from the haemolymph across the membrane is through simple diffusion. Transport of type II OC across the membrane into the lumen is mediated through an MDR or p-glycoprotein transporter.

Chapter 2 Cloning and mRNA Expression of *orct* and *orct2*

2.1 Synopsis

Organic cations are a common group of molecules that include endogenous metabolites and xenobiotics that must be effectively detoxified or eliminated in order for organisms to survive. The midgut and MTs of insects have been shown to play a role in the excretion of OCs (Rheault and O'Donnell, 2004; Rheault *et al*., 2005; Rheault *et al*., 2006). This chapter describes the cloning of two putative organic cation-like transporters, *orct* and *orct2*, from the fruit fly *D. melanogaster*. Sequence analysis of these clones supports the grouping of these genes into the major facilitator superfamily (MFS) and into the 2.A.1.19 group of electrochemical potential driven OCTs (Saier, 2000). Phylogenetic analysis of ORCT and ORCT2 sequences with insect and vertebrate orthologs indicated that two distinct insect clades exist that are equally divergent from vertebrate OC-like transporters. Relative mRNA expression of *orct* and *orct2* following exposure to a prototypical type I OC, TEA, was assessed in a number of *D. melanogaster* tissues. Transcripts of *orct* and *orct2* were detected in all tissues tested, with *orct* having high constitutive expression in MTs. Expression increased following exposure to TEA over 15 generations in all tissues tested for *orct* and in the midgut for *orct2*. The expression of *orct* and *orct2* in the MTs and midgut, the main excretory organs of *D. melanogaster* and tissues previously shown to transport TEA (Rheault *et al*., 2005), indicated that these transporters may play a role in the epithelial transport and elimination of OCs from adult *D. melanogaster*.

2.2 Materials and Methods

2.2.1 Insect Rearing

Oregon R strain *D. melanogaster* Meigen were raised on standard artificial fly media and maintained at 20-23°C in polystyrene shell culture vials (25x95 mm; Fisher Scientific, Nepean, ON, Canada). The artificial media was prepared as described by Chahine and O'Donnell (2009). Briefly two solutions were prepared separately. Solution A contained 50 g sucrose, 9 g agar, 4 g $KNaC_4H_4O_6 \bullet H_2O$, 0.5 g KH_2PO_4, 0.25 g NaCl, 0.25 g $MgCl_2 \bullet 6H_2O$, and 0.25 g $Fe_2(SO_4)_3$ in 400 mL of Milli-Q® filtered reverse osmosis water (Millipore, Billerica, MA, USA). Solution B consisted of 25 g of dry active yeast in 100 mL of Milli-Q® water (Millipore). The two solutions were autoclaved separately for 45 minutes, and then combined and stirred. After cooling to 50°C, 5 mL of an acid mixture (11 parts Milli-Q® water, 10 parts propionic acid and 1 part o-phosphoric acid) and 3.73 mL of a 10% (*w/v*) mixture of Tegosept (methyl-4-hydroxybenzoate) in ethanol were added to the mixture. For experiments where larval *D. melanogaster* were exposed to TEA in the rearing media, TEA was added following the addition of the acid mixture to final concentrations of 80 mmol L^{-1} or 150 mmol L^{-1}. The final solution is poured into *D. melanogaster* shell vials and agitated by hand until set. Concentrations for TEA-enriched media exposure were determined from larval LC_{50} data for TEA collected by Bijelic *et al*. (2005). Media was stored at 4°C for up to 30 days. Animals 4-7 days post emergence were used in all experiments.

2.2.2 RNA Extraction and Reverse Transcription

Tissues for 80 midgut, 200 Malpighian tubules, 50 ovary and 8 whole flies were harvested and pooled three separate times from adult *D. melanogaster* to make three

biological replicates. Tissues harvested were collected from flies raised on standard artificial media, 80 mmol L^{-1} TEA enriched media or 150 mmol L^{-1} TEA enriched media over 1 and 15 generations. The number of individuals to make each pooled sample as well as appropriate generation time for exposure experiments was determined previously by Chahine and O'Donnell (2009, 2010). RNA was extracted as described by Nawata and Wood (2008) and Chahine and O'Donnell (2009). Tissues were collected under nuclease-free *D. melanogaster* saline in a nuclease free work area and immediately transferred into TRIzol® Reagent (Invitrogen, Burlington, ON) for total RNA extraction. To prepare *D. melanogaster* nuclease-free saline for tissue collection, 500mL of Milli-Q® water was treated with 0.1% DEPC (diethylpyrocarbonate) for 2 hours at 37°C. The water was then autoclaved at 121°C for 30 minutes to remove the DEPC and saline components were added after cooling. The saline contained: 118 mmol L^{-1} NaCl, 20 mmol L^{-1} KCl, 10.2 mmol L^{-1} $NaHCO_3$, 8.5 mmol L^{-1} $MgCl_2 \bullet 6H_2O$, 2.0 mmol L^{-1} $CaCl_2 \bullet 2H_2O$, 7.87 mmol L^{-1} HEPES sodium salt and 3.78 mmol L^{-1} $NaH_2PO_4 \bullet 2H_2O$. RNA was isolated by adding 200 µL of chloroform, vortexing to mix, incubating for 2 minutes at room temperature and extracted by centrifugation at 12 000xg for 15 minutes at 4°C. The aqueous layer was treated with 500 µL of isopropanol and 1 µL of glycogen (20 mg mL^{-1}) to precipitate the RNA with centrifugation at 12 000xg for 15 minutes at 4°C. A single wash was performed with 70% ethanol and the dried RNA pellet was resuspended in 10µL of water from Milli-Q® water treated with 0.1% DEPC. RNA was treated with Ambion® Turbo DNA-*free*™ (Invitrogen) according to the manufacturers protocols to remove any genomic DNA contamination. RNA purity and quantity was assessed using a BioPhotometer Plus with a Hellma® TrayCell (Eppendorf, Hamburg, Germany). Typical RNA yields ranged from 227.3 ng μL^{-1} from Malpighian tubules to 3914.2 ng μL^{-1} from ovary with an A260/280 purity measurement

from 1.8-2.2 for all samples. Each RNA sample was then electrophoresed on 1% agarose gel stained with SYBR® Safe (Invitrogen) immediately following extraction to check RNA quality. Only RNA samples with a clear 18s ribosomal subunit RNA band, and lacking visible signs of genomic contamination were used for subsequent cDNA constructions. Invertebrate 28s ribosomal subunit RNA contains a cryptic nick that results in cleavage of this 28s subunit and thus this band may be absent when visualized through agarose gel electrophoresis. A sample RNA non-denaturing agarose gel is shown in Figure 2.1. cDNA was immediately synthesized from 1 μg of RNA using the Improm II™ Reverse Transcription System (Promega, Madison, WI) with oligo(dT) primers. cDNA construction was tested through polymerase chain reaction (PCR) with GoTaq® Green Master Mix (Promega) according to manufacturers instructions with primers for ribosomal protein 49 (*rp49*). cDNA samples were stored at -20°C.

2.2.3 Primer Design

Previously predicted organic cation transporter-like gene sequences from *D. melanogaster* (Taylor *et al.,* 1997; Hoskins *et al.,* 2007) were located in the National Center for Biotechnology Information (NCBI) GenBank database (www.ncbi.nlm.nih.gov). Cloning primers (Table 2.1) were designed at the 5' and 3' ends of the predicted sequences so that the predicted amplicons would contain the complete ORFs of *orct* (GenBank ascession number: NM_079755) and *orct2* (GenBank ascession number: NM_142981). Primers were designed for a *rp49* (GenBank ascession number: Y13939.1) as a positive control gene to test cDNA construction and amplification (5'-AGCATACAGGCCCAAGATCGTGAA/AATCTCCTTGCGCTTCTTGGAGGA-5'). Primers were designed and analyzed using Integrated DNA Technologies [IDT (www.idtdna.com)] PrimerQuest©

Software (2002), which incorporates the Primer3© Software (Rozen and Skaletsky, 1998). Specificity of primers was accessed using Basic Local Alignment Search Tool (BLAST) (www.ncbi.nlm.nih.gov/BLAST; Altschul *et al.,* 1990). In addition, all PCR amplicons were sequenced by the Nucleic Acid Protein Service (NAPS) Unit, Michael Smith Laboratories at the University of British Columbia (Vancouver, Canada) to ensure primer specificity and correct target amplification. Primers for quantitative real-time PCR (qPCR) were designed to span intron/exon junctions where possible using NCBI Primer-BLAST (www.ncbi.nml.nih.gov/tools/primer-blast), which employs Primer3© Software (Rozen and Skaletsky, 2000) and BLAST (www.ncbi.nlm.nih.gov/BLAST; Altschul *et al.,* 1990). Primers were designed for two genes of interest (*orct* and *orct2*) and for three reference genes; *rp49*, actin (*actin 42A*), a structural protein, and glyceraldehyde-3 dehydrogenase (*gapdh-1*), a glycolytic enzyme (Table 2). Primers were selected in order to minimized secondary structure using Oligo Analyzer 3.1® (www.idtdna.com/Scitools/Applications/Oligoanalyzer), which includes secondary structure analysis by UNAFold (Zuker, 2003). Primers were designed to have a length between 18-24 base pairs with an annealing temperature (Tm) from 52 - 60°C. Primer pair Tm mismatch between forward and reverse primers had to be <2°C. A GC% content of 40-70% was accepted and primers with a GC clamp in the last 3 bases of the primer were preferred but not required. Primer self-dimers and primer pair hetero-dimers were required to have a Gibbs free energy (ΔG) of association ≤-6.0 kcal. $mole^{-1}$. All primer sets were designed to amplify a product of 70 – 250 base pairs. The Tm of any secondary structure predicted by UNAFold (Zuker, 2003) for primers or amplicons, had to be >10°C lower than that primer sets predicted Tm to be used during amplification for the primers to be accepted.

2.2.4 Primer Optimization

Primers sets were tested to confirm amplicon size using a heterogeneous mixed whole body cDNA template from flies reared on non-enriched, control media using standard PCR. Cycling was performed on a C1000 Thermal Cycler (Bio-Rad, Hercules CA, USA) with the following PCR cycling parameters; an initial denaturing step of 95°C for 2 minutes, followed by 35 cycles of denaturing at 95°C for 30 s, an annealing step across a temperature gradient at 55°C - 63°C for 30 s, and an elongation step at 72°C for 60 s; followed by a final elongation at 72°C for 5 minutes. Each PCR reaction contained 12.5µL of GoTaq® Green Master Mix, 2 µL of cDNA, 1 µL each of 100 µmol L^{-1} forward and 100 µmol L^{-1} reverse primer and nuclease free water in a 25 µL reaction volume. Amplified products were verified for size by visualizing products on a 1.5% non-denaturing agarose gel stained with SYBR® Safe.

All qPCR primer sets were optimized for primer concentration and annealing temperature using SsoFast™ EvaGreen® Supermix (Bio-Rad). Whole body cDNA from flies raised on control media was used as a template at a relative concentration of $10^{-0.5}$. Whole body cDNA was used to represent a heterogeneous cDNA sample, which would include all tissues of interest. qPCR was performed on a CFX-96™ Real-Time PCR Detection System (Bio-Rad). The cycling protocol consisted of an initial denaturing step at 95°C for 30 s followed by 39 cycles of denaturing at 95°C for 5 s; and an annealing step over a temperature gradient of 50°C to 70°C for 5 s; for a total of 40 cycles. Following 40 cycles of amplification, a MELT curve analysis was done by incrementally increasing the block temperature from 65-95°C in steps of 0.5°C for 5 s. A sample MELT curve for *orct* primer optimization is shown in Figure 2.2. A single peak at 83.5°C indicated a single amplicon for *orct*, with all other peaks indicating primer dimer or non specific amplification falling below

detection threshold. Eight different temperatures (50°C, 51.3°C, 53.9°C, 57.8°C, 62.6°C, 66.6°C, 68.8°C, 70°C) were tested for each primer set. Optimal primer concentrations for each primer set over each of the 8 temperatures were evaluated using a primer mix so that each individual primer was used at a final concentration of 400 nmol L^{-1}, 500 nmol L^{-1} or 600 nmol L^{-1} in the reaction. Two technical replicates were performed for each concentration (Figure 2.3). No template controls (NTCs) were used to confirm that reaction components are free of contaminating DNA or fluorescent products, and to ensure that the observed Cq (quantification cycle) values are not the result of primer dimerization. Subsequently, sample wells for each primer and the NTCs were run on a 1.5% non-denaturing agarose gel stained with SYBR® Safe to check amplicon size and for significant primer dimer. A single annealing temperature was chosen to use in all subsequent reactions. The annealing temperature that was chosen resulted in a Cq of 20-35 for sample wells, Cq for the NTCs > 37, and a MELT curve indicating amplification of a single product for each primer set (Figure 2.4). Primer efficiencies were evaluated over a range of either 5-fold or 10-fold serial dilutions of a heterogeneous mixed whole body cDNA template collected from adults raised on control media. The dilution series is created such that it covers a wide dynamic range covering at least 3 orders of magnitude. This allows proper calculation of the linear phase of the calibration curve to establish efficiency of the primers. Primer efficiency is calculated as:

$$\text{Efficiency} = 10^{-1/\text{slope}} - 1 \qquad \text{Eq. 2.1}$$

Where the slope is calculated as the Cq divided by the logarithm of the concentration. Hence the theoretical ideal efficiency where the amount of product doubles with each additional cycle would be 1.00 or 100% (Bustin *et al.,* 2009). Three technical replicates were used for each template concentration in order to allow us to assess for

experimental pipetting errors (Figure 2.5). The reaction was cycled using the following parameters: a denaturing step of 95°C for 5 s and a combined annealing and elongation step of 58°C for 5 s. This protocol was repeated for 39 cycles for a total of 40 complete cycles followed by a standard MELT curve as described in the preceding paragraph. Cycling parameters were identical for each primer set evaluated. qPCR reactions were performed at a constant volume of 20 µL. Each reaction contained: 2 µL of cDNA template, 0.2 µL of primer mix (50 µmol L^{-1}), 10.0 µL of SsoFast™ EvaGreen® Supermix and 7.8 µL of nuclease free water. NTCs were performed for reasons explained above; in addition, no reverse transcription (NRT) controls were used to test for genomic DNA contamination of the samples. NRT controls are prepared at the same time as the cDNA samples and were stored at -20°C; these reactions contain RNA samples that have not undergone reverse transcription. NRTs were considered acceptable if the observed Cq value was >5 cycles higher than the Cq values observed in experimental samples. Statistical analysis of efficiency curves was performed after quality analysis and manual well exclusion using CFX Manager™ Software (Bio-Rad). Primer pairs with efficiencies between 90% and 110%, a slope ≈ -3.3 ±0.2, and an R-squared value ≥ 0.98 were accepted and used in subsequent analysis (Bustin *et al*., 2009) (Figure 2.6).

2.2.5 Cloning of Full Length cDNA Encoding *orct* and *orct2*

Amplification on whole body cDNA using Easy-A™ High-Fidelity PCR Cloning Enzyme & Master Mix (Agilent; Santa Clara, CA, USA) was performed with terminal primers for *orct* (5'-ATGGGCTACGACGACGTCATC /TTAGCCGGACTGTCCGTTCAGCATTC-5') and *orct2* (5'-ATGGGCTACGATGAGGCCATCATCCATCTG/ TTACTTGTGGCCATTGGCTATGGTTGATCC-5') to obtain the full length amplicons containing the complete ORFs. PCR was performed on a C1000™ Thermal

Cycler with the following parameters: an initial denaturing at 95°C for 2 min, followed by 30 cycles of denaturing at 95°C for 40 s, annealing at 60°C (*orct*) or 65°C (*orct2*) for 30 s and elongation at 72°C for 2 minutes, and ending with a final elongation of 72°C for 7 minutes for a total of 31 cycles. Each PCR reaction contained reagents according to manufacture instructions in a 50 µL volume with 2 µmol L^{-1} each of forward and reverse primers and 100 ng of template. Products were purified on a 1% agarose gel stained with SYBR® Safe. Products of interest were excised from the gel and purified using Wizard® SV Gel and PCR Cleanup system (Promega). Purified products were ligated using T4 DNA ligase (Promega) into pGEM®-T Easy Vector System (Promega) using a 3:1 insert to vector ratio corrected for genomic size. Resulting constructs were transformed into chemically competent JM109 *E. coli* cells (Promega) according to manufactures protocols. Transformed cells were spread on Luria-Bertani (LB) agar plates supplemented with 100µg mL^{-1} ampicillin, and previously spread with 40 µL 5-bromo-4-chloro-3-indolyl-beta-D-galactopyranoside (X-gal; 40 mg mL^{-1}) and 100 µL isopropyl β-D-1-thiogalactopyranoside (IPTG; 0.2 M). Plates were incubated at 37°C overnight in an inverted position. LB agar was prepared according to Sambrook and Russell (2001). Briefly, 10 g molecular grade tryptone, 5 g yeast extract and 10 g NaCl were added to 1000 mL Milli-Q® water and the pH was brought to 7.0 using HCl and NaOH. For liquid LB media, the solution was then autoclaved for 20 minutes. To create solid media 7 g of agar was added prior to the autoclaving step. Once cooled to 50°C, antibiotics were added for selection and plates were poured to set. Four single white colonies for each construct were selected by blue white screening and used to inoculate 5 mL of liquid LB media supplemented with 100 µg mL^{-1} ampicillin. Cultures were incubated at 37°C with shaking (170 rpm) until an optical density (OD_{600}) of 2.0-4.0 was achieved; determined using a BioPhotometer Plus with a Hellma® TrayCell. Plasmids were purified from single

isolate cultures using the PureYield™ Plasmid Mini Prep System (Promega) and quantified. Typical yields ranged from 427.1 ng μL^{-1} to 876.2 ng μL^{-1} with an A_{260}/A_{280} purity measurement of 1.85-1.89. Plasmids were digested with *EcoR*1 (New England Biolabs Ltd., Pickering ON) according to manufacturers instructions for a 10 µL reaction volume, and were visualized on a 1% agarose gel to confirm correct insert size (data not shown). Plasmids containing ligated products were sent for sequencing using a combination of T7, SP6 and gene specific nested primers (Table 2.3). All amplified products were sequenced for 5 times coverage at NAPS (Vancouver, BC, Canada).

2.2.6 *orct* and *orct2* Sequence Analysis

Sequencing results for *orct* and *orct2* were compiled using Geneious™ Pro (v5.0.4) (Drummond *et al.,* 2011) to produce a single contiguous consensus sequence from the 5 replicate sequencing reads using a 75% similarity threshold. Translation of the nucleotide sequences was done using Geneious™ Pro (Drummond *et al.,* 2011) and the presence of each genes complete open reading frame was confirmed through Geneious™ Pro (Drummond *et al.,* 2011) pairwise nucleotide global alignment with free end gaps to the predicted sequences of *orct* (Taylor *et al*., 1997) and *orct2* (Hoskins *et al*., 2007), using a 65% similarity (5.0/-4.0) cost matrix with a gap opening penalty of 12 and gap extension penalty of 3. Percent shared identity between representative OCT orthologs, from vertebrate and invertebrate species and *orct* and *orct2*, and identity between predicted and cloned sequences of *orct* and *orct2,* were determined using pairwise Geneious™ Pro (Drummond *et al.,* 2011) alignments of amino acid sequences with a Blosum62 cost matrix with a gap opening penalty of 12 and gap extension penalty of 3 in Geneious™ Pro (Drummond *et al.,* 2011).

The predicted molecular mass of ORCT and ORCT2 was calculated using the Compute pI/Mw Tool (Gasteiger *et al.,* 2005). Secondary structures were predicted using hydrophobicity analysis with TmPred (Hofmann and Stoffel, 1993) with final graphical output by Microsoft® PowerPoint® 2008 for Mac (v12.2.9). Alignments of TMDs using results from each genes hydrophobicity analysis with TmPred (Hofmann and Stoffel, 1993) were created using Microsoft® Excel® 2007 for Mac (v12.3) and were compared to multiple amino acid alignments containing OCT orthologs created in Geneious™ Pro (Drummond *et al.,* 2011). Potential protein family domains were predicted using the Simple Modular Architecture Research Tool [SMART (Schultz *et al.,* 1998)] and BLAST (Altschul *et al.,* 1990). Phosphorylation and glycosylation sites were predicted using PROSITE (Sigrist *et al.,* 2010) and N-myristolation sites were predicted with NMT-The MYR Predictor (Bohr-Gasse, 2007).

2.2.7 Phylogeny of Organic Cation Transporters

Representative amino acid sequences from the major facilitator superfamily (OCTs, OCTNs, insect OCT-like transporters) were retrieved from GenBank database using BLAST (Altschul *et al.,* 1990) with *orct* and *orct2* as query sequences (Table 2.4). Sequences with a similarity threshold (e-value) of < 0.001 were included in the alignment. The initial alignment was created using Geneious™ Pro (Drummond *et al.,* 2011) with parameters for a Geneious™ Pro (Drummond *et al.,* 2011) alignment as described in the previous section. An unrooted, neighbor-joining tree was generated with the Geneious™ Tree Builder (Drummond *et al.,* 2011) using a Jukes-Cantor distance model. Threshold was set to 75% and the alignment was bootstrapped over 10 000 iterations. Final graphical output was generated using Geneious™ Pro (Drummond *et al.,* 2011) and edited in Microsoft® PowerPoint® 2008 for Mac (v12.2.9).

2.2.8 Quantitative Real-Time Polymerase Chain Reaction

qPCR was performed on cDNA collected from whole body, midgut, MTs and ovary tissues collected from 4-7 day old adult *D. melanogaster*. Flies were raised on control media or media enriched with either 80 mmol L^{-1} or 150 mmol L^{-1} of TEA. Tissues were collected following 1 and 15 generations of exposure. Reactions were performed in 96 well low profile plates using the CFX96™ Real-Time PCR Detection System with the following cycling conditions: 30 s activation at 95°C, followed by 40 cycles of 5 s denaturation at 95°C and 5 s annealing/extension at 58°C followed by a standard MELT curve analysis (described in 2.2.4). Each experimental 20 µL reaction contained 10 µL of Ssofast™ EvaGreen® Supermix, 2 µL of 10x dilution of cDNA and 500 nmol L^{-1} of forward and reverse primer in nuclease-free water. Sample wells were visualized on a 1% agarose gel stained with SYBR® Safe to ensure that only a single amplified product was present with no significant primer dimer. Each qPCR experiment was conducted on 3 biological replicates of *D. melanogaster* and performed with 2 technical replicates. In addition to experimental samples, a single NTC for each gene was run on each plate and a single NRT for each sample was tested once with each primer set to test for primer dimerization and genomic contamination respectively. Observed Cq values for NRT and NTC controls were held to quality quidelines outlined previously (Section 2.2.4) and in the Bio-Rad CFX™ Manager Software Handbook (Bio-Rad).

Inter run calibration with a heterogeneous whole body sample was performed on each plate (Vermeulen *et al.,* 2009) for each primer set (Hellemans *et al.,* 2007) to normalize for variation between different plates. Plates were designed to follow sample maximization analysis (Hellemans *et al.,* 2007), which allowed for statistically relevant

analysis of the expression of a single gene across sample types and experimental conditions (Figure 2.8).

Expression of three reference genes was tested and the stability of each of these genes across tissues and experimental conditions was analyzed using GeNorm^{PLUS} (Biogazelle, Ghent University, Belgium). Reference genes were first ranked according to their stability, expressed as GeNorm M-values, and then a GeNorm V analysis was conducted to determine the optimal number of reference genes to be used in subsequent analysis (Hellemans *et al.,* 2007). M-values of >0.5 and <1.0 were accepted for reference genes across heterogeneous samples. GeNorm V output was generated by a comparison of M-values between reference gene (n) and gene (n+1) beginning with the most stable reference gene and ending with the least stable. As convention, the benefit of using additional reference targets (n+1) is limited when $V_{n/n+1} < 0.15$ (Hellemans *et al.,* 2007); this yields the optimal number of reference targets to use.

qPCR analysis was conducted using multiple reference genes (*gapdh-1* and *rp49*) for normalization, determined by the GeNorm analysis output (see Appendix 1 for additional information on normalization using multiple reference genes). Analysis of qPCR data was done using CFX™ Manager Software which employs the Hellemans *et al.* (2007) method of data normalization and allows proper error propagation through inter run calibration.

2.2.9 Data Analysis

To determine if differences in relative mRNA expression were significantly different two successive criteria had to be met. First, relative fold differences between mean expression values had to be > than 2-fold (Bubner, Gase and Baldwin, 2004). Second, fold differences in expression had to be determined to be mathematically significant by an

applied statistical test. Final statistical analysis was performed using Graphpad Prism™ (v5) (www.graphpad.com) by one-way analysis of variance (ANOVA) followed by Dunnett's multiple comparison post-hoc test to analyze tissue distribution relative to whole body An Unpaired Student's *t*-test was used to compare mRNA expression of control tissues at 1 and 15 generations. Two-way ANOVA with a Bonferroni post-hoc test was used to assess the effect of TEA exposure and generation time in individual tissues and one-way ANOVA with a Dunnett's multiple comparison test was conducted to assess effect of TEA exposure within each generation. Data was expressed as mean ± standard error of the mean (SEM) with a $p<0.05$ considered significant. For direct comparison of the relative expression of each gene of interest within a certain tissue, data was normalized to the gene with the lowest expression value. Means were divided to yield the normalized mean. Error was normalized by taking the square root of the sum of squares of the fractional SEM.

Ex. Calculate total error (dX) when normalized value (X) = A/B

$$dX/X = \mathrm{sqrt}((dA/A)^2 + (dB/B)^2) \qquad \text{Eq. 2.5}$$

2.3 Results

2.3.1 Sequence and Structural Features

The cloned *orct* cDNA consisted of 1647 nucleotides and contained an open reading frame encoding a 548-amino acid (aa) residue protein that was 99.7% similar to the predicted protein (GenBank accession number: NM_079755). A comparison of the cloned *orct* cDNA to the predicted sequence showed 2 single nucleotide transitions at 438 and 1636 from A→C that corresponded to amino acid substitutions (Table 2.5). The substitution at 146 fell within TMD2 where as the substitution at 546 (K→Q) was within the intracellular carboxyl end. A fully annotated sequence for cloned *orct* cDNA is shown in Figure 2.9. Analysis via SMART (Schultz *et al.,* 1998) and BLAST (Altschul *et al.,* 1990), indicated that domains in the *orct* amino acid sequence were consistent with members of the MFS. The predicted molecular mass of the protein was 61 kDa (Compute pI/Mw Tool; Gasteiger *et al*., 2005). Hydrophobicity analysis using TmPred (Hoffman and Stoffel, 1993) indicated the protein possessed 12 putative TMDs each with 21-25 aa residues (Figure 2.9). The secondary structure of ORCT was modeled to human OCT orthologs to give a predicted cytoplasmic amino terminus (19aa) and carboxyl terminus (45aa). The model predicted a large extracellular loop (84aa) between TMD1 and TMD2 consistent with human OCT orthologs (Dresser *et al.,* 2001; Wright and Dantzler, 2004), which contained 4 putative N-linked glycosylation sites (N*x*(T/S)*x*) at positions 55, 67, 89 and 97. The predicted protein also contained a large intracellular loop (72aa) between TMD6 and TMD7, and a putative protein kinase C-dependent (PKC) phosphorylation site (SAR-267) and a cAMP dependent protein kinase (PKA) phosphorylation site (RRKT-333). Additional PKC phosphorylation sites were predicted at 152 (SDK), 213 (SYR), as well as an additional PKA phosphorylation site at 157 (RKPT).

The cloned cDNA of *orct2* consisted of 1701 nucleotides encoding a 567 aa residue protein, which was 99.6% similar to its predicted sequence (GenBank accession number: NM_142981). Multiple single nucleotide polymorphisms were found between the predicted *orct2* sequences and the cloned cDNA (Table 2.6). Of these substitutions, only 2 caused amino acid transitions at residue 58 (S→I), which lies within a predicted N-linked glycosylation site, and at residue 60 (D→E). Full annotation of the cloned *orct2* cDNA is shown in Figure 2.10. Similar to *orct*, SMART (Schultz *et al.,* 1998) and BLAST (Altschul *et al.,* 1990) analysis of *orct2* showed that domains of the sequence are consistent with other members of the MFS transporters. The predicted molecular mass was 63.2 kDa (Compute pI/Mw Tool; Gasteiger *et al.,* 2005). Hydrophobicity analysis with TmPred (Hoffman and Stoffel, 1993) indicated that the protein possessed the characteristic 12 TMDs with an N-amino terminus (18aa) and carboxyl terminus (58aa) on the cytoplasmic side of the membrane (Figure 2.11). The model predicted a characteristic extracellular loop (84aa) between TMD1 and TMD2 as well as a large intracellular loop (81aa) between TMD6 and TMD7. ORCT2 has 5 total predicted N-linked glycosylation sites (N*x*(T/S)*x*), 4 in the extracellular loop between TMD1 and TMD2 (sites 55, 67, 89 and 97) and an additional site at 364 between TMD7 and TMD8. PKC phosphorylation sites were predicted at 152 (SDK) and 267 (SAR) as well as a PKA phosphorylation site at 341 (RRKT).

Figure 2.12 shows an alignment of ORCT and ORCT2, and candidate vertebrate OCT orthologs, with a number of conserved domains highlighted. TMDs were conserved between ORCT, ORCT2 and vertebrate orthologs, with an additional TMD predicted for human FLIPT1 (Figure 2.13). The first conserved 13 residue region was found in ORCT and ORCT2 between TMD2 and TMD3 with the sequence GQ-(ML)-SDK-(LY)-GRKP-(TI)-(FL) and is comparable to the sequence found in vertebrates in the form G-(RKPATY)-L-(GAS)-

(DN)-(RK)-(FY)-G-G-(RK)-(RKP)-(LIVGST)-(LIM) (Wright and Dantzler, 2004). An 8-residue domain was found just upstream of TMD2 with the sequence VTEWNLVC. This sequence is identifiable in 9 orthologs of OCT-like vertebrate transporters with the sequence STIVTEW-(DN)-LVC (Schomig *et al*., 1998). Variations in the sequence included a tryptophan (W) in OCTNs rather than a phenylalanine (F) in OCTs at residue 7 and a serine (D) at residue 2 in OCT1 and OCT2 rather than the threonine (T) present in other OCT and OCTN orthologs. Sequences of EQFPT following TMD10 and M-(PL)-ETI after TMD12 were found to be similar to signature sequences for vertebrate orthologs identified by Schomig *et al.,* (1998).

Figure 2.14 displays an alignment with a number of insect OCT-like orthologs, which shared conserved domains with vertebrate OCT sequences and to each other. All insect species used in this study had peptide sequences with 10-12 predicted TMDs in conserved areas, with the same characteristic intracellular and extracellular loops as the vertebrate OCTs (Figure 2.15). Insect peptide chains ranged in length from 512-aa (*Tribolium castaneum*) to 570-aa (*Anopheles gambiae*). In addition to conserved signature sequences between insect and vertebrate species, there were a number of domains seemingly conserved in only insect species (excluding *A. gambiae* MFS). These domains included: a 12-aa sequence within TMD4, (AS)(TS)-TSG-(VL)(FY)-L-(VA)-AYV; a 6-aa sequence within TMD6, (ILV)-A-(ILV)-T-(ILV)-P; a 8-aa sequence just following TMD6, IPES-(APVS)-RWL; a 6-aa long sequence within TMD7, Y-(VY)-GLS-(WY); a 5-aa sequence within TMD10, IT-(AS)-SY; a 9-aa sequence between TMD10 and TMD11, EQFPTV-(VI)-RN; and a 7-aa sequence within TMD12, SL-(LV)-LPET. These proposed insect orthologs signature domains, taken with the conserved domains between insect and vertebrate species

indicates a higher degree of similarity between insect sequences as compared to vertebrate OCT orthologs.

2.3.2 Alignments and Phylogenetic Relationships

ORCT has the highest pairwise identity (72.4%) with the other *D. melanogaster* (Order: Diptera) sequence ORCT2 (Table 2.7). Similar high identity was shared between another dipteran, *Culex quinquefasciatus* (southern house mosquito) and ORCT (63.3%) and ORCT2 (60.7%). Insect sequences from the coleopteran *T. castaneum* (red flour beetle) had 57.6% identity with ORCT and 53.6% identity with ORCT2, and the hymenopteran *Apis mellifera* (western honey bee) had 56.5% identity to ORCT and 51.8% identity to ORCT2. *A. gambiae* (African malaria mosquito), another dipteran, and close *Culex* relative (Family: Culicidae) had the lowest shared identity with predicted insect proteins (35.9% to ORCT, 33.1% to ORCT2, 29.1% *A. mellifera* MFS). Similarity between ORCT and vertebrate orthologs ranged from 35.6% (human FLIPT1) to 39.4% (human OCT3); with similarity for ORCT2 and vertebrate orthologs ranging from 30.4% (human FLIPT1) to 33.6% (human OCT3). In summary, ORCT and ORCT2 had higher similarity with other insect transporters with the exception of *A. gambiae*. *A. gambiae* does not show high similarity to other insect or vertebrate species, indicating this predicted sequence might represent a distinct transporter type unrelated to ORCT, ORCT2 or vertebrate OCT orthologs.

In a phylogenetic analysis, ORCT and ORCT2 were compared to putative MFS transporters from insects and candidate OCT-like transporters from vertebrates (Figure 2.16). 36 sequences were aligned including 9 sequences from insects. The analysis revealed that insect sequences fell into two distinct clades with *A. gambiae* and the hymenoptera *Camponotus floridanus* (Florida carpenter ant) separate from the other insect

MFS putative transporters. ORCT and ORCT2 are equally divergent from OCT1, OCT2, OCT3 and OCTN transporters (branch length 0.5) and are more distantly related to the human FLIPT (branch length 0.56 and 0.62) and *A. gambiae* MFS (branch length 0.65) transporters. A distinct clade of insect OCT-like transporters separate from vertebrate orthologs might suggest a early branching of this transporter family during its evolution.

2.3.3 Gene Expression Analysis of *orct* and *orct2* Using Quantitative Real-Time Polymerase Chain Reaction

The stability of the reference genes *gapdh-1*, *rp49*, and *actin 42A* were assessed using GeNorm^{PLUS} (Biogazelle) analysis software. The results of this analysis indicated that M-values for stability of the reference genes were higher than the theoretical optimal value for heterogeneous samples (M < 1) (Hellemans *et al.,* 2007), with *actin 42A* being the least stable reference gene with a value of 1.76 (Figure 2.17.A). Based on the GeNorm V analysis, the variability between subsequently tested reference targets (based on the n and n+1 least variable reference targets) was high (GeNorm V >0.15). GeNorm V analysis thus indicated that the ideal number of reference genes to use for this experiment was two (Figure 2.17.B). Therefore all subsequent qPCR data analysis and normalization was done using *gapdh-1* and *rp49 as* the reference targets.

Figure 2.18 shows tissue distribution analysis of mRNA of *orct* and *orct2* in whole body, midgut, MTs and ovary from flies raised on control media. The relative amount of mRNA in each tissue is shown normalized to each genes whole body mRNA expression. Detectable amounts of mRNA were present in each of the tissues tested for each gene. mRNA expression for *orct* was significantly higher in the MTs (Figure 2.18.A), suggesting high constitutive expression of *orct* in the insect renal tissue. In contrast, mRNA expression

of *orct2* was significantly lower in the MTs and ovary compared to whole body expression (Figure 2.18.B).

Relative amounts of expression between *orct* and *orct2* in each of the tissues tested under control conditions were compared (Figure 2.19). mRNA levels for *orct2* were greater than 4-fold higher than *orct* in whole body (Figure 2.19.A), 8-fold higher in ovary (Figure 2.19.B), and 3-fold higher in midgut (Figure 2.19.D); whereas expression of *orct* was over 8-fold higher than *orct2* in the MTs (Figure 2.19.C). Expression values for each gene were normalized to the gene with the lowest expression within a certain tissue. Results of this analysis showed *orct2* to have higher basal expression across a wider range of tissues were *orct* is more highly and locally expressed in the MTs.

Expression of *orct* and *orct2* was measured in midgut, MTs and ovary following one and 15 generations of exposure to 80 mmol L^{-1} and 150 mmol L^{-1} TEA and expressed relative to the control tissue level of expression measured at 1 and 15 generations. Unpaired Student's *t*-tests between expression values in control tissues collected at 1 and 15 generations confirmed that mean Cq values were not significantly different, therefore values were pooled to give one control value for the final analysis. Following 1 generation of either 80 mmol L^{-1} or 150 mmol L^{-1} TEA exposure, there was an almost 5-fold increase in expression of *orct* in the midgut, independent of the concentration of TEA exposure, which increased to almost 10-fold over 15 generations of exposure (Figure 2.20.A). Expression levels of *orct* increased over 3-fold at the 80 mmol L^{-1} TEA exposure in the MTs (Figure 2.20.B) following 15 generations of exposure only. Ovary expression increased over 4-fold at each concentration of exposure after 15 generations (Figure 2.20.C). Expression in these tissues after 1 generation was not significantly different from control.

The expression profile of the midgut for *orct2*, showed a greater than 5-fold increase in expression following exposure to TEA after 1 generation (Figure 2.21.A), and an almost 10-fold increase in expression after 15 generations. All increases in expression were independent of the concentration of TEA exposure. There were no significant changes in *orct2* expression after exposure to TEA in the MTs (Figure 2.21.B) and the ovary (Figure 2.21.C).

2.4 Summary

This chapter described the cloning of two putative OCTs from *D. melanogaster*. Sequencing of *orct* and *orct2* showed the two sequences to have divergences from the predicted sequences, resulting in substitutions at the protein level. Pairwise alignments between the genes indicated high similarity (72.4%), which was nearly double the percent similarity shared between of any of the vertebrate OCT isoforms (32.2% between human OCT1 and human OCT3), with the exception of the high degree of similarity between human OCT1 and human OCT2 (69.8%). Each of the cloned genes possessed 12 conserved TMDs with intracellular and extracellular loops characteristic of this transporter superfamily. A number of conserved domains first identified in vertebrates were conserved in insect orthologs, as well with additional conserved domains found between insect sequences. Sequence analysis supports the grouping of ORCT and ORCT2 into the MFS 2.A.1.19 (2, electrochemical potential driven porters; A, uniporter/symporter/antiporter; 1, MFS; 19, OCTs) according to Saier (2000). Phylogenetic analysis showed the ORCT and ORCT2 peptide sequences to fall into an insect specific clade that is equally divergent from OCT3 and OCTN orthologs, and OCT1 and OCT2 orthologs. Results of sequence analysis and phylogenetic analysis indicated a high degree of similarity between insect orthologs and

could indicate an ancestral relationship of ORCT and ORCT2 to vertebrate OCT-like sequences. Gene expression results indicated that *orct* had constitutive high expression in the MTs, whereas *orct2* was not highly expressed under control conditions in any tissue tested compared to whole body. Expression of *orct2* was higher relative to *orct* in whole body, ovary and midgut tissue. Following exposure to TEA, there was a significant increase in midgut expression for both *orct* and *orct2* as well as an increase in *orct* expression following 15 generations of exposure in the MTs and ovary tissues. This supports the physiological evidence describing TEA transport across midgut and MTs. An alternative explanation would be that transcript regulation of *orct* and *orct2* is mediated through a generalized stress response to toxicity. Transport across the MTs is most likely mediated by ORCT, whereas transport across the midgut could be regulated by exposure to TEA and is mediated by ORCT and ORCT2 based on mRNA tissue distribution profiles.

Table 2.1 Cloning primers.

Gene name	Forward/reverse sequence (5'-3')	Amplicon size (bp)	Accession number
orct	ATGGGCTACGACGACGTCATC/TTAGCCGGACTGTCCGTTCAGCATTC	1647	NP_524479
orct2	ATGGGCTACGATGAGGCCATCATCCATCTG/ TTACTTGTGGCCATTGGCTATGGTTGATCC	1704	NM_142981

Table 2.2 Quantitative real-time PCR primers.

Gene name	Forward/reverse sequence (5'-3')	Efficiency	R^2	Slope	y-intercept	Amplicon size (bp)	Amplicon start (bp)	Accession number
orct	GCAGCAACGAAACCAAGACCTGTT/ GCACGCCCAGCATGAATAACGAAT	100.3%	0.990	-3.314	27.064	141	284	NM_079755
orct2	ACCAAGACCTGTTCCAGCTACGTT/ ACCAAACACAATGCTGCCCAGAAG	112.3%	0.981	-3.059	27.147	153	295	NM_142981
gapdh-1	TGAAGGGAATCCTGGGCTAC/ ACCGAACTCGTTGTCGTACC	99.9%	0.995	-3.325	19.538	149	862	NM_080369.2
actin 42A	GCTTCGCTGTCTACTTTCCA/ CAGCCCGCATACTGCTTAGA	92.8%	0.985	-3.509	23.111	105	1172	NM_078901.2
rp49	TGCTAAGCTGTCGCACAAATGG/ ACTTCTTGAATCCGGTGGG	96.9%	0.994	-3.397	18.746	145	81	Y13939.1

Table 2.3 Sequencing primers.

Primer name	Gene name	Forward sequence (5'-3')	Starting position
T7	*orct/orct2*	TAATACGACTCACTATAGGG	-69
SP6	*orct/orct2*	ATTTAGGTGACACTATAG	+93
dmorctvC2f1	*orct*	ACCAAGACCTGTTCCAGCTACGTT	295
dmorctvC2f2	*orct*	AGTACCTGAATGGCAGCATTCCAC	257
dmorctvC2f3	*orct*	GAGTCTTCCTGGTTGCCTATGTCA	590
dmorct2seqf1	*orct2*	TTCTGGGCAGCATTGTGTTTGGTC	425

Table 2.4 Protein sequences for alignments.

Protein	Species	Accession number	Protein	Species	Accession number
ORCT	*Drosophila melanogaster*	*NM_079755	mOCT2	*Mus musculus*	NP_038695
ORCT2	*Drosophila melanogaster*	*NM_142981	MdOCT2	*Monodelphis domestica*	XP_001381474
TcMFS	*Tribolium castaneum*	XP_974554.1	CfOCT2	*Canis familiaris*	XP_862848
ApMFS	*Acyrthosiphon pisum*	XP_001952793	SsOCT2	*Sus scrofa*	NP_999067
AgMFS	*Anopheles gambiae*	XP_3155304	PtOCT2	*Pan troglodytes*	XP_518840
AmMFS	*Apis mellifera*	XP_395856	GgOCT2	*Gallus gallus*	XP_419622
CqMFS	*Culex quinquefasciatus*	XP_001843197	TgOCT2	*Taeniopygia guttata*	XP_002189094
NvMFS	*Nasonia vitripennis*	XP_00167895	hOCT3	*Homo sapiens*	BAA76350
CflMFS	*Camponotus floridanus*	EFN71065	CfOCT3	*Canus familiaris*	XP_542706
hOCT1	*Homo sapiens*	NP_003048	MmOCT3	*Macca mulatta*	XP_00108733
rOCT1	*Rattus norvegicus*	NP_036829	PtOCT3	*Pan troglodytes*	XP_526175
mOCT1	*Mus musculus*	NP_033228	CmOCTN1	*Callicebus moloch*	ACB21280
BtOCT1	*Bos Taurus*	NP_001094568	CmOCTN2	*Callicebus moloch*	ACB21281
CfOCT1	*Canis familiaris*	XP_541185	OaOCTN2	*Oryctolagus anatinus*	XP_001510318
GgOCT1	*Gallus gallus*	XP_419621	PaOCTN2	*Papio anubis*	ABW96797
OcOCT1	*Oryctolagus cuniculus*	NP_001075491	hOCTN2	*Homo sapiens*	NP_003051
hOCT2	*Homo sapiens*	NP_003049	hFLIPT1	*Homo sapiens*	AAN52927.1
rOCT2	*Rattus norvegicus*	NP_113772	hFLIPT2	*Homo sapiens*	AAN52928.1

*Accession number for available predicted sequence from GenBank database (NCBI). Cloned sequences were used for generation of the multiple alignment and subsequent phylogenetic tree.

Table 2.5 Sequence analysis for *orct* showing nucleotide substitutions between the cloned and predicted sequence (NP_524479) of *orct*.

Colony designation	SNP position (bp)	Transition	Amino acid position	Substitution
orct C1 *orct* C2	438	A → C	146	L → F
orct C3 *orct* C4	1636	A → C	546	K → Q

Table 2.6 Sequence analysis for *orct2* showing nucleotide substitutions between the cloned and predicted sequence (NM_142981) of *orct2*.

Colony designation	SNP position (bp)	Transition	Amino acid position	Substitution
orct2 C1 *orct2* C2 *orct2* C3 *orct2* C4	173	G → T	58	S → I
	180	C → G	60	D → E
	207	G → A	69	Silent
	474	A → G	158	Silent
	562	A → C	188	Silent
	567	G → A	189	Silent
	600	C → T	200	Silent
	705	C → T	235	Silent
	1671	A → G	557	Silent

Table 2.7 Sequence identity shared between organic cation transporter-like representative proteins. Column and row headings indicate assigned protein name: *Tc*, *Tribolium castaneum* protein; *Ag*, *Anopheles gambiae* protein; h, human proteins.

	ORCT	ORCT2	*Tc*MFS	*Ag*MFS	hOCT1	hOCT2	hOCT3	hOCTN2	hFLIPT1
ORCT									
ORCT2	72.4%								
*Tc*MFS	57.6%	53.6%							
*Ag*MFS	35.9%	33.1%	29.5%						
hOCT1	37.4%	31.1%	31.7%	29.0%					
hOCT2	36.5%	32.3%	31.5%	28.9%	69.8%				
hOCT3	39.4%	33.6%	31.9%	28.3%	32.2%	30.8%			
hOCTN2	38.0%	31.3%	33.7%	28.2%	34.0%	32.4%	32.4%		
hFLIPT1	35.6%	30.4%	32.7%	26.4%	29.3%	30.1%	29.9%	29.8%	

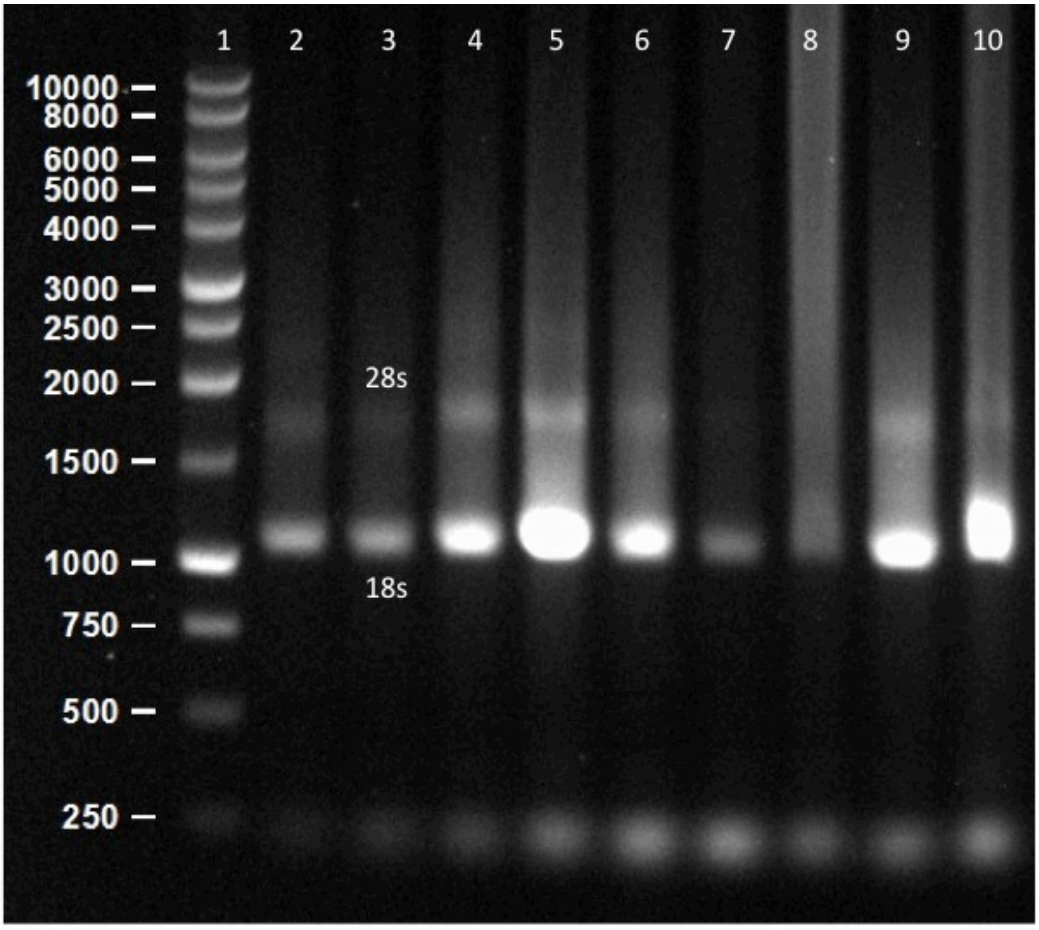

Figure 2.1 Representative RNA gel for qPCR tissue samples from control and TEA exposed individuals after 1 generation. Ribosomal mRNA 18s and 28s bands were labeled. Invertebrate RNA contains nicks that can cause 28s bands to be faint or absent, even in intact RNA. Lanes contain the following: 1) 1kb DNA Ladder (New England Biolabs Ltd.) 2) whole body control, 3) midgut control, 4) ovary control, 5) 150 mmol L^{-1} TEA whole body, 6) 150 mmol L^{-1} TEA midgut, 7) 150 mmol L^{-1} TEA ovary, 8) 80 mmol L^{-1} TEA whole body, 9) 80 mmol L^{-1} TEA midgut, 10) 80 mmol L^{-1} TEA ovary.

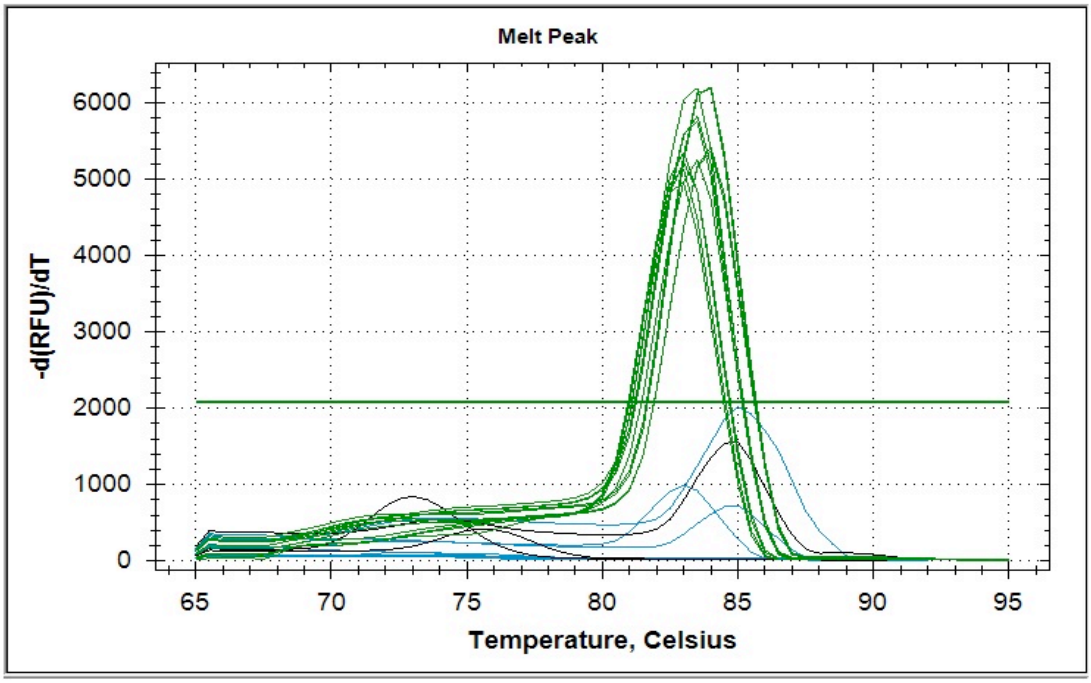

Figure 2.2 Sample MELT curve analysis for *orct*. MELT curve was generated by plotting the change in the inverse of the measured fluorescence value over time (vertical axis) by the temperature of the block (horizontal axis). Double-stranded DNA products created through amplification denature at unique temperatures and cause fluorescence to decrease. This method allows determination of the number of unique amplicons present (having the same peak position) across a qPCR plate. Trace colors: *orct* amplification, green; NRT, blue; NTC, black. Horizonal green bar indicates fluorescence threshold value.

		1	2	3	4	5	6	7
A	70.0	**Unk-1** orct 400nM	**Unk-1** orct 400nM	**Unk-9** orct 500nM	**Unk-9** orct 500nM	**Unk-17** orct 600nM	**Unk-17** orct 600nM	**NTC** orct 600nM
B	68.8	**Unk-2** orct 400nM	**Unk-2** orct 400nM	**Unk-10** orct 500nM	**Unk-10** orct 500nM	**Unk-18** orct 600nM	**Unk-18** orct 600nM	
C	66.6	**Unk-3** orct 400nM	**Unk-3** orct 400nM	**Unk-11** orct 500nM	**Unk-11** orct 500nM	**Unk-19** orct 600nM	**Unk-19** orct 600nM	
D	62.6	**Unk-4** orct 400nM	**Unk-4** orct 400nM	**Unk-12** orct 500nM	**Unk-12** orct 500nM	**Unk-20** orct 600nM	**Unk-20** orct 600nM	**NTC** orct 600nM
E	57.8	**Unk-5** orct 400nM	**Unk-5** orct 400nM	**Unk-13** orct 500nM	**Unk-13** orct 500nM	**Unk-21** orct 600nM	**Unk-21** orct 600nM	
F	53.9	**Unk-6** orct 400nM	**Unk-6** orct 400nM	**Unk-14** orct 500nM	**Unk-14** orct 500nM	**Unk-22** orct 600nM	**Unk-22** orct 600nM	
G	51.3	**Unk-7** orct 400nM	**Unk-7** orct 400nM	**Unk-15** orct 500nM	**Unk-15** orct 500nM	**Unk-23** orct 600nM	**Unk-23** orct 600nM	
H	50.0	**Unk-8** orct 400nM	**Unk-8** orct 400nM	**Unk-16** orct 500nM	**Unk-16** orct 500nM	**Unk-24** orct 600nM	**Unk-24** orct 600nM	**NTC** orct 600nM

Figure 2.3 Sample plate schematic for temperature and primer concentration optimization using quantitative real-time PCR. Identical unknown numbers represent technical replication. NTCs were run at various temperatures to assess primer dimer effects at low and high temperatures. Plate was designed using CFX Manager™ Software.

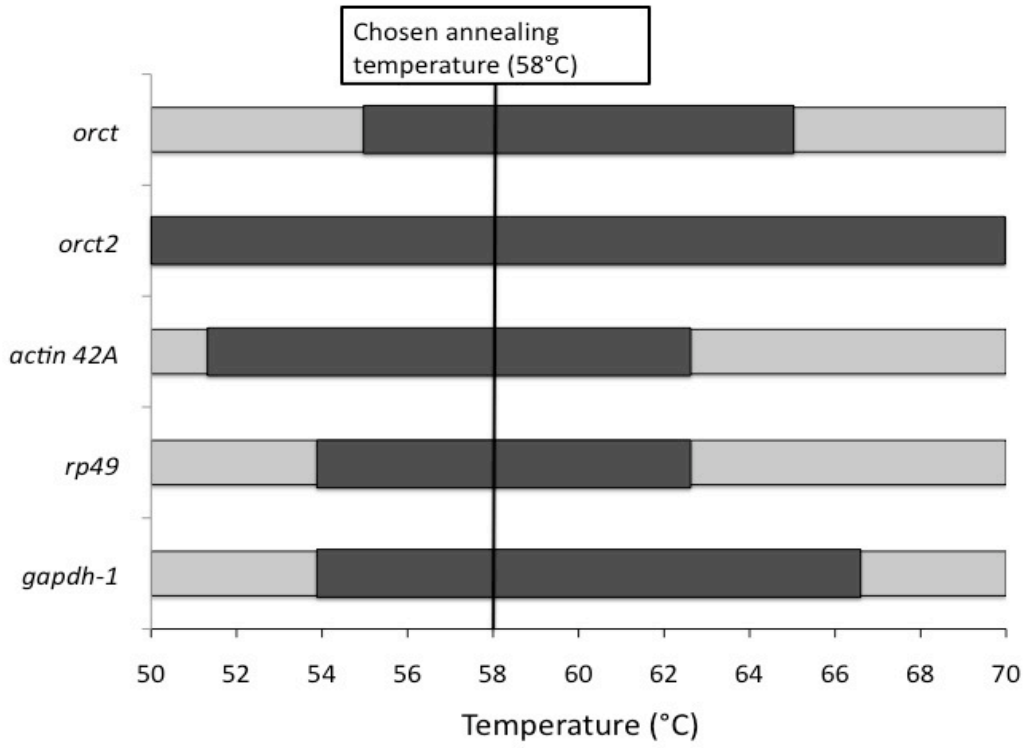

Figure 2.4 Optimal temperature ranges for quantitative real-time PCR primer sets (*orct*, *orct2*, *actin 42A*, *rp49*, *gapdh-1*) indicated by dark gray bars. Light gray regions indicated the full range of temperatures tested.

	1	2	3
A	Std-1 orct WB	Std-1 orct WB	Std-1 orct WB
B	Std-2 orct WB	Std-2 orct WB	Std-2 orct WB
C	Std-3 orct WB	Std-3 orct WB	Std-3 orct WB
D	Std-4 orct WB	Std-4 orct WB	Std-4 orct WB
E	Std-5 orct WB	Std-5 orct WB	Std-5 orct WB
F	Std-6 orct WB	Std-6 orct WB	Std-6 orct WB
G	NTC-1 orct WB	NTC-1 orct WB	
H	NRT-1 orct WB	NRT-1 orct WB	

Figure 2.5 Sample plate schematic for determination of primer set efficiency using 6 serial 5 or 10- fold dilutions of template. Plate was designed using CFX Manager™ Software. NTCs and NRT controls were performed to test for primer dimer and genomic DNA contamination.

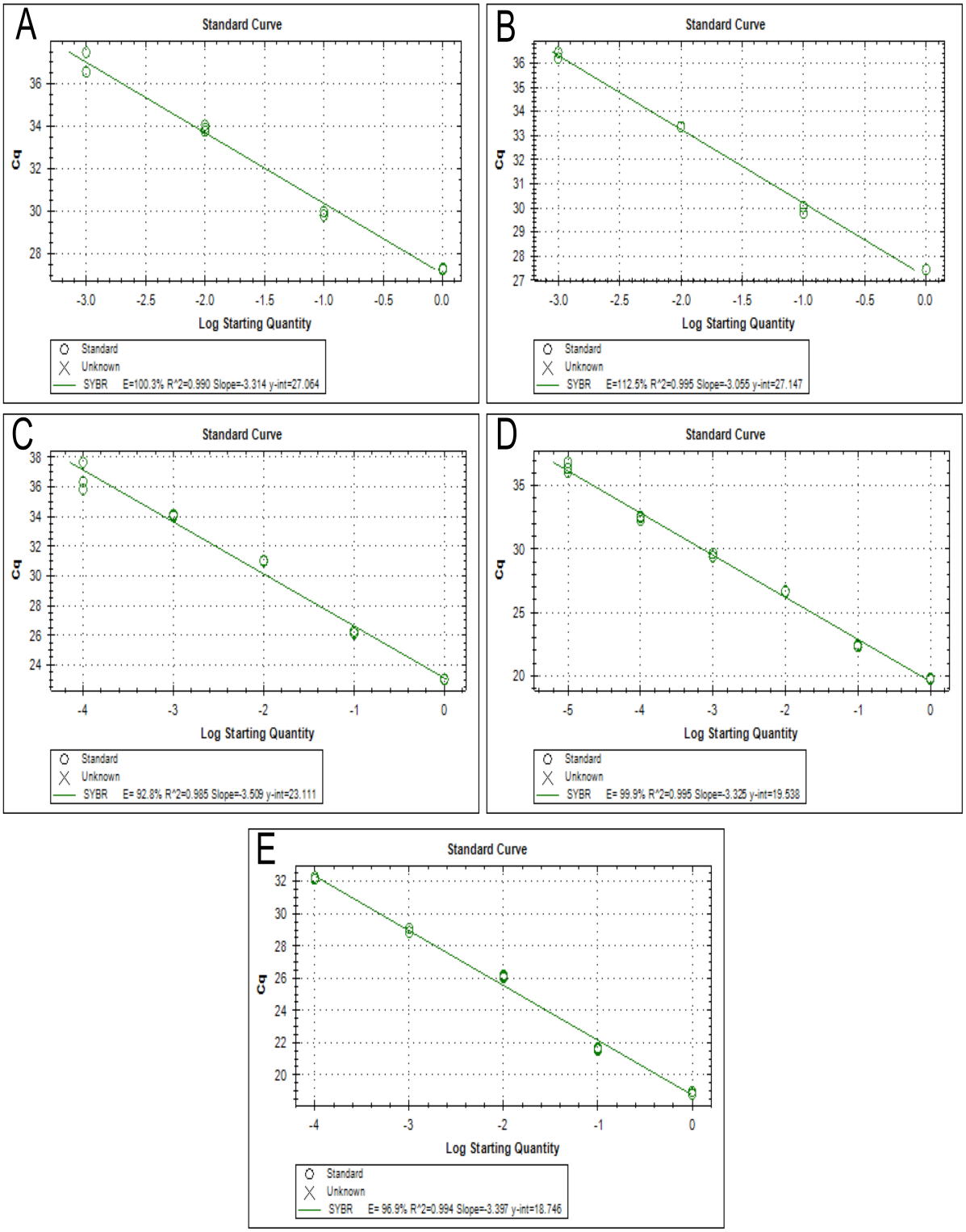

Figure 2.6 Efficiency curves for *orct* (A), *orct2* (B), *actin 42A* (C), *gapdh-1* (D) and *rp49* (E). The legend on each graph displays: primer efficiency (E), R^2 value, y-intercept and slope. Quantification cycle (Cq) is present on the vertical axis while the horizontal axis displays the logarithmic value of the starting template quantity.

	1	2	3	4	5	6	7	8	9	10	11	12
A	**Unk-1** orct WB	**Unk-5** orct WB	**Unk-9** orct WB	**Unk-13** orct 79WBF1	**Unk-17** orct 79WBF1	**Unk-21** orct 79WBF1	**Unk-25** orct 150WBF1	**Unk-29** orct 150WBF1	**Unk-33** orct 150WBF1	**Unk-37** orct WB		
B	**Unk-1** orct WB	**Unk-5** orct WB	**Unk-9** orct WB	**Unk-13** orct 79WBF1	**Unk-17** orct 79WBF1	**Unk-21** orct 79WBF1	**Unk-25** orct 150WBF1	**Unk-29** orct 150WBF1	**Unk-33** orct 150WBF1	**Unk-38** orct2 WB		
C	**Unk-2** orct OV	**Unk-6** orct OV	**Unk-10** orct OV	**Unk-14** orct 79OVF1	**Unk-18** orct 79OVF1	**Unk-22** orct 79OVF1	**Unk-26** orct 150OVF1	**Unk-30** orct 150OVF1	**Unk-34** orct 150OVF1	**Unk-39** gapdh1 WB		
D	**Unk-2** orct OV	**Unk-6** orct OV	**Unk-10** orct OV	**Unk-14** orct 79OVF1	**Unk-18** orct 79OVF1	**Unk-22** orct 79OVF1	**Unk-26** orct 150OVF1	**Unk-30** orct 150OVF1	**Unk-34** orct 150OVF1	**Unk-40** actin42a WB		
E	**Unk-3** orct MT	**Unk-7** orct MT	**Unk-11** orct MT	**Unk-15** orct 79MTF1	**Unk-19** orct 79MTF1	**Unk-23** orct 79MTF1	**Unk-27** orct 150MTF1	**Unk-31** orct 150MTF1	**Unk-35** orct 150MTF1	**Unk-41** rp49 WB		
F	**Unk-3** orct MT	**Unk-7** orct MT	**Unk-11** orct MT	**Unk-15** orct 79MTF1	**Unk-19** orct 79MTF1	**Unk-23** orct 79MTF1	**Unk-27** orct 150MTF1	**Unk-31** orct 150MTF1	**Unk-35** orct 150MTF1	**NTC** orct2	**NTC** gapdh1	
G	**Unk-4** orct MG	**Unk-8** orct MG	**Unk-12** orct MG	**Unk-16** orct 79MGF1	**Unk-20** orct 79MGF1	**Unk-24** orct 79MGF1	**Unk-28** orct 150MGF1	**Unk-32** orct 150MGF1	**Unk-36** orct 150MGF1	**NTC** rp49	**NTC** actin42a	
H	**Unk-4** orct MG	**Unk-8** orct MG	**Unk-12** orct MG	**Unk-16** orct 79MGF1	**Unk-20** orct 79MGF1	**Unk-24** orct 79MGF1	**Unk-28** orct 150MGF1	**Unk-32** orct 150MGF1	**Unk-36** orct 150MGF1	**NTC** orct	**NTC** orct	

Figure 2.7 Sample schematic for a quantitative real-time PCR experimental plate designed according to the sample maximization method (Hellemans *et al.,* 2007). The same unknown value represents technical replication of the same biological sample. Unknowns 37-41 were performed on every experimental plate with the same whole body sample to act as inter run calibrators. NTCs were run on every plate. NRTs for each sample were tested one time for each gene on separate plates with inter-run calibrators.

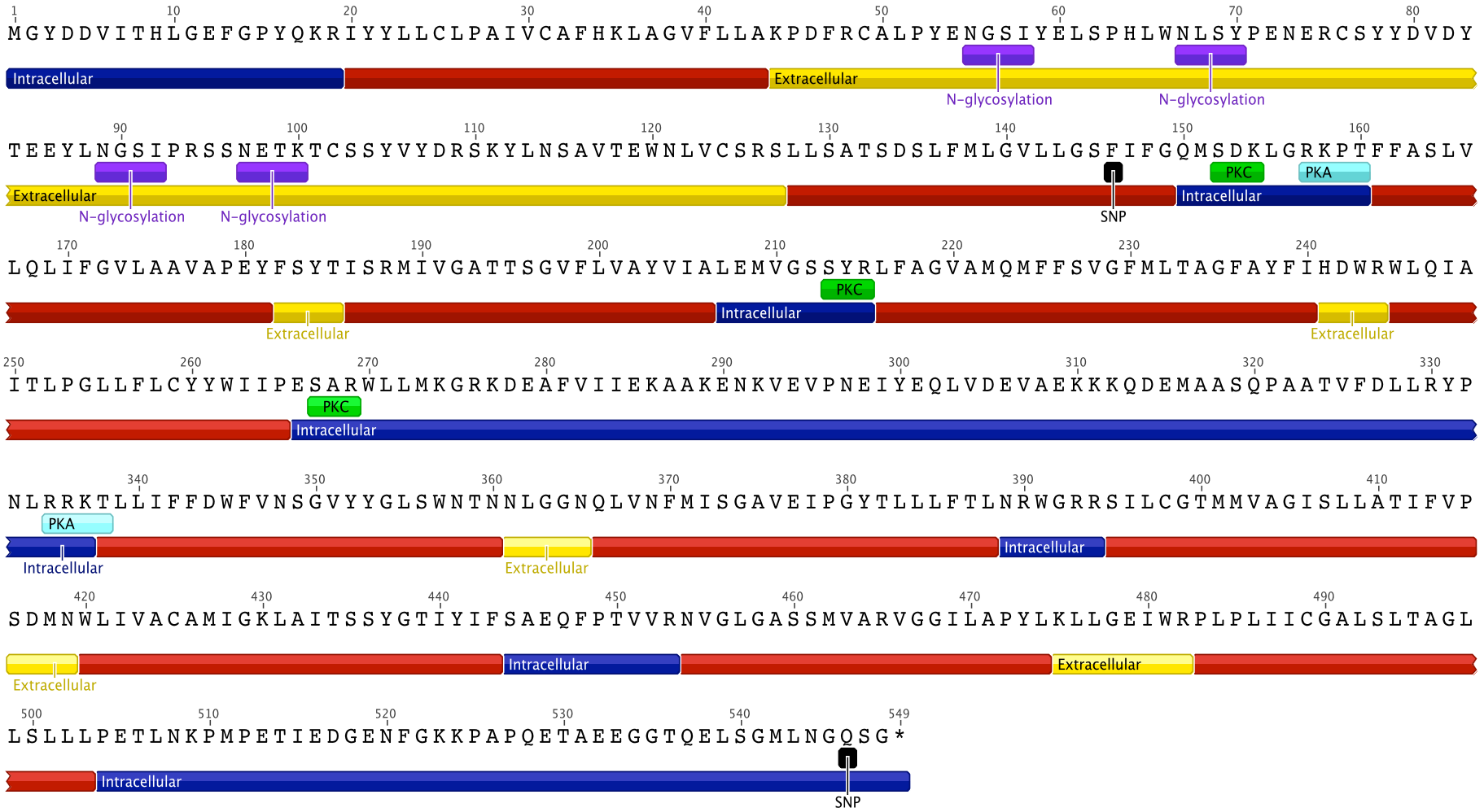

Figure 2.8 Annotated protein sequence of ORCT. Colored bars indicate the following: blue, intracellular domain; red, TMD; yellow, extracellular domain; purple, N-glycosylation site; green, PKC phosphorylation site; light blue, PKA phosphorylation site; black, single nucleotide polymorphism (SNP) from predicted sequence.

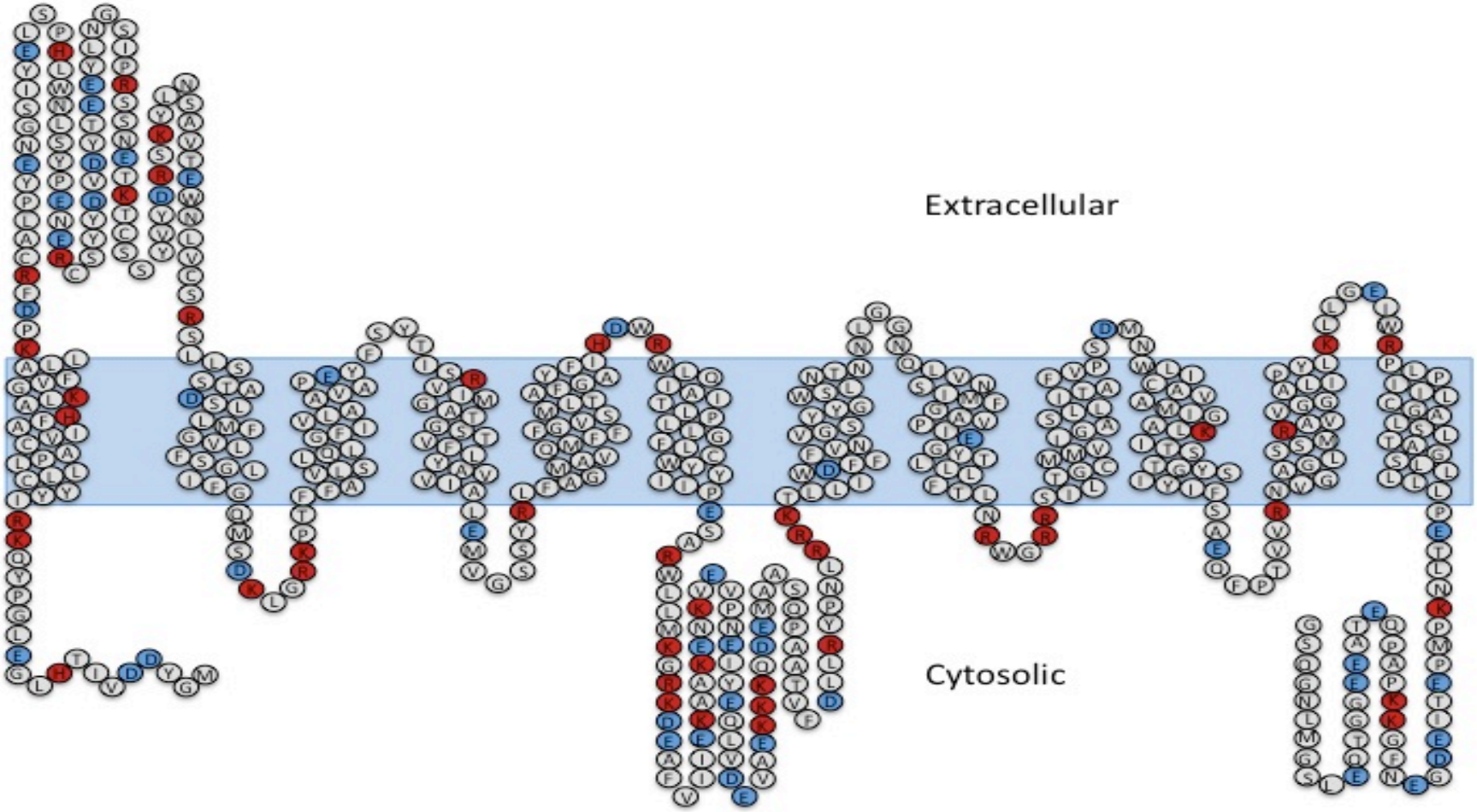

Figure 2.9 Schematic representation of the predicted secondary structure of ORCT. Hydrophobicity analysis with TmPred (Hoffman and Stoffel, 1993) predicts 12 TMDs with intracellular amino and carboxyl ends. Image was generated using Microsoft® PowerPoint® 2008 for Mac. Non-polar amino acids are shown in white, positively charged amino acids are blue, and negatively charged amino acids are red.

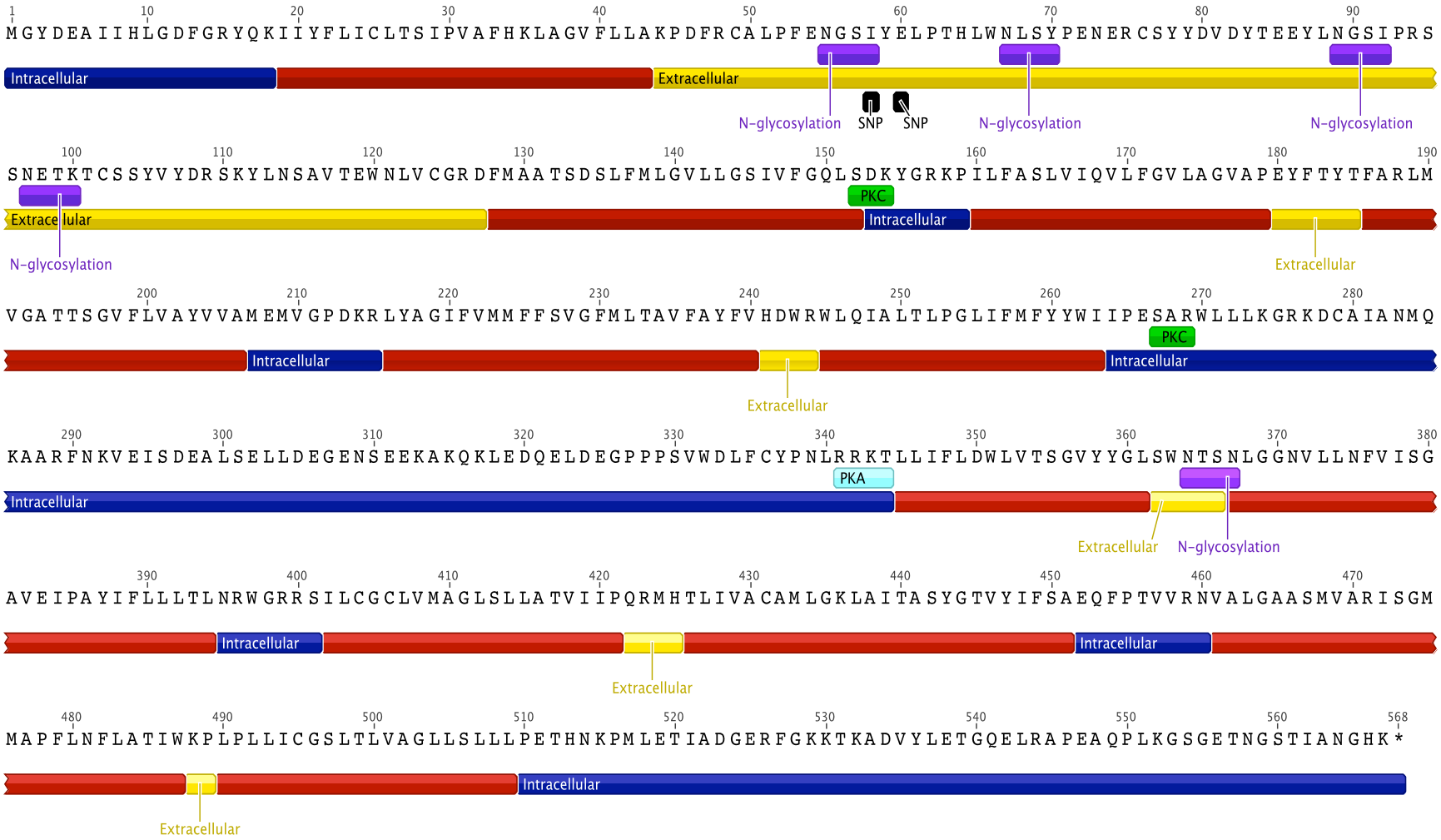

Figure 2.10 Annotated Protein sequence of ORCT2. Colored bars indicate the following: blue, intracellular domain; red, TMD; yellow, extracellular domain; purple, N-glycosylation site; green, PKC phosphorylation site; light blue, PKA phosphorylation site; black, single nucleotide polymorphism (SNP) from predicted sequence.

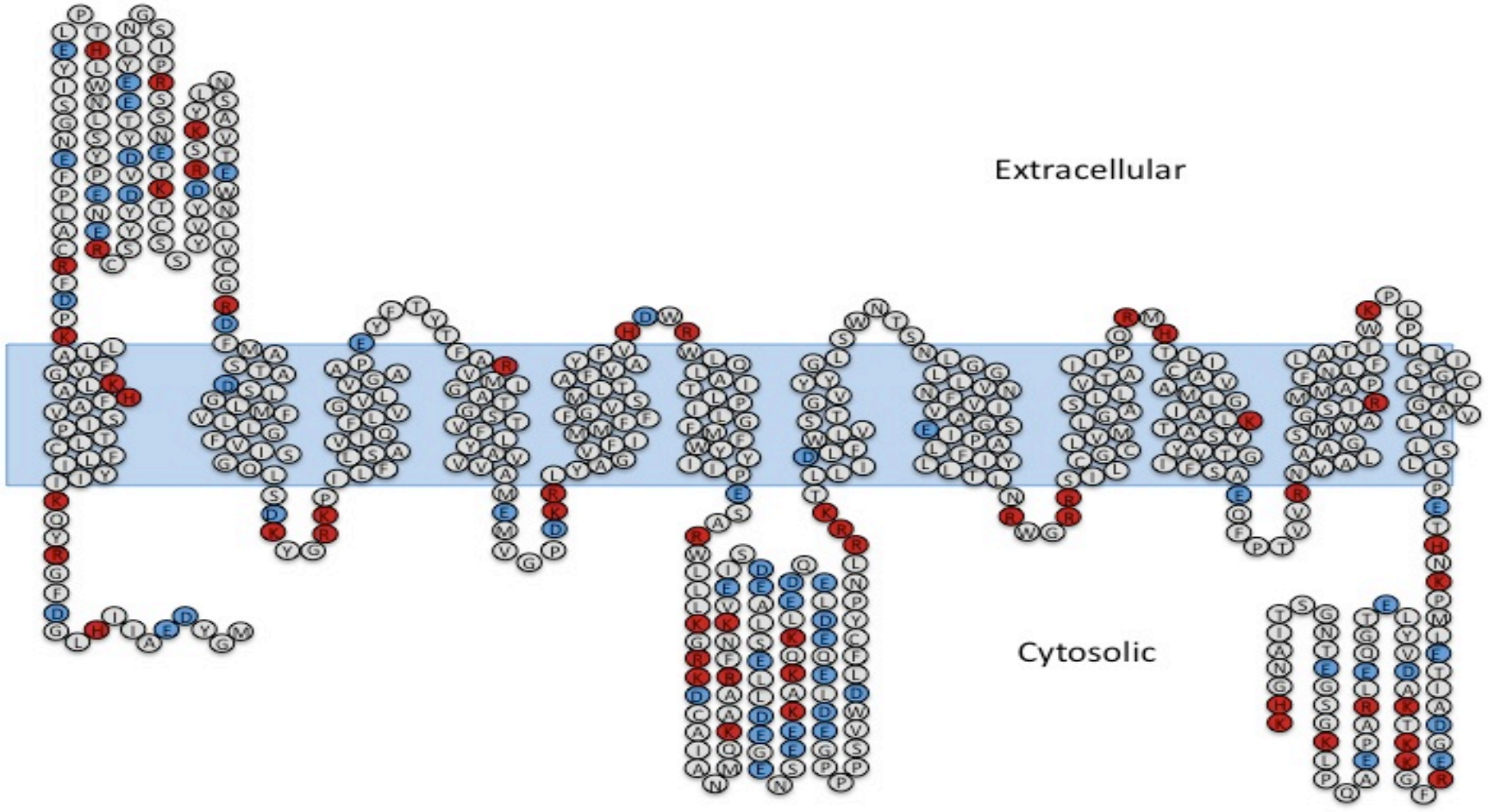

Figure 2.11 Schematic representation of the predicted secondary structure of ORCT2. Hydrophobicity analysis with TmPred (Hoffman and Stoffel, 1993) predicts 12 TMDs with intracellular amino and carboxyl ends. Image was generated using Microsoft® PowerPoint® 2008 for Mac. Non-polar amino acids are shown in white, positively charged amino acids are blue, and negatively charged amino acids are red.

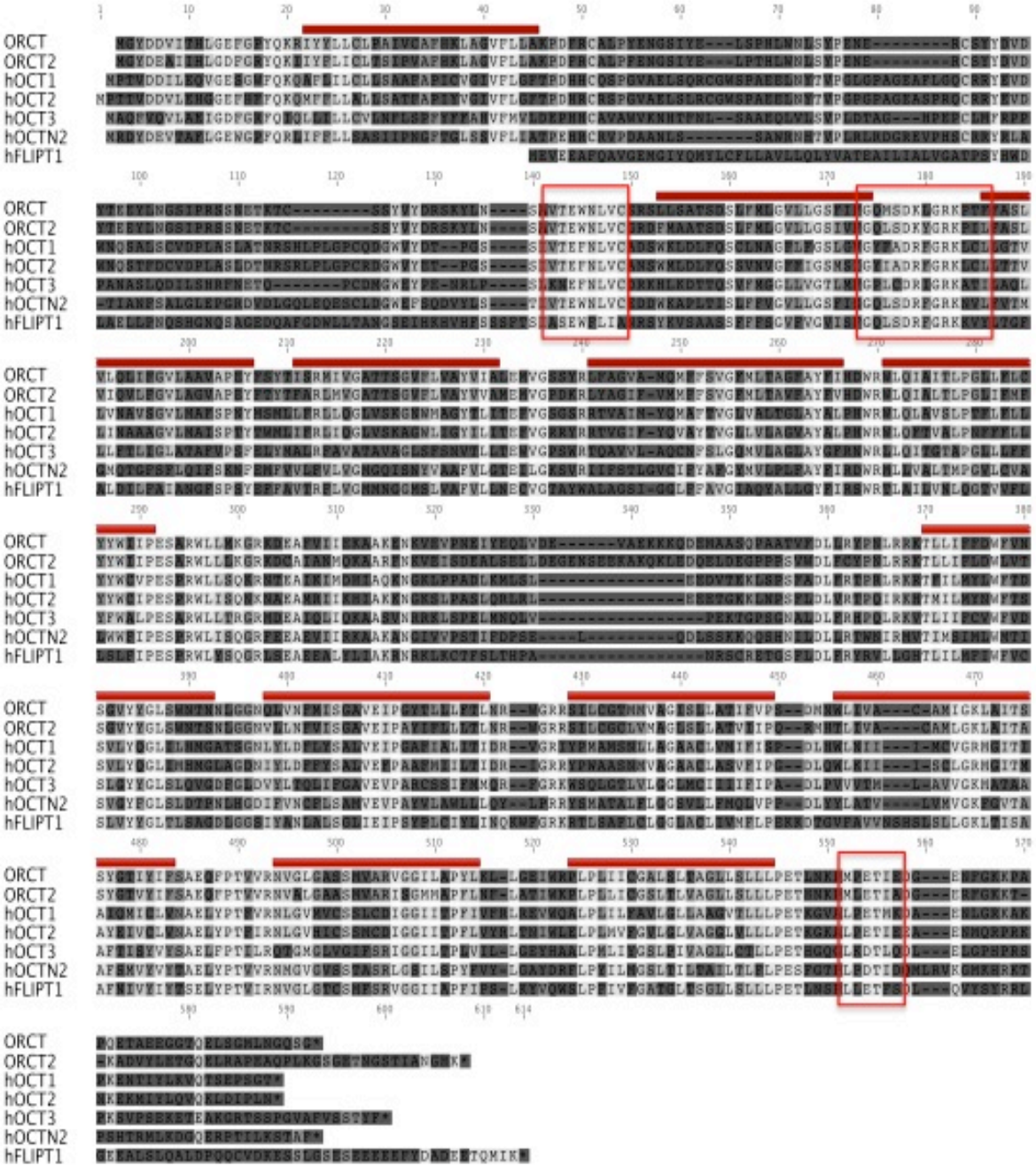

Figure 2.12 Alignment of representative vertebrate organic cation transporters and organic cation transporter orthologs with sequences from *D. melanogaster*. Human OCT isoforms were used as well as OCTN and FLIPT transporters. Sequences found using NCBI BLAST (Altschul *et al.,* 1990) with ORCT as the input query sequence. Alignment constructed using Geneious™ Pro software (Drummond *et al.,* 2011). Red bars indicate TMDs for ORCT, red boxes indicate conserved regions between all sequences. Dark shaded regions indicate low similarity, where as light shaded regions indicate similar amino acids. Unshaded regions indicate identical sites. h indicates human protein.

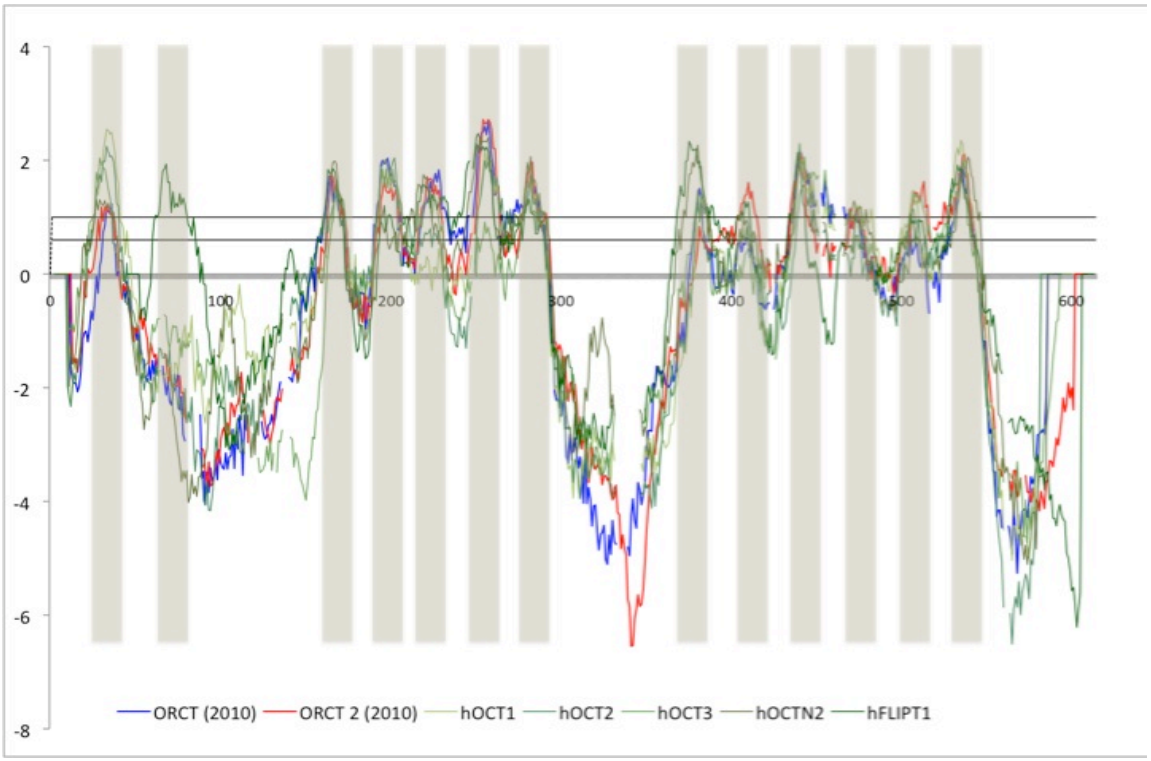

Figure 2.13 Hydrophobicity plots of ORCT and ORCT2 with representative vertebrate organic cation transporter orthologs using TMpred (Hoffman and Stoffel, 1993) with a given TMD range of 17-33 aa. Sequences were aligned relative to amino acid position from a multiple alignment (Figure 2.13) (horizontal scale). Transmembrane spanning regions predicted for all sequences were indicated by the vertical bars. All sequences shared 12 conserved trans membrane domains, with human FLIPT protein having an additional predicted TMD between positions 50 – 100. Upper threshold for predicting TMD is indicated by the grey horizontal bar at 1.0 and the lower threshold at 0.6. Vertical axis indicates a hydrophobicity value predicted by TMpred, which uses the Kyte-Doolittle scale for amino acid hydrophobicity. A value between 0.6 to 1.0 indicates a TMD.

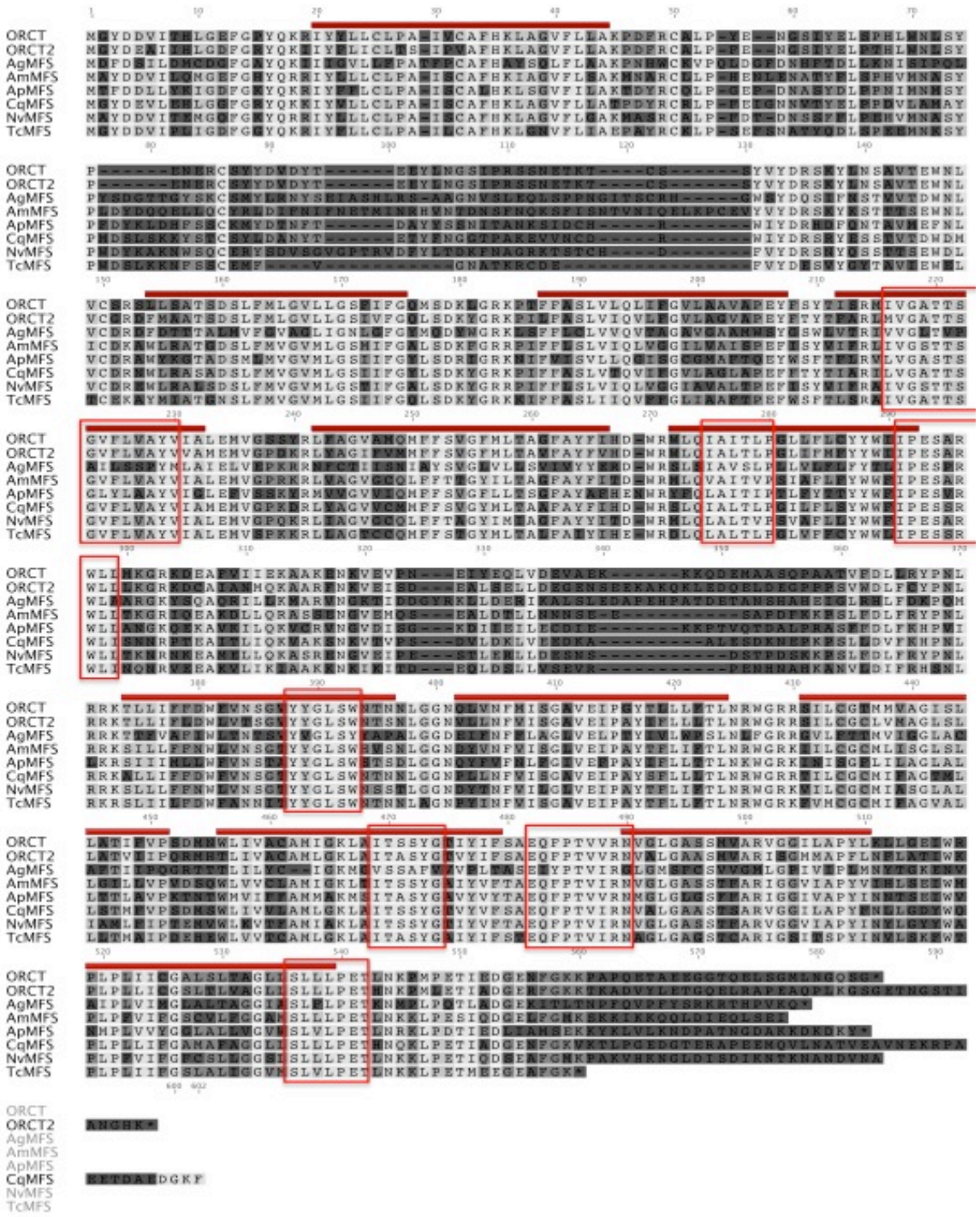

Figure 2.14 Alignment of representative insect organic cation transporter-like orthologs. Sequences found using NCBI BLAST (Altschul *et al.,* 1990) with ORCT as the input query sequence. Alignment constructed using Geneious™ Pro software (Drummond *et al.,* 2011). Red bars indicate TMDs for ORCT, red boxes indicate conserved regions between all sequences. Dark shaded regions indicate low similarity, where as light shaded regions indicate similar amino acids. Unshaded regions indicate identical sites. Legend indicates the protein: *Ag*, *Anopheles gambiae* protein; *Am*, *Apis mellifera* protein; *Ap*, *Acyrthosiphon pisum* protein; *Cq*, *Culex quinquefasciatus* protein; *Nv*, *Nasonia vitripennis* protein; *Tc*, *Tribolium castaneum* protein.

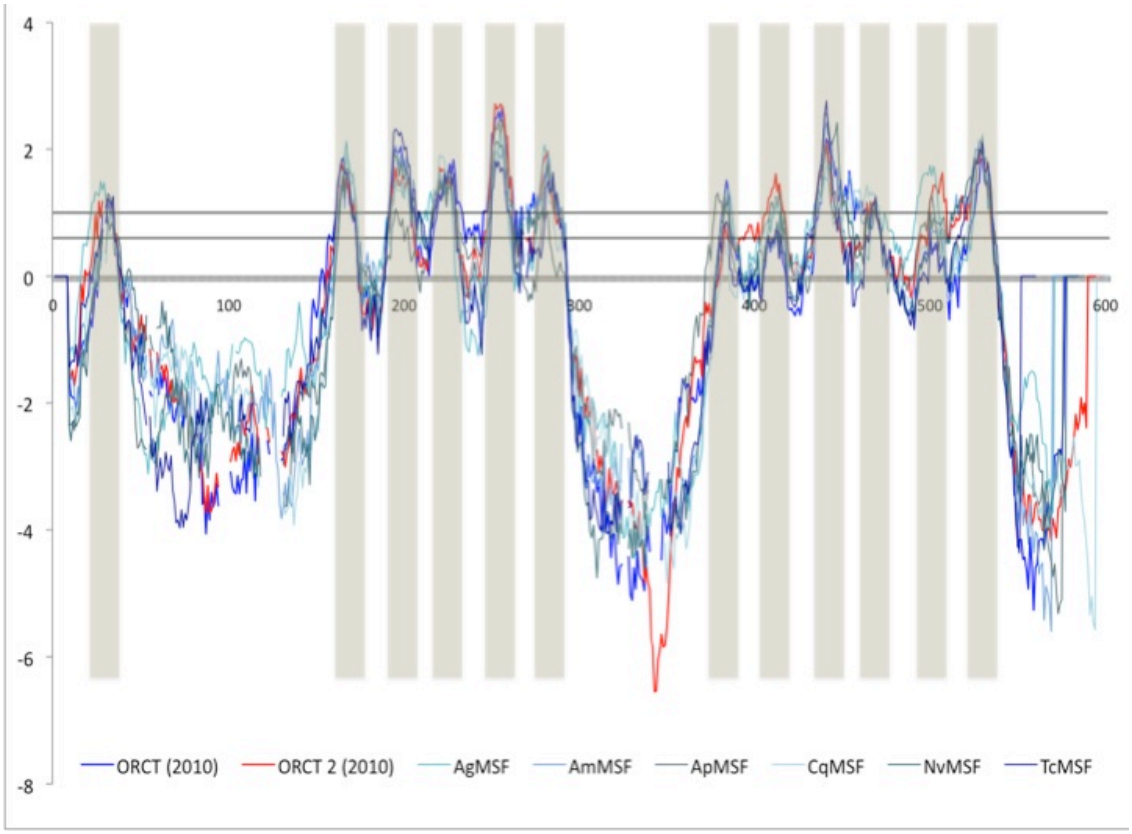

Figure 2.15 Hydrophobicity plots of ORCT and ORCT2 with representative insect organic cation transporter-like orthologs using TMpred (Hoffman and Stoffel, 1993) with a given TMD range of 17-33 amino acids. Sequences were aligned relative to amino acid position from a multiple alignment (Figure 2.14) (horizontal scale). Transmembrane spanning regions predicted for all sequences were indicated by the vertical bars. The majority of sequences shared 12 conserved trans membrane domain, with the exception of *T. castaneum* which had 10 predicted domains. Upper threshold for predicting TMD is indicated by the horizontal bar at 1.0 and the lower threshold at 0.6. Vertical axis indicates a hydrophobicity value predicted by TMpred, which uses the Kyte-Doolittle scale for amino acid hydrophobicity. A value between 0.6 to 1.0 indicates a TMD. Legend indicates the protein: *Ag*, *Anopheles gambiae* protein; *Am*, *Apis mellifera* protein; *Ap*, *Acyrthosiphon pisum* protein; *Cq*, *Culex quinquefasciatus* protein; *Nv*, *Nasonia vitripennis* protein; *Tc*, *Tribolium castaneum* protein.

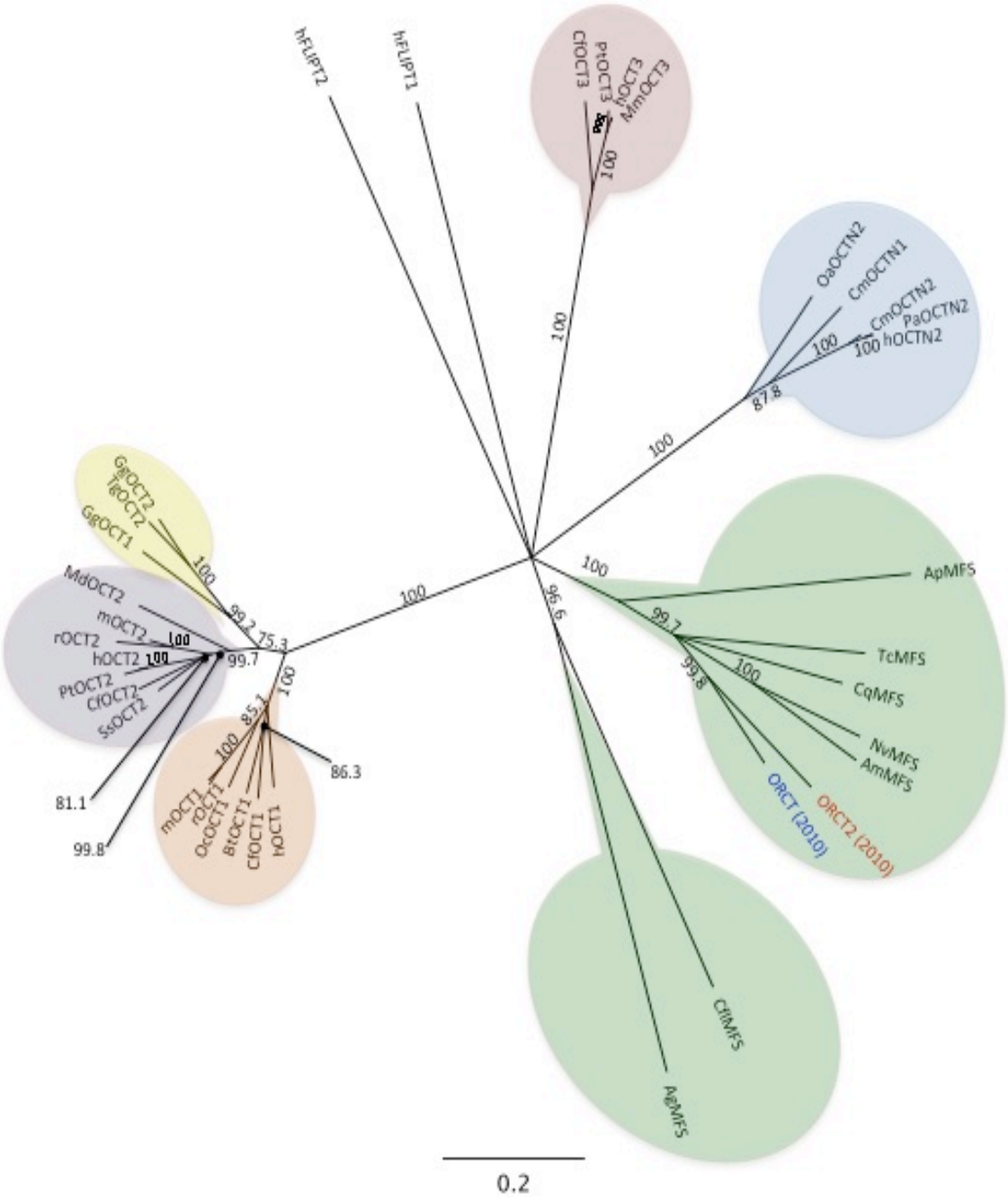

Figure 2.16 Phylogenetic analysis of representative organic cation transporter-like orthologs from the major facilitator superfamily. The tree was constructed in Geneious™ Pro (Drummond *et al.,* 2011) using the Jukes-Cantor method for a Neighbor Joining tree and is displayed as an unrooted tree. Likelihood values are shown at branch nodes. The scale bar represents the number of amino acid substitutions per site. ORCT is highlighted in blue, ORCT2 highlighted in red. Background shading: OCT1, orange; OCT2, purple; OCT3, pink; Bird OCT1-2, yellow; OCTN, blue; Insect MSF, green.

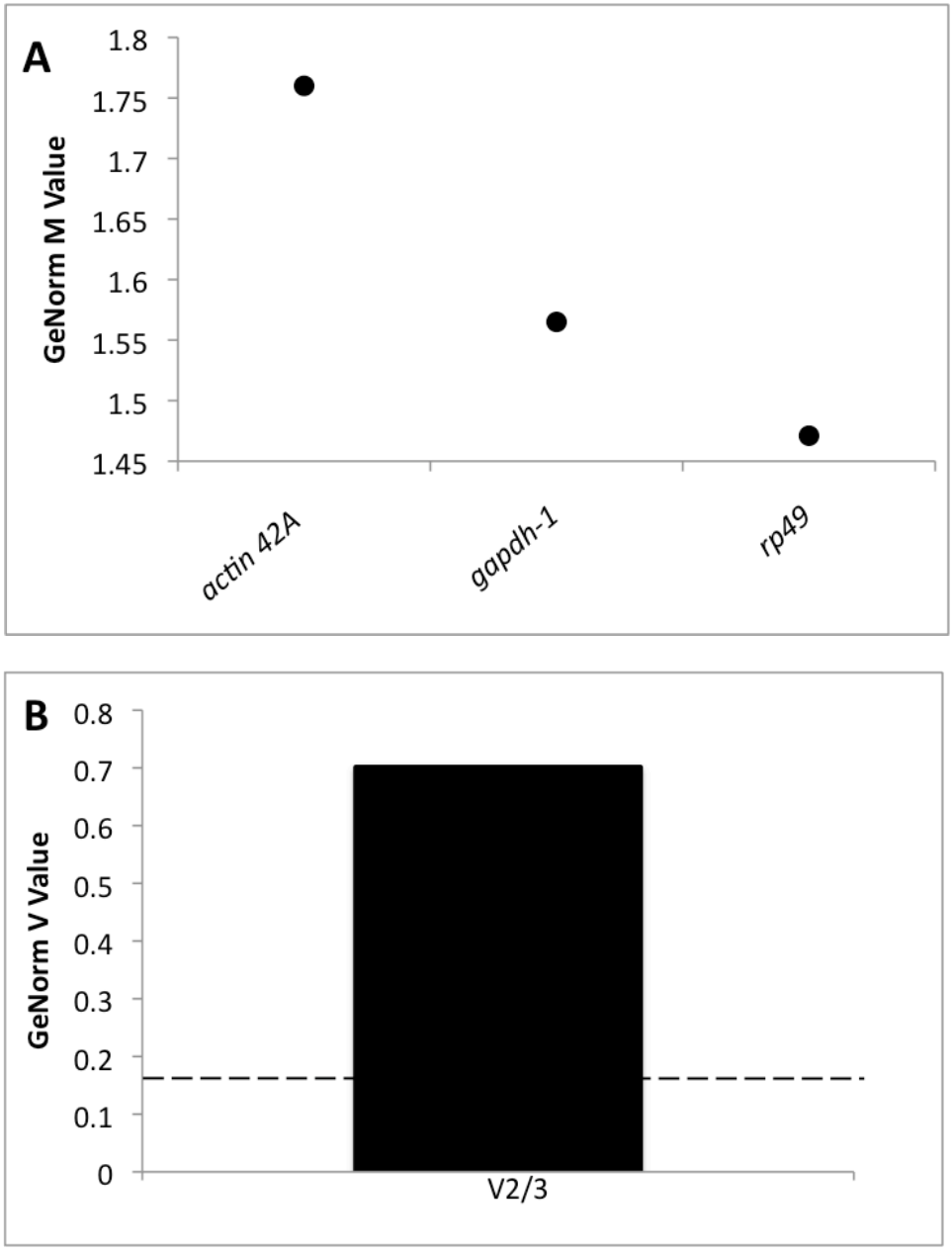

Figure 2.17 Reference gene stability analysis. A) GeNorm M analysis (BioGazelle) showed ranked stability of tested reference genes. M-values for a heterogeneous sample should be less than <1. B) GeNorm V analysis (BioGazelle) determined the ideal number of reference genes to be n-1. A GeNorm V value for n-1 reference genes was above threshold for a heterogeneous sample (0.16). *actin 42A* was the least stable gene, therefore *gapdh-1* and *rp49* were used in all final analyses.

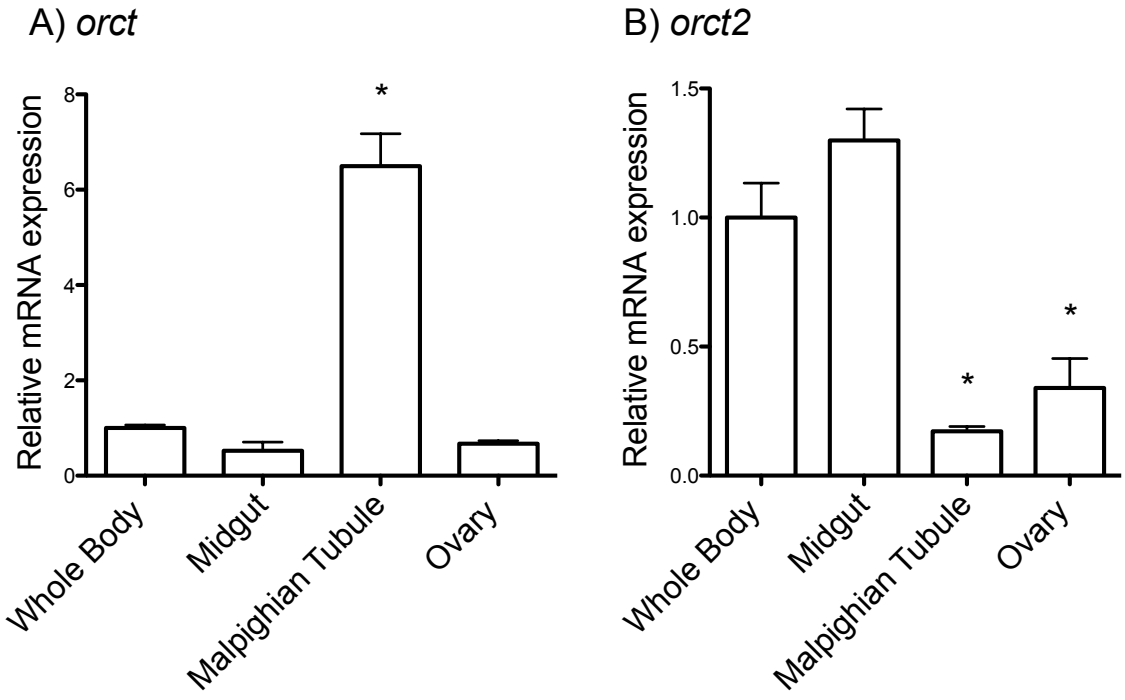

Figure 2.18 Tissue distribution profiles of *orct* (A) and *orct2* (B). Relative mRNA fold expression of each gene was measured in whole body, midgut, Malpighian tubule, and ovary tissues and results are expressed calibrated to the whole body expression of each gene. Statistical significance from whole body expression (*) was assessed using a one-way ANOVA with a Dunnett's multiple comparisons post-test. Statistical tests and final graphical output was done using Graphpad Prism™ (v5) with a p-value <0.05 considered significant.

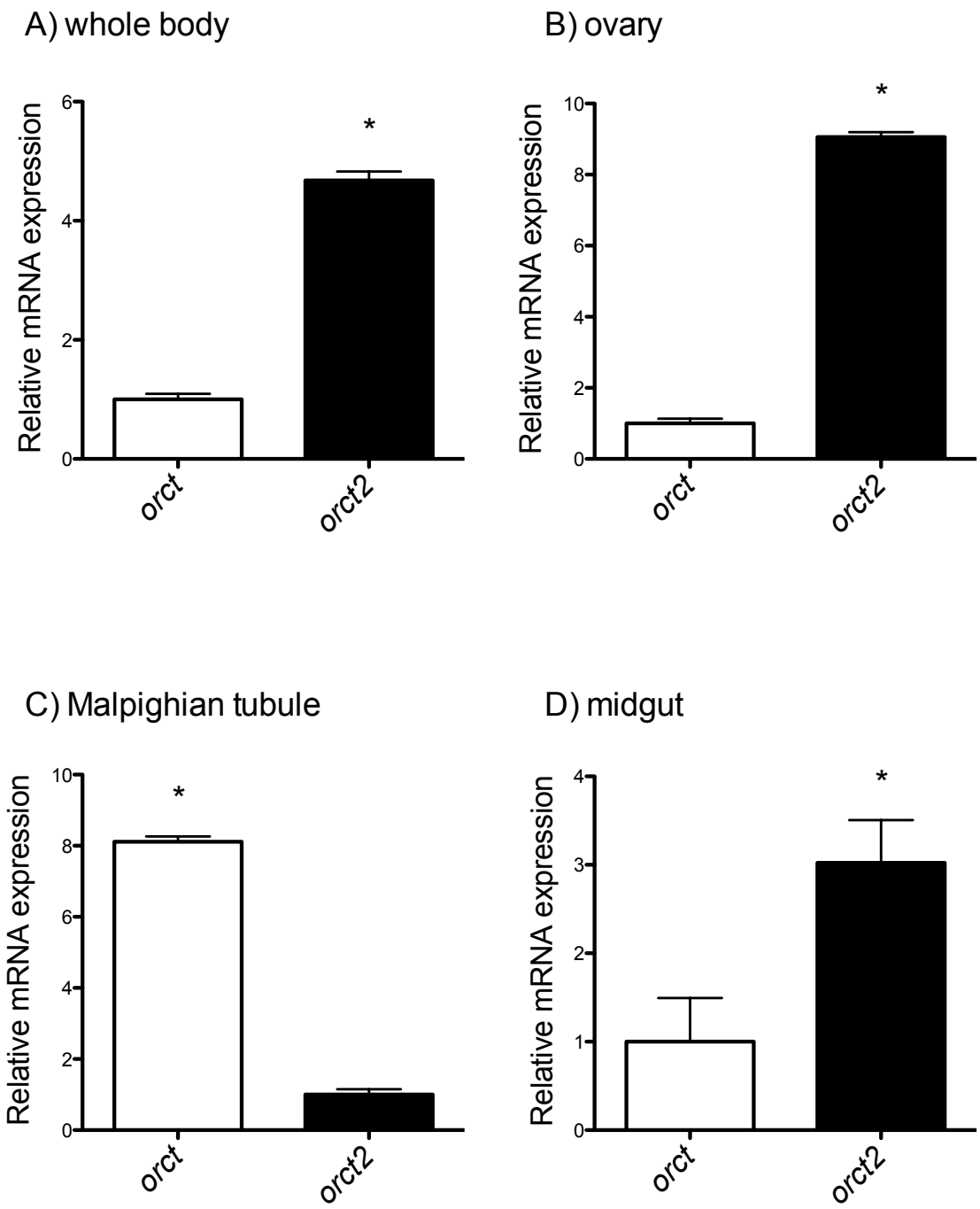

Figure 2.19 Comparative expression of *orct* and *orct2* within *D. melanogaster* tissues. A) whole body, B) ovary, C) Malpighian tubule, D) midgut. Expression values were normalized to the gene with the lowest expression value in each tissue tested. Unpaired Student's *t*-tests were used to compare mRNA expression values. Statistical tests and final graphical output was done using Graphpad Prism™ (v5) with a p-value <0.05 considered significant.

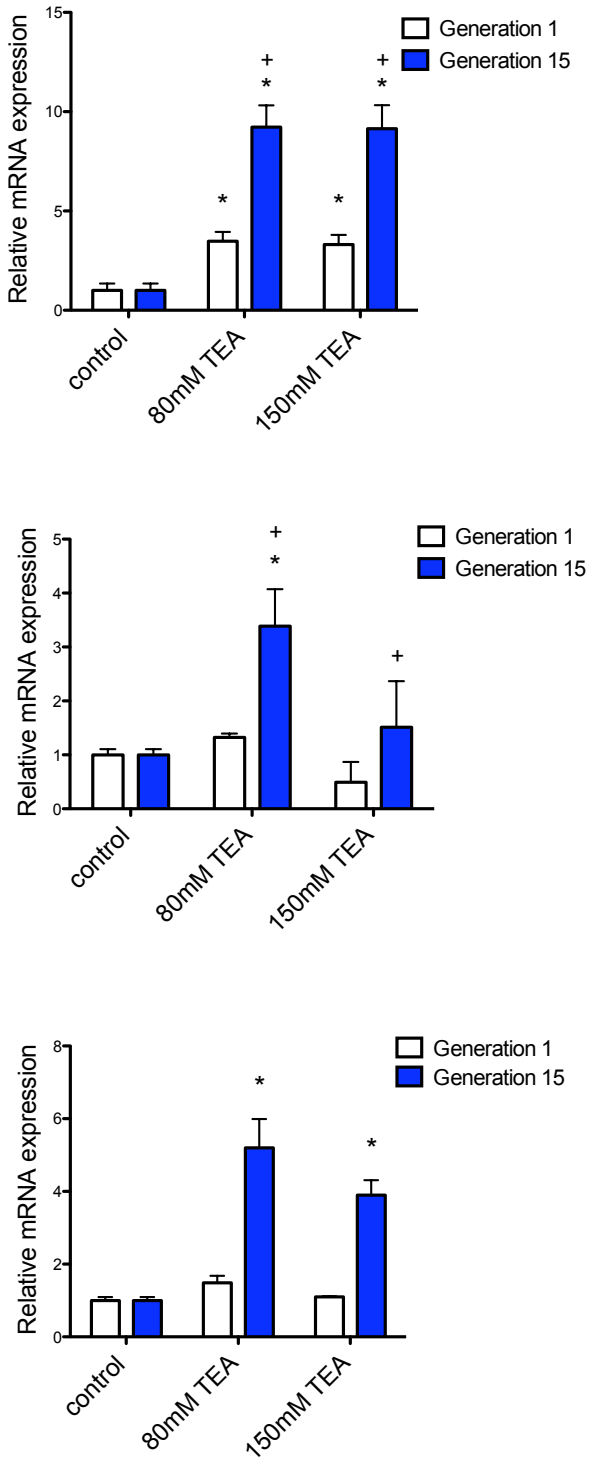

Figure 2.20 Relative expression of *orct* mRNA following exposure to tetraethylammonium after 1 (white) and 15 (blue) generations. A) midgut, B) Malpighian tubules, C) ovary. Expression values were normalized to control conditions within each generation. Significant differences in expression due to exposure are indicated by *; significant differences between generations subjected to the same exposure of TEA are indicated by +. Two-way ANOVA with a Bonferroni post-hoc test was used to assess the affect of treatment and generation time. One-way ANOVA with a Dunnett's post-hoc test was used to determine statistical changes in exposure within a generation. Statistical tests and final graphical output was done using Graphpad Prism™ (v5) with a p-value <0.05 considered significant.

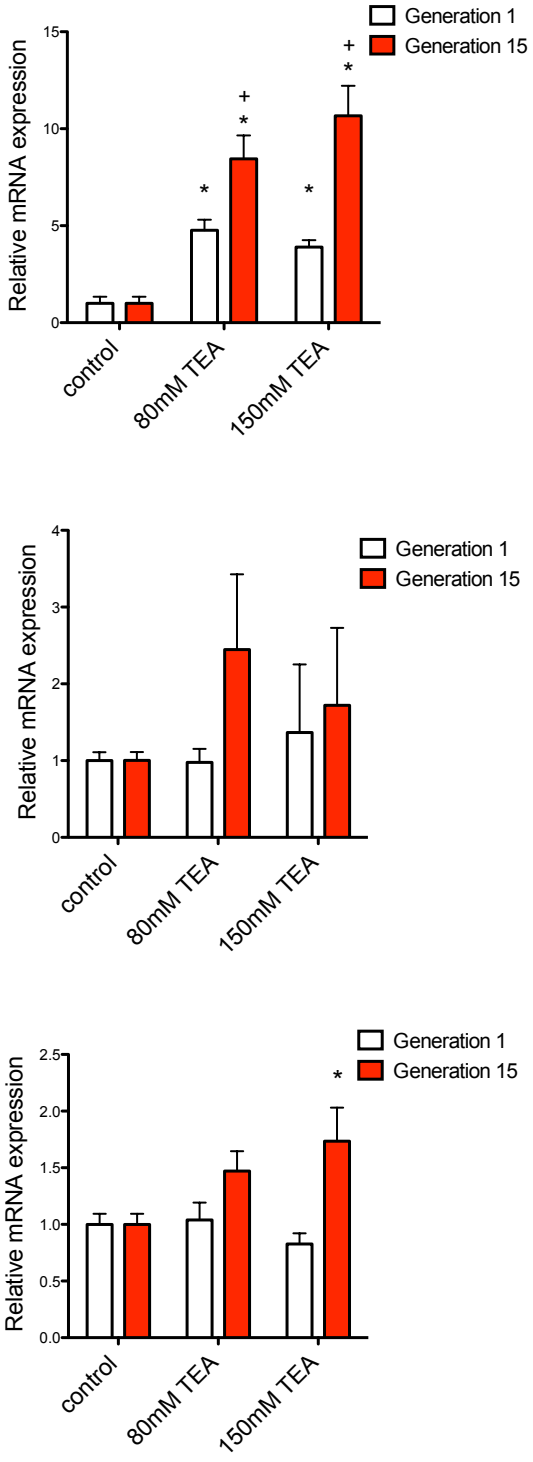

Figure 2.21 Relative expression of *orct2* mRNA following exposure to tetraethylammonium after 1 (white) and 15 (red) generations. A) midgut, B) Malpighian tubules, C) ovary. Expression values were normalized to control conditions within each generation. Significant differences in expression due to exposure are indicated by *; significant differences between generations subjected to the same exposure of TEA are indicated by +. Two-way ANOVA with a Bonferroni post-hoc test was used to assess the affect of treatment and generation time. One-way ANOVA with a Dunnett's post-hoc test was used to determine statistical changes in exposure within a generation. Statistical tests and final graphical output was done using Graphpad Prism™ (v5) with a p-value <0.05 considered significant.

Chapter 3 Expression of the ORCT Protein in Insect Cell Lines

3.1 Synopsis

In order to conduct functional assays of the isolated ORCT and ORCT2 proteins, an appropriate heterologous expression system had to be tested. In contrast to the option of expressing the protein in a heterologous expression system, a homologous expression system derived from *D. melanogaster* is commercially available. However, Kc1 and SL2 cell lines from *D. melanogaster* were not used in this research for a number of reasons. First, previous studies have shown Kc1 and SL2 cells to be ineffective at correctly transporting and inserting foreign proteins into the cell membranes (Hegedus *et al*., 1999). Second, there may exist native constitutive expression of the genes of interest in *D. melanogaster* cell lines, which would obscure results obtained from functional studies. Finally, Sf9 cells were made readily available to use from collaborators at Pacific Agri-Foods Research Center, Summerland, B.C. A series of expression constructs for ORCT were prepared that allowed expression of the ORCT protein in Sf9 cell lines derived from the fall army worm, *Spodoptera frugiperda* (Lepidoptera). Prokaryotic heterologous protein expression systems such as *Escherichia coli* (*E. coli*) and yeast, despite their wide use and appeal, lack the necessary intracellular processing for correct assembly of a eukaryotic protein (Hegedus *et al.,* 1999). Expression of ORCT in a eukaryotic, insect expression system allowed protein processing to occur in a cellular environment that more closely mimics the natural environment for this protein. Over the last 30 years, manipulation of baculovirus genomes lead to the development of a number of expression vectors for transfection of insect cell lines (Pfeifer *et al.,* 1999; Smith *et al.,* 1983). Sf9 cells using a baculovirus expression vector have been recently used to express and characterize a number of vertebrate membrane

transport proteins (Sarkade *et al.,* 1992; Hegedus *et al.,* 1999; Bakos *et al.,* 2000; Ozvegy *et al.,* 2001).

Transient and constitutive expression of ORCT was mediated by a plasmid vector, p2ZOPe2, which exploits the immediate-early 2 (ie2) promoter from the *Orgyia pseudotsugata* multicapsid nuclepolyhedrosis virus (*Op*MNPV) (Hegedus *et al.,* 1998). ORCT was expressed transiently using the baculovirus vector p*Ac*Bac mediated by the polyhedrin promoter from *Autographica californica* multicapsid nucleopolyhedrosis virus (*Ac*MNPV) (Luckow and Summers, 1988; Miller, 1988). Budded virus constructs were collected following transfection with p*Ac*Bac for subsequent infection of Sf9 cells. Protein expression was assessed through Coomassie staining for total protein and through Western blotting. Site-specific detection of ORCT is possible through the addition of an HA-tag sequence (YPY DVP DYA) from human influenza hemagglutinin. ORCT-HA constructs were detected as soon as 24 hpt with the plasmid vector p2ZOPe2 and increased in intensity at 48 hpt. Protein from transfections with p*Ac*Bac was detectable only at 48 hpt; however protein from subsequent infections with budded virus was detectable 24 hours post infection (hpi) and increased in intensity up to 96 hpi. Results of the Western blots did not correspond to the predicted 60 kDa size of ORCT in all cases, however post-translational modification of the protein may have affected protein migration. Functional assays are needed to confirm correct assembly of the ORCT protein, and to characterize ORCT as an organic cation transporter.

3.2 Materials and Methods

3.2.1 Insect Rearing

Oregon R strain *D. melanogaster* Meigen were raised on standard artificial fly media and maintained in laboratory culture. Artificial media was prepared as described by Chahine and O'Donnell (2009). Full protocol for media preparation was outlined in Chapter 2. Media was stored at 4°C for up to 30 days. Insects 4-7 days post emergence were used in all experiments.

3.2.2 RNA Extraction and Reverse Transcription

Adult 4-7 day post emergence *D. melanogaster* were harvested for total RNA extraction. Eight whole flies were transferred into 1mL TRIzol® reagent and RNA was extracted as described by Chahine and O'Donnell (2009) and Nawata and Wood (2008). A complete protocol for RNA extraction is outlined in Chapter 2. Typical RNA yields ranged from 528.0 ng/µL to 1171.7 ng/µL with A260/280 of 2.1. RNA was stored at -80°C for 6 months with no loss of yield. RNA was treated with Ambion® Turbo DNA-*free*™ to remove any contaminating genomic DNA prior to cDNA construction. cDNA was synthesized from 1µg of RNA in the Improm II™ Reverse Transcription System with oligo(dT) primers. Temperature cycling for reverse transcription was performed using a C1000™ Thermal Cycler according to manufacturer directions. cDNA was stored at -20°C.

3.2.3 Primer Design

A predicted OCT-like gene (*orct*) was previously cloned and sequenced (Chapter 2). A full length amplicon of the *orct* gene was obtained using terminal primers that enclose the ORF with 5' modifications. A Kozac sequence (5'-GCCACC) was added to the 5' forward

primers for ribosomal recognition. Appropriate restriction sites (*Hind*III and *BamH*I) corresponding to each expression vector (p2ZOPe2, pFastBac™1 (Invitrogen)) were included in the primer. Additionally, one forward and one reverse primer for each vector construct was created with a 27bp long HA-tag sequence (5'-TACCCCTACGACGTGCCCGACTACGCC) from human influenza hemagglutinin (GenBank accession number: AEG65813.1) corresponding to the amino acid sequence YPY DVP DYA, for which there is a commercially available antibody for site specific detection. Table 3.1 lists primers for the amplification of *orct* for each vector with modifications outlined. Primers were designed and analyzed using Integrated DNA technologies [IDT; (www.idtdna.com)] which employs IDTs PrimerQuest® Software (2002). Specificity of primers was accessed using BLAST (Altschul *et al.,* 1990).

3.2.4 Amplification and Preparation of Amplicons

For each expression vector (p2ZOPe2, pFastBac™1) 3 amplicons were designed. The first had an HA-tag on the forward strand designated 5'HA-*orct*, the second had an HA-tag on the reverse strand designated *orct*-HA3' and final amplicon lacked the HA-tag sequence designated *orct*N (Figure 3.1; Figure 3.2). The HA-tag sequence was added to the forward and reverse strands so that the resulting proteins could be detected from either the amino or carboxyl terminus. The untagged construct was created for use as a control as well as for use in future functional assays. Amplification on whole body cDNA using Easy-A™ High-Fidelity PCR Cloning Enzyme and Master Mix was performed to obtain full length amplicons of *orct*. Each PCR reaction contained 2.0 µL cDNA template and 1.0 µL of forward (100 µmol L^{-1}) and 1.0 µL of reverse (100 µmol L^{-1}) primer in a total reaction volume of 50 µL according to manufacturer's protocol. Cycling was performed on C1000™ Thermal Cycler

with the following parameters: initial denaturing at 95°C for 2 minutes, followed by 30 cycles of 40 s denaturing at 95°C, 30 s annealing at 69°C and 2 minutes elongation at 72°C, with a final elongation step at 72°C for 5 minutes.

PCR reactions were purified using either QIAquick® PCR Purification Kit (Qiagen, Toronto, ON) or E.Z.N.A.® Gel Extraction and PCR Cleanup Kit (Omega Bio-Tek, Norcross, GA) according to manufacturer. Amplicons and vectors were digested using *Hind*III and *BamH*I restriction enzymes (New England Biolabs Ltd.) using 1-4 µg DNA in NEB2 buffer according to manufacturer's directions. All digestion reactions were incubated at 37°C for 1 hour. Restriction digest reactions were purified on a 0.7% agarose gel stained with SYBR® Safe. Bands of interest were excised and recovered using either QIAquick® Gel Extraction Kit (Qiagen) or E.Z.N.A.® Gel Extraction Kit (Omega Bio-Tek). Ligation of *orct* amplicons into the baculovirus system (pFastBac™1; pAcBac) was done at Pacific Agri-Foods Research Center, Summerland, B.C. by Nadia Sokal. Ligations of *orct* amplicons into the transient p2ZOPe2 vector were performed at the University of British Columbia, Kelowna, B.C. by the author. Purified DNA was assessed for quantity and quality using a BioPhotometer Plus with Hellma® Tray Cell. Concentrations of purified DNA ranged from 7.5-20.5 ng μL^{-1} and had A260/A280 purity ratios of 1.7–2.2.

3.2.5 Cloning into p2ZOPe2

Amplicons of *orct* were ligated into p2ZOPe2 using T4 DNA ligase (Promega) with an insert to vector ratio of 3:1, for 2 hours at room temperature before transformation into high efficiency JM109 *E.coli* cells (Promega) according to manufacturer's protocols. Resultant *orct*-p2ZOPe2 constructs were designated: pZOP$^{5'HA\text{-}orct}$, pZOP$^{orct\text{-}HA3'}$, and pZOP^{orctN} to reflect the presence of the HA-tag sequence (Figure 3.1). Cells were plated onto

LB agar plates supplemented with 30 μg mL^{-1} zeocin and incubated 37°C overnight. No insert control plasmids ($pZOP^{ctl}$) were transformed and plated as a negative control. Colonies were screened for positive inserts using PCR on a C1000™ Thermal Cycler with the following cycling conditions: an initial denaturing for 10 minutes at 95°C, followed by 35 cycles of denaturing at 95°C for 30 s, annealing at 69°C for 30 s and elongation at 72°C for 2 minutes. Each PCR reaction contained 12.5 μL GoTaq® Hot Start Green Master Mix, 0.13 μL Triton-X and 1 μL each of forward and reverse primer (100 μmol L^{-1}) in a total reaction volume of 25 μL. The tip of a pipette was used to select a colony that was transferred to the inside of a 0.2mL PCR tube to supply template for the reaction. The tip was subsequently used to streak an LB agar plate that was grown overnight at 37°C. Products from the PCR were visualized on a 1% agrose gel stained with SYBR® Safe. Based on the results of the PCR, 5 positive colonies were randomly chosen for each construct for long-term storage in a 10% (*v/v*) glycerol solution, and of these stored colonies, 1 clone for each construct was selected to inoculate 5 mL of LB media. The colony was incubated for 16 hours at 37°C with shaking (170 rpm) and zeocin selection (30 μg mL^{-1}). After this first incubation and selection a 50 mL volume of LB media with 30 μg mL^{-1} zeocin was subsequently inoculated and incubated for 24 hours at 37°C. The OD600 of the 50 mL inoculum was assessed repeatedly using a Biophotometer plus with a Hellma® TrayCell until an optical density of 2-4 was reached. Plasmids were purified using E.Z.N.A.® Midi Prep Kit (Omega Bio-Tek) according to manufacturer protocols, with resulting plasmid yields from 71.5 ng μL^{-1} – 299.8 ng μL^{-1} with A260/A280 between 1.7- 1.88. Plasmids for each construct were digested in a 10μL volume with *BamH*I and *Hind*III using NEB2 Buffer according to manufacturer's instructions and visualized on a 1% agarose gel stained with SYBR® Safe to confirm the correct insert size (data not shown).

3.2.6 Cloning into p*Ac*BAC

In order to produce a final bacmid containing *orct*, the *orct*-HA constructs were first inserted into the transfer vector pFastBac™1. A single bacterial colony containing the pFastBac™1 plasmid was isolated from an LB-agar plate and used to inoculate a 3 mL culture of LB media supplemented with 100 μg mL^{-1} of ampicillin and 7 μg mL^{-1} of gentamycin. Plasmids were isolated using EZ-10 Spin Column Plasmid DNA Minipreps Kit (Bio Basic Inc., Markham, ON). pFastBac™1 contains two Tn7 transposition sites encompassing the multiple cloning site of the vector as well as conferring ampicillin and gentamycin resistance to the transfected bacteria (Figure 3.2). pFastBac™1 was linearized with *Hind*III according to manufacturer's protocols for 2 hours at 37°C in a 50 μL reaction volume. After 2 hours the buffer was adjusted with 50 mmol L^{-1} NaCl to optimize for *BamH*I. *BamH*I was added bringing the reaction volume to 55 μL, and the reaction was incubated an additional hour at 37°C. Digests were purified on a 0.7% agarose gel stained with ethidium bromide. The linear plasmid was excised and purified using QIAquick® Gel Extraction Kit (Quiagen). Previously prepared amplicons (5'HA-*orct*, *orct*-HA3', *orct*N) were ligated using a 3:1 insert to vector ration with T4 DNA ligase into pFastBac™1 in a 20 μL reaction volume at 16°C for 4 hours. Constructs for pFastBac™1 (pFastBac$^{5'HA\text{-}orct}$, pFastBac$^{orct\text{-}HA3'}$, pFastBac^{orctN} and pFastBac^{ctl}) were transformed into electrocompetent DH10β cells (Sharma and Shimke, 1996), and cells were spread onto LB-agar plates supplemented with 50 μg mL^{-1} ampicillin and 7 μg mL^{-1} gentamycin and incubated overnight at 37°C. Two colonies for each construct were isolated and used to inoculate 3mL cultures of LB media supplemented with ampicillin (50 μg mL^{-1}) and gentamycin (7 μg mL^{-1}). The cultures were incubated with shaking (170 rpm) overnight at 37°C and plasmids were isolated using EZ-10 Spin Column Plasmid DNA Kit (Bio Basic Inc.). Products were

visualized on a 0.7% agarose gel stained with ethidium bromide to determine plasmid quality and quantified using a Biophotometer (Eppendorf). Plasmids were digested with *Hind*III and *BamH*I (described above) and resolved on a 0.7% agarose gel with ethidium bromide to confirm the presence of the *orct* insert (data not shown).

Competent cells containing the the *Ac*MNPV bacmid, bmon14272 (p*Ac*Bac) and pmon7124 helper plasmid were provided by Dr. G. Blisserd's Lab (Cornell University, Ithaca, NY) in 2005 and have been stored by Dr. D. Theilmann's Lab (PARC, Summerland, BC).

Competent cells were prepared by inoculating a 3 mL culture of LB media supplemented with 50 μg mL^{-1} kanamycin and 10 μg mL^{-1} tetramycin and incubating the culture overnight at 37°C with shaking at 170 rpm. The 3 mL culture was used to inoculate 100 mL YENB media (3.75 g Bacto© Yeast Extract, 4 g Difco© Nutrient Broth in 500 mL distilled water adjusted to pH7.5 with NaOH and autoclaved to sterilize) supplemented with 50 μg mL^{-1} kanamycin and 10 μg mL^{-1} tetramycin and was incubated at 37°C with shaking (170 rpm) until an OD600 of >0.7.

Cells were chilled in a 4°C fridge for 5 minutes and collected by centrifugation at 4 000xg for 10 minutes at 4°C. Duplicate washes were performed by resuspending cells in 50 mL of cold distilled water and collecting cells by centrifugation at 4 000xg for 10 minutes at 4°C. Cells were resuspended in 20 mL of cold 10% (*v/v*) glycerol solution, collected by centrifugation at 4 000xg for 10 minutes at 4°C and resuspended once more in 1 mL 10% (*v/v*) glycerol.

Transformation capability of competent cells was tested by electroporating with a pGEM®-T vector (Promega).

Constructs of *orct*-pFastBac™1 were transformed by combining 100 ng of plasmid with 20 µL of competent cells containing p*Ac*Bac and the helper plasmid pmon7124 and electroporating the cells (Sharma and Shimke, 1996). Cells were incubated in 750 µL LB media overnight at 37°C with shaking (170 rpm) to allow site-specific transposition of *orct* from pFastBac™1 to p*Ac*Bac. Cells were plated onto LB agar supplemented with kanamycin (50 µg mL^{-1}), tetramycin (10 µg mL^{-1}), gentamycin (7 µg mL^{-1}), 10 µL of 0.5 mol L^{-1} isopropyl β-D-1-thiogalacropyranoside and 40 µL of 20 mg mL^{-1} 5-bromo-4-chloro-3-indolyl-β-D-galacropyranoside. Successful transformants designated p*Ac*Bac$^{5'\text{HA-}orct}$, p*Ac*Bac$^{orct\text{-HA3'}}$, p*Ac*Bac$^{orct\text{N}}$ and p*Ac*Bac$^{\text{ctl}}$, were white in color and were restreaked on LB agar supplemented with gentamycin (7 µg mL^{-1}) and kanamycin (50 µg mL^{-1}) for selection and incubated overnight at 37°C. For each construct, a single colony was used to inoculate a 3 mL culture of LB media with gentamycin (7 µg mL^{-1}) and kanamycin (50 µg mL^{-1}) selection. Each bacmid was isolated using a modified plasmid mini kit for bacmid DNA. 1.5 mL of a 3 mL overnight culture of LB media was used to pellet cells at 10 000xg for 1 minutes. Cells were resuspended in 0.25 mL of Solution 1 (15 mM Tris pH 8, 10 mM EDTA with 100 µg mL^{-1} RNase A). Cells were lysed by adding 0.25 mL of Solution 2 (0.2 N NaOH, 1% sodium dodecyl sulfate) and the mixture was incubated at room temperature until the lysate cleared. Cell debris were precipitated by adding 0.25 mL cold Solution 3 (3 mol L^{-1} potassium acetate adjusted with glacial acetic acid to pH 5.5) and mixing by inversion. Tubes were incubated for 10 minutes on ice and centrifuged for 10 minutes at 4°C at 10 000xg. The supernatant was removed by pipetting and DNA was pelleted by adding 0.8 mL isopropanol and spinning at 13 000xg for 15 minutes. The pellet was washed with 0.7 mL of 70% ethanol. The dry pellet was resuspended in 40 µL of Tris-EDTA buffer with 0.2 µL RNase A. DNA was incubated for 20 minutes at 37°C to allow the RNase A to work. The

RNase was degraded by heating to 65°C for 10 minutes and allowing the DNA to cool. DNA was stored at -80°C.

3.2.7 Transfection and Collection of Budded Virus

Transfections with *orct*-HA constructs ligated into p2ZOPe2 (pZOP$^{5'HA\text{-}orct}$, pZOP$^{orct\text{-}HA3'}$, pZOP^{orctN} and pZOP^{ctl}) or p*Ac*Bac (p*Ac*Bac$^{5'HA\text{-}orct}$, p*Ac*Bac$^{orct\text{-}HA3'}$, p*Ac*Bac^{orctN} and p*Ac*Bac^{ctl}) were performed using Sf9 cells cultured in TC100 media supplemented with 10% fetal bovine serum (FBS) and 0.1% gentamycin (50 mg mL^{-1} stock). Transfections were performed in 6 well plates in duplicate on 1x10^6 cells. Liposomes were previously prepared by combining DDAB (dimethyldioctadecyl-ammonium bromide) and DOPE (L-alpha-phosphatidylethanolamine dioleoyl) in a 1:2 molar ratio. Transfection cocktail for each well contained 15 µL lipofectin, 85 µL Grace's Insect Media (Sigma-Aldrich, Oakville, ON) and 1 µg DNA adjusted for genome size. Grace's Insect Media was added to bring the mixture to a volume to give 1 mL/well of transfection cocktail following a 15 minute incubation of the components at room temperature. Transfections with uncut plasmids (pZOP^{ctl} and AcBac^{ctl}) acted as negative controls. A parallel transfection with a plasmid containing a green fluorescent protein (GFP) construct, 501 pE38-GFP, was used as a positive control. Mock transfections, which underwent the same washes but lacked the addition of DNA, were used to compare the health of the cells following transfection. Cells were prepared by duplicate washes with 1.5 mL of Grace's Insect Media prior to the addition of 1 mL of the transfection cocktail, containing 1 µg DNA to each well. Plates were incubated for 4 hours at 27°C in a humid container. Following incubation, the transfection cocktail was aspirated off and cells were washed once with 1.5 mL Grace's Insect Media and left to incubate overlaid with 1.5 mL TC100 Media (400 mL Grace's Insect Media, 50 mL FBS, 50 mL lactalbumin/TC-

Yeastolate, 500 µL gentamycin (50 mg mL^{-1})) for 24 and 48 hours from the addition of the transfection cocktail at 27°C.

Cells were collected into 1.5 mL tubes at 24 and 48 hpt following two washes of 1x phosphate buffered saline (PBS; 137 mmol L^{-1} NaCl, 2.7 mmol L^{-1} KCl, 8.1 mmol L^{-1} $Na_2HPO_4 \bullet H_2O$, 1.76 mmol L^{-1} KH_2PO_4 with pH 7.4) by scraping the wells with a rubber policeman. Cells were pelleted by centrifugation at 1000xg for 5 minutes and the supernatent removed. Cells were stored at -80°C until further analysis.

Budded virus (v5'HA-*orct*, v*orct*-HA3', v*orct*N) was collected 5 days post transfection by collecting the overlaid TC100 media through pipetting. Collected media was centrifuged at 1000xg for 5 minutes to remove cellular debris and the supernatant containing the BV was transferred to a new tube. Budded virus was stored at 4°C until future use.

Images were captured at 24 and 48 hpt using a Nikon Diaphot microscope outfitted with a Nikon D700 camera using Nikon Camera Control Pro Software (Nikon Instruments Inc., Melville, NY). Bright field shutter speed was 1/125 seconds and shutter speed for GFP images was 0.5 s using a DM501 Nikon Filter and a Nikon Super Hi Pressure Mercury Lamp (Nikon Instruments Inc.).

3.2.8 Infection

Previously collected BV (v5'HA-*orct*, v*orct*-HA3', v*orct*N) was used to infect Sf9 cell lines. Infections were performed in 6 well plates in duplicate for each construct on $1x10^6$ cells. Cells were plated and left to adhere to the wells for 1 hour at 27°C in a humid incubator. Budded virus was applied at a multiplicity of infection of 5, assuming a virus titre of $1x10^8$ plaque forming units/mL (D. Theilmann, personal communication). Plates were incubated for 1 hour at 27°C with manual agitation every 10 minutes. Following

incubation the virus was removed and the cells underwent triplicate washes with 1.5 mL Grace's Insect Media. Cells were overlaid with 1.5 mL of TC100 media and left to incubate at 27°C. Cells were collected at 24, 48, 72 and 96 hpi using the collection method described in the previous section. Mock infections served as negative controls and were collected at 24, 72 and 96 hpi.

3.2.9 Protein Preparation and Sodium Dodecyl Sulfate Polyacrylamide Gel Electrophoresis

To prepare protein for gel loading, $1x10^6$ cells were resuspended in a solution of 50 µL 2x SDS PAGE (sodium dodecyl sulfate polyacrylamide gel electrophoresis) loading buffer (100 mmol L^{-1} Tris-HCl pH 6.8, 4% SDS, 0.2% bromophenol blue, 20% glycerol, 200 mmol L^{-1} β-mercaptoethanol), 1 µL 100x protease inhibitor (P8340-5mL, Sigma-Aldrich), 1 µL β-mercaptoethanol, 48 µL 1x PBS. Genomic DNA was sheared by passing cells through a 25 gauge syringe needle 3 times with subsequent heat denaturing for 10 minutes at 100°C. The SDS PAGE matrix was prepared according to Sambrook and Russell (2001) for a 4% stacking and 10% resolving gel using the Mini PROTEAN® II Electrophoresis Cell (Bio-Rad). Briefly, the 4% Stacking gel consisted of: 1.85 mL Distilled water, 750 µL 0.5 mol L^{-1} Tris-HCl pH 6.8, 15 µL 20% SDS, 0.35 µL 30% acrylamide/bis-acrylamide, 15 µL 10% ammonium persulfate and 6 µL TEMED (N,N,N',N'-tetramethylethylenediamine), and the 10% resolving gel consisted of a solution of: 4.07 mL distilled water, 2.5 mL 1.5 mmol L^{-1} Tris-HCl pH 8.8, 50 µL 20% SDS, 3.33 mL 30% acrylamide/bis-acrylamide, 50 µL 10% ammonium persulfate, 5 µL TEMED. One lane was loaded with 10 µL COLORPLUS™ Prestained Protein Ladder (New England Biolabs Ltd.) and 5.5 µL of sample was loaded to

represent protein from 50 000 cells. Gels were prepared in duplicate and run at 70 mV through the stacking gel and then at 125 mV through the resolving gel.

3.2.10 Coomassie Staining and Western Blotting

To visualize total protein, 1 SDS-PAGE gel was stained with Coomassie® Brilliant Blue R250 (Invitrogen) overnight at room temperature with shaking. Stain is prepared by dissolving 1 g Coomassie® Brilliant Blue R250 in 400 mL 95% ethanol, 100 mL glacial acetic acid and 500 mL distilled water. Gels were destained the following day with a solution of 400 mL 95% ethanol, 100 mL glacial acetic acid and 500 mL distilled water at room temperature with shaking until protein bands were visible.

Western blotting was used for site-specific detection of the HA-tagged ORCT protein. Protein was transferred from an SDS-PAGE gel by electroblotting to a 6 cm X 8.5 cm piece of polyvinylidene fluoride membrane (Immobilon-P, Millipore) previously soaked in methanol to wet. Transfer buffer consisted of 6.06 g Tris base, 28.82 g glycine, 400 mL methanol and 1600 mL water. The Mini Trans-Blot® Cell (Bio-Rad) was assembled according to manufacturer's directions and left overnight at 4°C at 50 V for transfer.

Membranes were blocked in excess blocking solution (20% (*w/v*) skim milk powder, 0.5% Tween-20 in 1xPBS) for one hour at room temperature with shaking. Blots were probed using a mouse monoclonal anti-HA antibody (Covance, Princeton NJ) applied at a 1:10 000 dilution in 10 mL of blocking solution and left to shake for 1 hour. The secondary peroxidase-conjugated goat anti-mouse IgG antibody (Medicorp Inc., Montreal, QC) was applied at 1:10 000 dilution in 10 mL of blocking solution and left for 1 hour. Membranes were washed 3 times for 15 minutes with a solution of 1xPBS and 0.5% Tween-20. Blots were exposed with Western Lighting® Plus ECL Enhanced Chemiluminescence System

(PerkinElmer, Ma, USA) and developed using autoradiographic film (GE Healthcare Ltd., Mississauga ON) following standard darkroom procedures, with 1 s exposure, 2 minute development, 30 s stop and a 2 minute fixation. Ladders were visualized by exposing film overnight, developing the film, and manually overlaying the images.

3.2.11 Selection for Stable Expressing Polyclonal Cell Line

Transient transfections with p2ZOPe2 containing *orct* inserts were performed in T25 flasks seeded with $1x10^6$ cells using the lipofectin protocol described in the previous sections. The transfection cocktail was removed following a 4 hour incubation at 27°C and replaced with 2.0 mL fresh TC100 media supplemented with 10% FBS and 0.1% gentamycin. At 72 hpt, cells expressing ORCT were selected for with supplemented TC100 media containing 250 ug mL^{-1} zeocin for 2 weeks to generate polyclonal stably transformed cell lines. These cells were collected and stored at -80°C

3.3 Results

3.3.1 Proof of Method

Figure 3.3 showed the successful transfection of the pE38-GFP control plasmid 24 and 48 hpt. Images were taken of Sf9 cells under UV conditions to visualize the GFP. Fluorescent signals from the GFP were detectable 24 hpt and expression appeared to increase over the next 24 hours (Figure 3.3.A; C). Images of mock transfected Sf9 cells 48 hpt showed no detectable background fluorescence indicating that any fluorescent signal seen was due to successful transfection of the control plasmid. Images taken of cells using a light microscope confirmed that cell morphology remained unchanged between the mock and transfected cells over 48 hours.

3.3.2 Transfection Results

Sf9 cells were collected at 24 and 48 hours following transfection with constructs of p*Ac*Bac (p*Ac*Bac$^{5'HA\text{-}orct}$, p*Ac*Bac$^{orct\text{-}HA3'}$, p*Ac*Bac^{orctN}) and p2ZOPe2 (pZOP$^{5'HA\text{-}orct}$, pZOP$^{orct\text{-}HA3'}$, pZOP^{orctN}) and protein expression was analyzed through Western blotting and Coomassie staining.

Figure 3.4 showed transfection results from p2ZOPe2. Western blotting with an HA antibody revealed distinct bands for both constructs containing the HA-tag sequence at both 24 and 48 hpt. At 24 hpt, a clear band was visible at 60 kDa and a strong band was visible at 40 kDa (Figure 3.4.A). These bands were also visible at 48 hpt, with an additional strong band at 80 kDa (Figure 3.4.B). Mock cells and cells transfected with the p2ZOPe2 circular plasmid and the pZOP^{orctN} construct had no visible bands following Western development. This indicated the specificity of the HA antibody for the HA-tag sequence.

Coomassie stained gels representing total protein from transfected cells collected 24 hpt (Figure 3.4.C) and 48 hpt (figure 3.4.D) showed no distinct bands corresponding to bands detected through Western blotting.

Figure 3.5 showed the Western blot and Coomassie staining results from cells collected 24 and 48 hpt with the baculovirus vector p*Ac*Bac. Western blotting of cells collected 24 hpt (data not shown) did not reveal any detectable HA-tagged ORCT protein. However, the blot using cells collected 48 hpt showed distinct bands >80 kDa and between 40 kDa and 60 kDa (Figure 3.5.A). Lanes containing mock transfected cells and cells transfected with p*Ac*Bac^{orctN}, and the p*Ac*Bac bacmid had no detection of the HA-tag sequence. Distinct bands corresponding to results of the Western blot were not detected with Coomassie staining (Figure 3.5.B; C).

3.3.3 Infection Results

Sf9 cells were infected with collected budded virus from transfections conducted previously. Cells were collected 24, 48, 72, 96 hpi and ORCT protein expression was analyzed by Western blot and Coomassie stains.

Figure 3.6 showed the Western blot results of infection with v5'HA-*orct* and v*orct*-HA3' over four collection time points. Bands were visible at all time points following infection with each of the 2 viruses with the HA-tag sequence.

Infection with v5'HA-*orct* (Figure 3.6.A) showed a single faint band at 60 kDa at 24 hpi that became distinct at 48 hpi. The band at 60 kDa was observable at 72 and 96 hpi, however, the signal is nearly undetectable due to the high amount of HA detection of indiscriminate sizes from the top of the membrane to approximately 40 kDa. Starting at 72 hpi a band was detected at 30 kDa and was also present at 96 hpi.

Figure 3.6.B showed results of the Western blot following infection with v*orct*-HA3'. At 24 hpi a single, distinct band at 60 kDa was detected. The band at 60 kDa was also observed at 48, 72, and 96 hpi, however, the signal was obscured at these time points by high amounts of signal from the top of the blot to 40 kDa of indeterminable sizes. The 60 kDa band is clearly represented on the original autoradiography film, but digital reproduction is less clear. At 48 hpi a double band just below 40 kDa, a band just below 30 kDa and 2 bands between 20 kDa and 25 kDa were also detected. The same band pattern is observed at 72 and 96 hpi, with intensities increasing over time. Lanes with protein from mock wells showed no signal, indicating the specificity of the HA antibody for the HA-tag sequence (data not shown).

A Coomassie stained gel representing total protein from infected cells with the virus v5'HA-*orct* (Figure 3.6.C) showed no distinct bands corresponding to bands detected

through Western blotting. Figure 3.6.D showed results of Coomassie staining protein collected from cells infected with v*orct*-HA3'. Cells collected 24 – 72 hpi showed no distinct bands corresponding to the bands detected by Western blotting. At 96 hpi dark protein bands were observed between 50-60 kDa, a doublet was seen between 40-50 kDa as well as a band slightly larger than 30 kDa and slightly less than 30 kDa. These signals correspond with signals observed on the v*orct*-HA3' Western blot (Figure 3.6.B, Lanes 7-8).

3.4 Summary

ORCT was expressed successfully in insect Sf9 cell lines using both transfections with a transient and baculovirus vector, and infection with collected BV. Proof of method was confirmed through the parallel transfections with a plasmid containing a GFP construct. GFP production was observed through fluorescent imaging as soon as 24 hpt and appeared to increase in intensity over the next 24 hours. Following transfection with p2ZOPe2 constructs, the HA-tag was detected at all time points tested, although protein was not detected through Coomassie staining. Bands detected through Western blotting near 60 kDa (Figure 3.4.A; Figure 3.6.B) correspond to the predicted molecular weight of the ORCT protein (Chapter 2). Bands less than 60kDa are most likely the result of protein turnover and degradation within the cells. Bands larger than 60 kDa could be the result of post-translational modifications of the protein. Alternatively, multiple banding patterns could be due to non-specific binding of the secondary antibody. Transfection with p*Ac*Bac was detected through Western blotting at 48 hpt, but not at 24 hpt. The blots included bands > 80kDa and between 40 – 60 kDa. No protein was detected for p*Ac*Bac transfection through Coomassie staining. Following infection with BV, the HA-tag was detected at all time points tested, and bands increased in intensity from 24 hpi to 96 hpi. Protein bands

were detected by Coomassie staining following infection with v*orct*-HA3' only at 96 hpi. These bands correspond to bands detected through Western blotting. The specificity of the HA antibody for the HA-tag sequence indicated successful expression of the ORCT protein. Protein was detected through both transfections and infections with various expression vectors. Functional studies using transfected Sf9 cells expressing the ORCT protein are needed to confirm that the protein is functional and expressed to a level high enough to be physiologically relevant. Results of this chapter indicated that Sf9 cells could be a potential expression system for the study of ORCT and ORCT2 function.

Table 3.1 Expression primers for cloning into pFastBac™1 (FB) and p2ZOPe2 (OP). Primer color coding: black, 5' end tag; red, restriction site; blue, Kozac sequence; tan, HA-tag sequence; green, gene of interest with bolded start and stop codons. Primer naming code: FB, pFastBac™1; OP, p2ZOPe2; f, forward; r, reverse; 1 or 2, pair number; HA, HA-tag; NHA, no HA-tag; bam, *BamH*I; hind, *Hind*III.

		Primer Qualities			Attributes	
Primer Name	Primer Sequence (5' →)	Length	GC %	Tm	RE	Tag
FBf1HAbam	5' – cgc gga tcc gcc acc **atg** tac ccc tac gac gtg ccc gac tac gcc ggc tac gac gac gtc atc acc	66	62.1	74.5	BamHI	HA
FBf2NHAbam	5' – cgc gga tcc gcc acc **atg** ggc tac gac gac gtc atc acc	39	66.7	73.0	BamHI	X
FBr1NHAhind	5' –gac aag ctt **tta** gcc gga ctg tcc gtt cag cat tc	35	51.4	65.7	HindIII	X
FBr2HAhind	5' – gac aag ctt **tta** ggc gta gtc ggg cac gtc gta ggg gta gcc gga ctg tcc gtt cag cat tc	62	58.1	72.8	HindIII	HA
OPf1HAhind	5' – tta aag ctt gcc acc **atg** tac ccc tac gac gtg ccc gac tac gcc ggc tac gac gac gtc atc acc	66	59.1	73.9	HindIII	HA
OPf2NHAhind	5' – tta aag ctt gcc acc **atg** ggc tac gac gac gtc atc acc	39	53.8	68.8	HindIII	X
OPr1NHAbam	5' – gat gga tcc **tta** gcc gga ctg tcc gtt cag cat tc	35	54.3	66.2	BamHI	X
OPr2HAbam	5' – gat gga tcc **tta** ggc gta gtc ggg cac gtc gta ggg gta gcc gga ctg tcc gtt cag cat tc	62	59.7	73.0	BamHI	HA

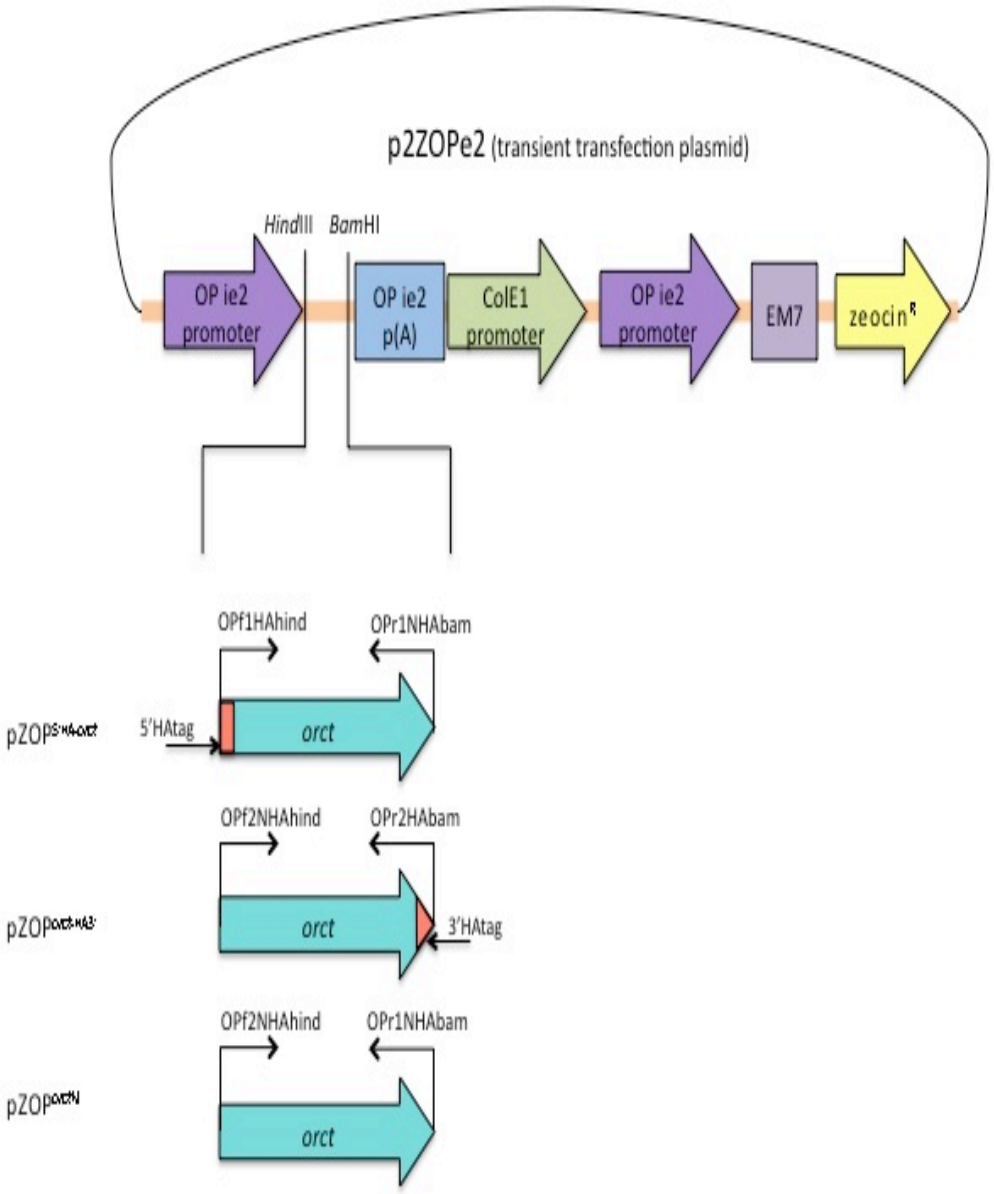

Figure 3.1 Schematic diagram showing constructs and cloning into p2ZOPe2. The vector is under the control of 2 ie2 promoters. One controls transcription of the foreign gene, the other controls transcription of zeocin resistance in Sf9 cells. The ColE1 promoter controls replication of the plasmid in bacterial cells, while a bacterial promoter (EM7) controls transcription of a zeocin resistant gene in bacterial cells. Each construct was flanked by *Hind*III and *BamH*I restriction sites for insertion into the plasmid, and has a Kozac sequence for ribosomal recognition at the 5' end. Additionally, an HA-tag sequence was added to one construct at the N-terminus and one construct at the C-terminus.

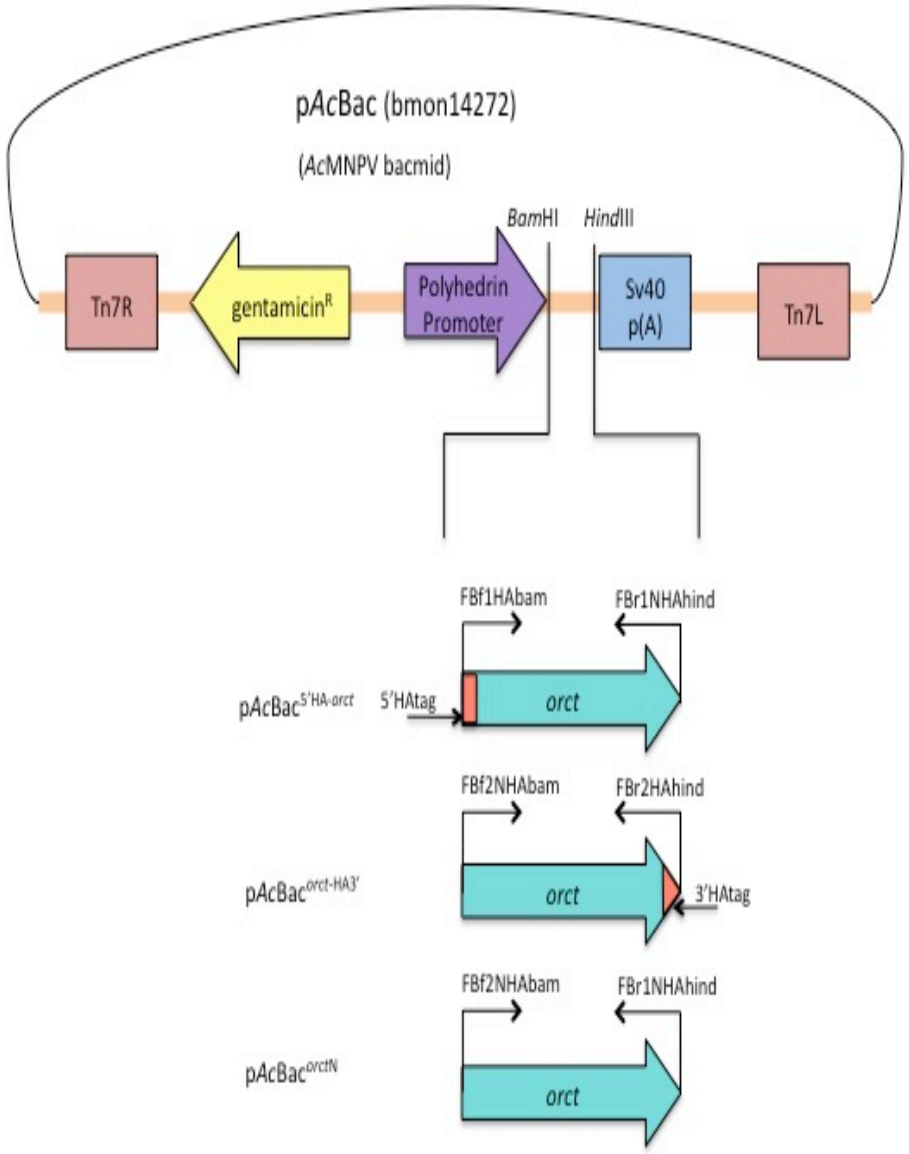

Figure 3.2 Schematic diagram showing constructs and cloning into p*Ac*Bac. Insertion of the Tn7 transposition sites from the shuttle vector pFastBac™-1 containing the foreign gene are shown. Transcriptional regulation of the foreign gene is under the control of a polyhedrin promoter. The vector contains an Sv40 poly-A tail that is added to the foreign gene transcript. A gentamicin resistance gene confers selection to both p*Ac*Bac and to the shuttle vector pFastBac™-1. Each construct was flanked by *Hind*III and *BamH*I restriction sites for insertion into the plasmid, and had a Kozac sequence for ribosomal recognition at the 5' end. Additionally, an HA-tag sequence was added to one construct at the N-terminus and one construct at the C-terminus.

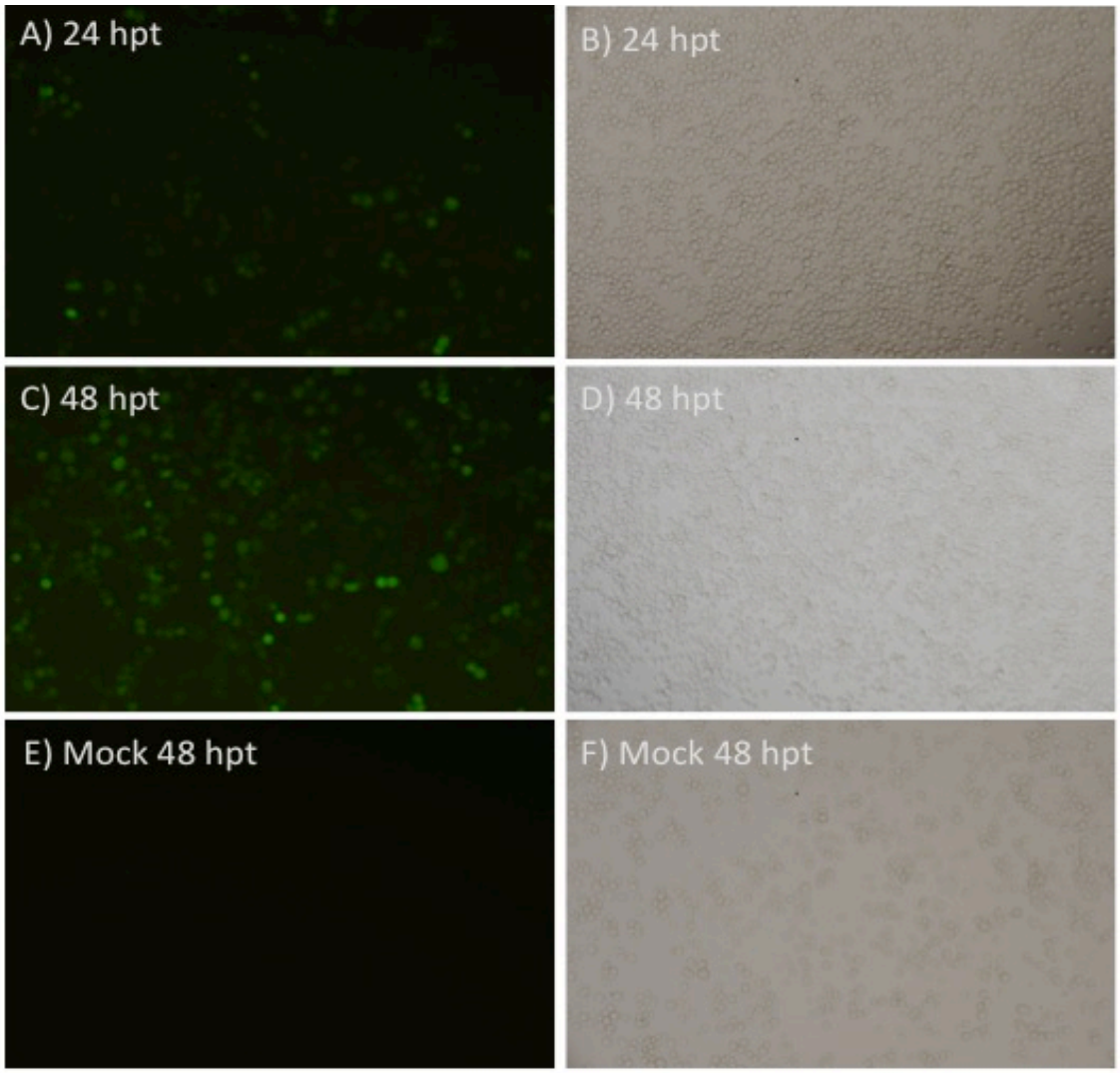

Figure 3.3 Images of Sf9 cells following transfection with pE28-GFP. GFP images 24 hpt (A) and 48 hpt (C) showed positive transfections. Bright field images 24 hpt (B) and 48 hpt (D) showed the health of the Sf9 cells following transfections. Mock transfections showed no background fluorescence (E) and were used to compare cell morphology to Sf9 cells that had undergone transfection (F). Images were taken at 40x total magnification.

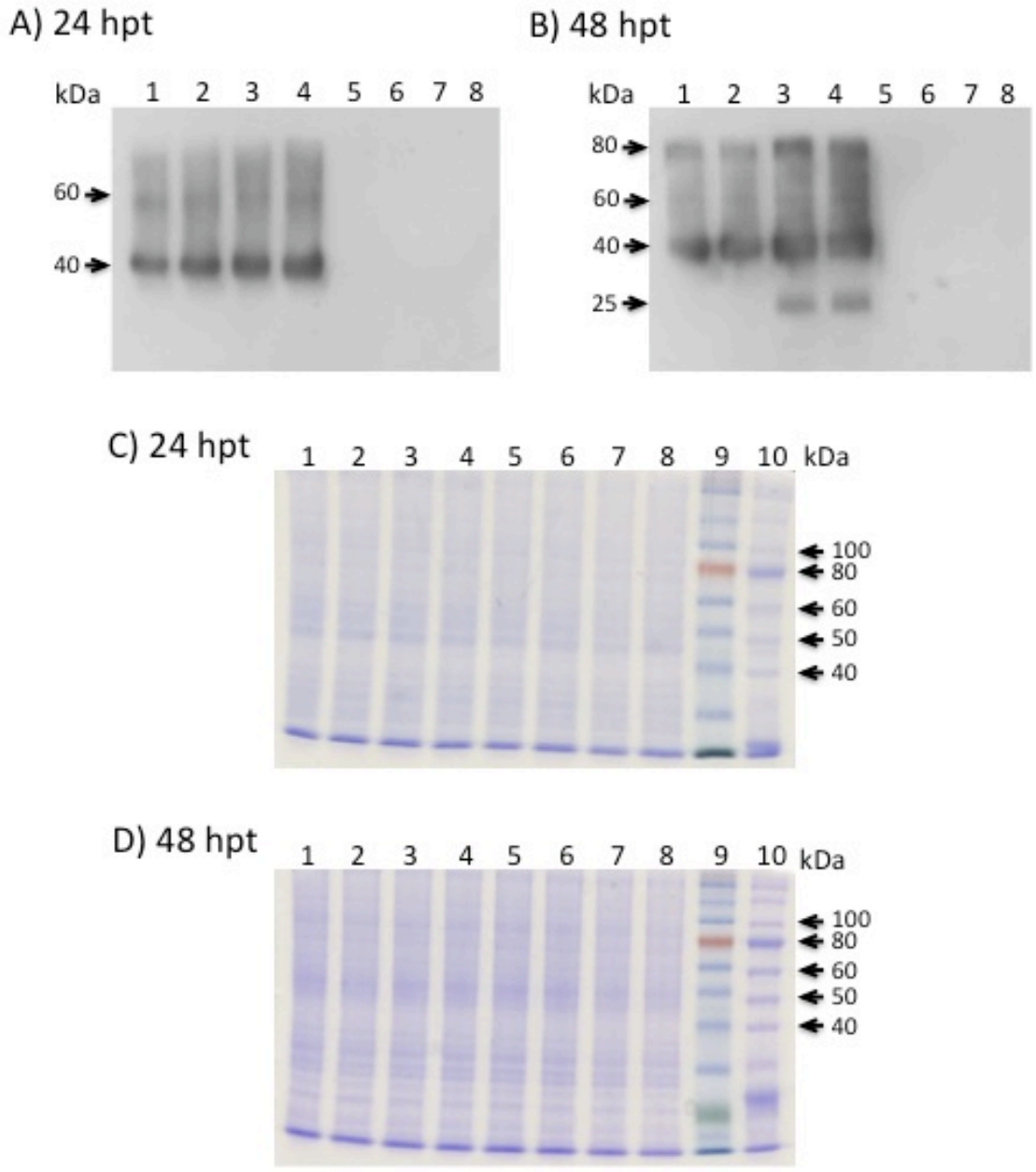

Figure 3.4 Results of transfection with p2ZOPe2 constructs. Western blots of ORCT constructs at A) 24 hpt and B) 48 hpt were probed with a primary mouse anti-HA antibody and a secondary peroxidase-conjugated goat anti-mouse IgG antibody. Lanes were loaded with two technical replicates for the following proteins: 1-2, pZOP$^{5'\text{HA-}orct}$; 3-4, pZOP$^{orct\text{-HA3'}}$; 5-6, pZOP^{orctN}; 7, pZOP^{ctl}; 8, mock. Coomassie stained SDS-PAGE gels loaded with protein from cells collected from C) 24 hpt and D) 48 hpt show no distinct bands associated with the Western blot. Lanes were loaded with two technical replicates for the following protein: 1-2, pZOP$^{5'\text{HA-}orct}$; 3-4, pZOP$^{orct\text{-HA3'}}$; 5-6, pZOP^{orctN}; 7, pZOP^{ctl}; 8, mock; 9, COLORPLUS™ Prestained Protein Ladder; 10, protein ladder.

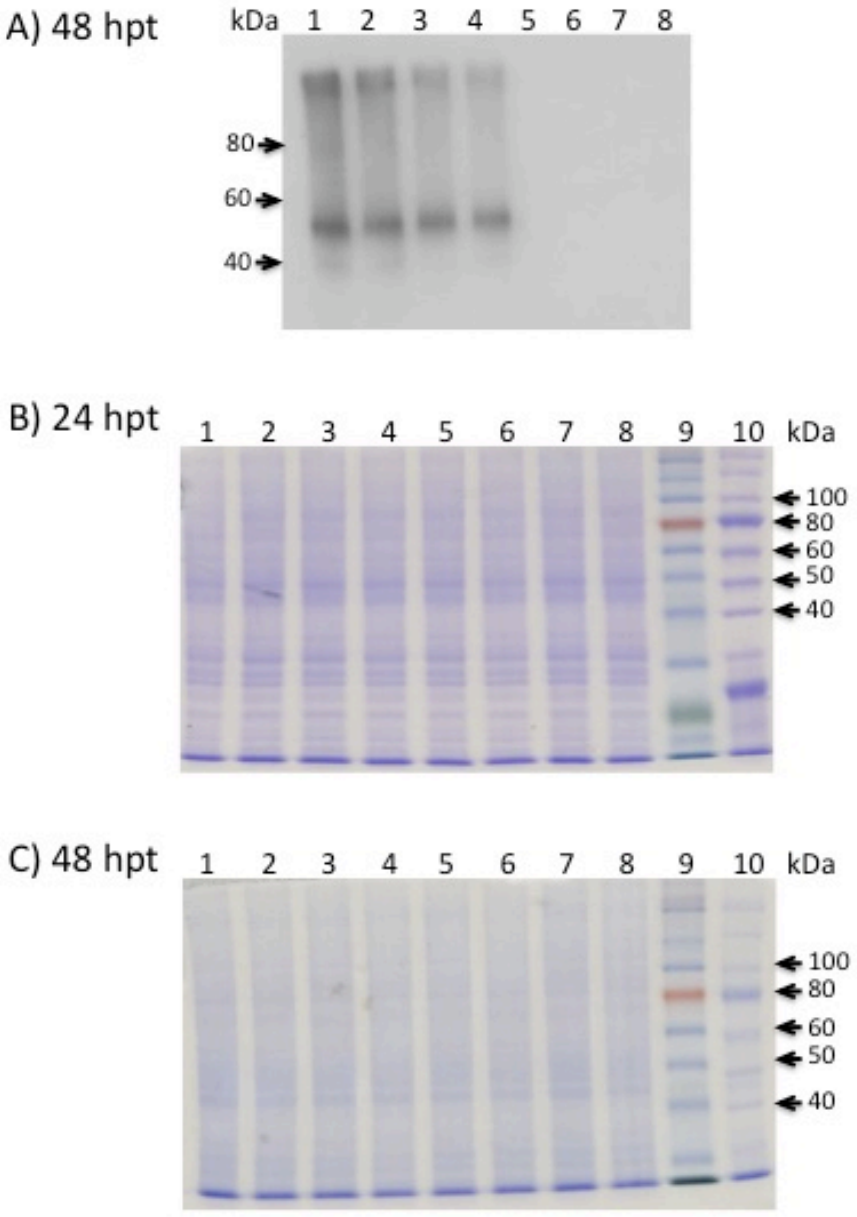

Figure 3.5 Results of transfection with p*Ac*Bac constructs. Western blots of ORCT constructs at A) 48 hpt were probed with a primary mouse anti-HA antibody and a secondary peroxidase-conjugated goat anti-mouse IgG antibody. Lanes were loaded with the following protein: 1-2, p*Ac*Bac$^{5'HA\text{-}orct}$; 3-4, p*Ac*Bac$^{orct\text{-}HA3'}$; 5-6, p*Ac*Bac^{orctN}; 7, p*Ac*Bac^{ctl}; 8, mock. Coomassie stained SDS-PAGE gels loaded with protein from cells collected from B) 24 hpt and C) 48 hpt show no distinct bands associated with the Western blot. Lanes were loaded with the following: 1-2, p*Ac*Bac$^{5'HA\text{-}orct}$; 3-4, p*Ac*Bac$^{orct\text{-}HA3'}$; 5-6, p*Ac*Bac^{orctN}; 7, p*Ac*Bac^{ctl}; 8, mock. ; 9, COLORPLUS™ Prestained Protein Ladder (NEB); 10, protein ladder.

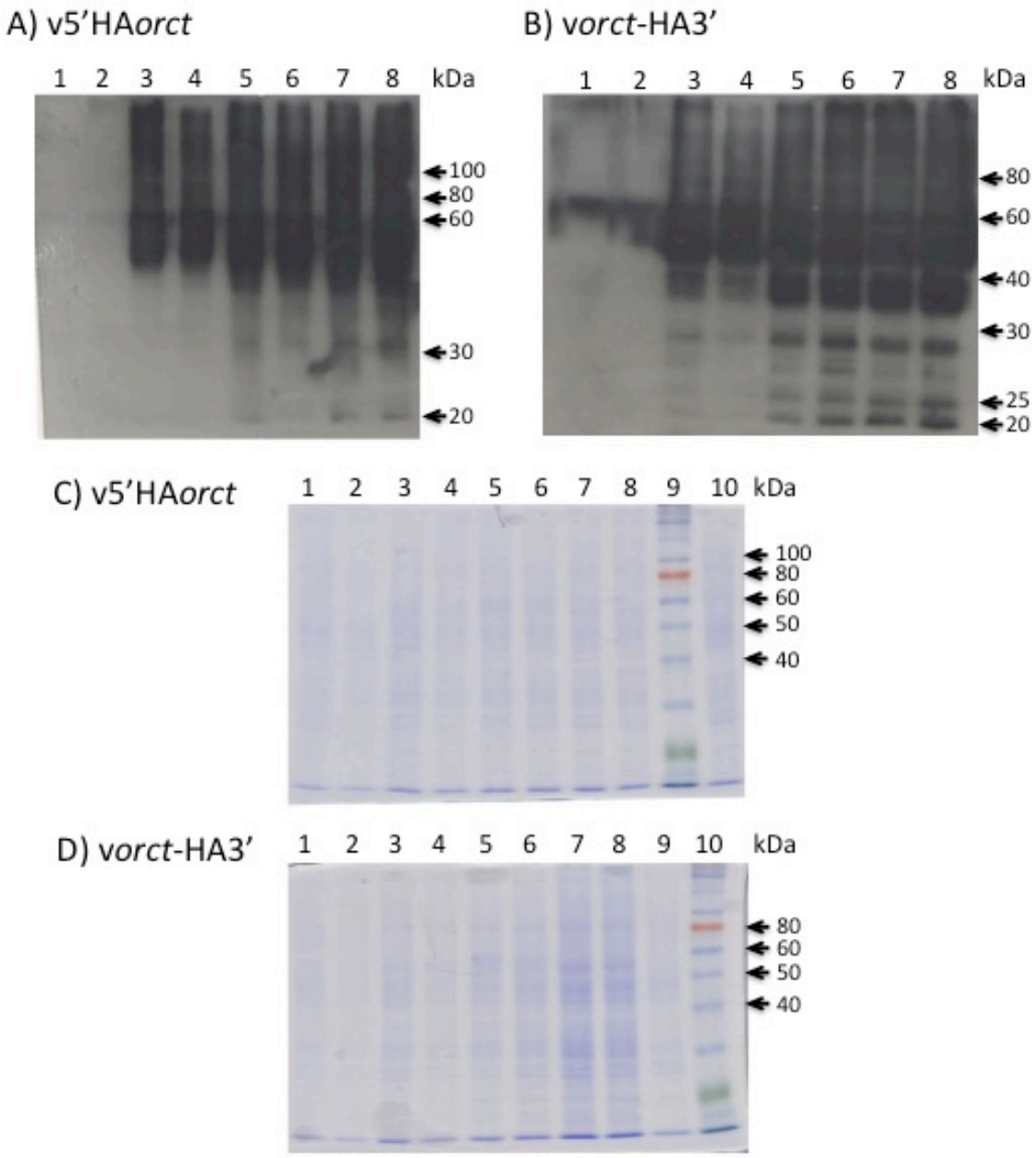

Figure 3.6 Results of infection with budded virus constructs. Western blots of A) v5'HA-*orct* and B) v*orct*-HA3' probed with a primary mouse anti-HA antibody and a secondary peroxidase-conjugated goat anti-mouse IgG antibody. Lanes were loaded with the following: 1-2, 24 hpi; 3-4, 48 hpi; 5-6, 72 hpi; 7-8, 96 hpi. Mock wells and controls were probed but are not shown as they were identical to previous controls (Figure 3.4; Figure 3.5). Coomassie-stained SDS-PAGE gels loaded with protein from cells collected from C) v5'HA-*orct* and D) v*orct*-HA3'. Lanes were loaded with the following: 1-2, 24 hpi; 3-4, 48 hpi; 5-6, 72 hpi; 7-8, 96 hpi. 9, COLORPLUS™ Prestained Protein ladder (D)-Mock); 10 mock infection (D) - COLORPLUS™ Prestained Protein Ladder.

Chapter 4 Discussion

4.1 General Discussion

Previous chapters of this thesis described the molecular identification and heterologous expression of two putative organic cation transporter genes, *orct* and *orct2*, from the fruit fly *Drosophila melanogaster*. Cloning of these transporters has provided new insights into the molecular basis of organic cation transport across *D. melanogaster* tissues by classifying the cloned sequences and elucidating the mRNA expression profiles. Previous studies had shown the ability of *D. melanogaster* MTs and midgut to transport OCs (Rheault and O'Donnell, 2004; Rheault *et al*., 2005). However, the transporter(s) governing the transcellular movement of these compounds in insects had yet to be determined. Expression of these transport proteins in insect Sf9 cell lines marks the first step at determining the function of a predicted OCT from an insect. Successful production of the ORCT and ORCT2 proteins in Sf9 cells could lead to the development of new physiological assays for the study of insect OCT proteins. The study of insect proteins within an insect expression system allows production and modification of the protein within a relatively native intracellular environment that would help to remove speculation surrounding conclusions drawn with respect to protein function when proteins are expressed in a more distantly related system (i.e. yeast, mammalian cells). Relative mRNA expression of the two gene transcripts was studied according to the newest and most stringent guidelines for qPCR analysis. The qPCR assay developed for this thesis will serve to train future students and researchers in correct experimental qPCR design. Chapter 2 describes the sequence analysis and molecular identification of the two gene transcripts as well as examination of the mRNA expression of these two genes following exposure to the prototypical type I OC, TEA. Chapter 3 is the first study to express an isolated insect OCT in a heterologous

expression system. Thus the results of this thesis provide the first molecular candidates to support previous physiological evidence for TEA transport across the tissues of *D. melanogaster*.

4.2 Molecular Identification of Organic Cation Transporters in *D. melanogaster*

Two putative OCT genes had been previously identified in *D. melanogaster* and named *orct* (Taylor *et al.*, 1997) and *orct2* (Hoskins *et al.*, 2007). I have cloned and conclusively sequenced these putative genes for the first time. Using sequence analysis tools, these genes have been molecularly classified based on peptide sequence and phylogenetics. Alignments between the cloned nucleotide sequences and the predicted sequence for *orct* and *orct2* showed a number of silent nucleotide substitutions, as well as substitutions which resulted in amino acid transitions (Table 2.5; Table 2.6, Chapter 2). The contiguous sequence for each gene that was created from 5 times sequencing coverage of 4 isolated clones, yielded identifiable nucleotide sequences for *orct* and *orct2* that were more robust than predicted sequences gathered from shotgun genome sequencing. I identified amino acid differences from the predicted genome sequence in the putative ORCT protein, which fell within TMD2 and within the intracellular carboxyl end, whereas amino acid differences in ORCT2 fell within the large extracellular loop between TMD1 and TMD2. Predicted post-translational modification sites were unaffected by any amino acid substitution. One substitution in the ORCT2 peptide sequence fell within a predicted N-linked glycosylation site. Mutation of the N-glycosylation sites of the rabbit OCT2 protein expressed in Chinese hamster ovary cells has been shown to have functional effects on the OCT2 protein (Pelis *et al.,* 2006). In that study individual mutation of the three glycoslylation sites resulted in decreased plasma membrane expression and increased

protein turnover. As a result, the transport of TEA was reduced accordingly in these mutants (Pelis *et al*., 2006). Mutation at all three N-glycosylation sites resulted in OCT2 being sequestered to an unidentified intracellular compartment (Pelis *et al*., 2006). In this study the mutation of a predicted N-glycoslylation site might suggest an effect on protein function. Further studies using mutation analysis and Western blotting to determine levels of N-glycoslylation as well as expression of mutant and wild-type ORCT and ORCT2 may provide interesting functional information with regard to insect OCT.

Additionally, a number of conserved sequence motifs indicative of vertebrate members of the major facilitator superfamily were identified in these *D. melanogaster* transporters. This supports the grouping of ORCT and ORCT2, based on sequence, into the MFS 2.A.1.19 category (2, electrochemical potential driven porters; A, uniporter/symporter/antiporter; 1, MFS; 19, organic cation transporters) (Saier, 2000). Insect orthologs of ORCT and ORCT2 shared domains with representative vertebrate orthologs, along with sharing a number of conserved sequences among themselves. This thesis proposed a number of identifiable conserved domains in insect OCT-like orthologs. This indicated a higher degree of similarity between insect orthologs compared to vertebrate orthologs. Shared identity could allow inference of function between insect orthologs following characterization of ORCT and ORCT2. Not included in this analysis was the insect orthologs from *A. aegypti*. The sequence from *A. aegypti* was observed to be highly dissimilar to both vertebrate and insect orthologs within noted conserved domains. Topology analysis yielded predicted secondary structures for ORCT and ORCT2 that contained 12 TMDs and intracellular amino and carboxyl ends. Each peptide sequence was predicted to have a large extracellular loop between TMD1 and TMD2 and a large intracellular loop between TMD6 and TMD7; both are characteristic of vertebrate orthologs

(Wright and Dantzler, 2004). A similar number of post-translational N-linked glycosylation sites were predicted between TMD1 and TMD2 in ORCT and ORCT2 as vertebrate transporters. Thus ORCT and ORCT2 based on sequence topology and conserved domains, appeared to be closely related to vertebrate OCT orthologs. Given these similarities, pairwise alignments and phylogenetic analysis were performed with the goal of further classifying and categorizing the ORCT and ORCT2 proteins.

When orthologous peptide sequences were compared, ORCT and ORCT2 had higher similarity to each other than any other ortholog pairs tested (Table 2.7, Chapter2). Similarity was high between insect orthologs with the exception of the *A. aegypti* ortholog. Rheault *et al*. (2006) found that TEA was not transported by the MTs of *A. aegypti*. The proposed rational was that *A. aegypti*, being hematophagous, possess a life history that did not require excretion of plant defensins and pesticides and had therefore not allowed the evolution of an organic cation transporter. Similarity in the *D. melanogaster* peptide sequences to individual OCT isoforms from humans was low, averaging ~30%. As well, similarity between *D. melanogaster* sequences to the predicted orthologs in *A. aegypti* was equally low (35% to ORCT), as was similarity between *A. aegypti* and human orthologs (Table 2.7, Chapter 2).

Similarity from pairwise alignments was reflected in the phylogenetic analysis of 37 ortholog sequences, representing OCT isoforms as well as OCTN isoforms and predicted insect orthologs. Also represented in the phylogram are sequences identified by Eraly and Nigam (2002, 2004), named fly-like putative transporters, or FLIPT1 and FLIPT2. These gene sequences have been included in analysis of vertebrate organic cation transporters and thus have been included in this phylogram. Preliminary studies of these proteins have shown them to be importers of an anticancer agent doxorubicin in human tumor cells

(Okabe *et al*., 2005), although functional characterization of these proteins is incomplete. Results of the phylogram indicated that ORCT and ORCT2 exist within an insect specific clade, equally divergent from OCT1 and OCT2, and OCT3 and OCTN isoforms (Figure 2.17, Chapter 2). Also reflected in the phylogram was the divergence of the *A. aegypti* predicted sequence from other transporters. Evidence described in this thesis expands upon previous research (Rheault *et al*., 2006) to suggest that *A. aegypti* may not possess a specific organic cation transporter and thus elimination of these compounds may occur through either a paracellular or p-glycoprotein mediated transport pathway.

Phylogenetic analysis was originally undertaken in the attempt to answer the question: can function of ORCT and ORCT2 be inferred by sequence similarity to a single isoform of OCT? The answer, based on the presented phylogram, is no. Although sequence domains support the grouping of OCRT and ORCT2 into the family of OCT-like transporters, equal divergence from functionally characterized transporters from vertebrates does not allow further grouping of these transporters into an identified isoform group. This could indicate that the *D. melanogaster* proteins share functional kinetic properties and substrate specificities from all isoforms found in vertebrates, or more likely, the *D. melanogaster* proteins have their own unique functional profiles. Therefore previous studies elucidating the function and substrate associations of OCT1, OCT2, and OCT3, can be used as guidelines only as to the assays that should be performed on ORCT and ORCT2, but should not be used as a predictive model as to how these transporters will function. The next step in classifying the ORCT and ORCT2 proteins then, is to functionally characterize the isolated proteins in a heterologous expression system.

4.3 Heterologous Protein Expression in Insect Sf9 Cells

This thesis described the preliminary steps of evaluating a protein expression system using a number of delivery systems with the future goal of ascertaining function of the *D. melanogaster* proteins. This is the first time any insect OCT protein would be expressed in a heterologous system for study. Insect Sf9 cells were chosen as an expression system, because as insect derived cells, previously proven to express heterologous membrane proteins (Hegedus *et al*., 1999), these cells would most closely mimic the native environments of the *D. melanogaster* proteins to allow correct post translational modification and membrane lipid composition. A BLAST search of the Sf9 cell line genome did not reveal an ortholog sequence to ORCT or ORCT2. It is possible that Sf9 cells, because of their derivation from pupal ovary, lack an OCT, which would mean that background levels of TEA transport for physiological assays should be low. Transfection of Sf9 cells with a plasmid vector as well as transfection and subsequent, parallel infection with a baculovirus were used to deliver the foreign protein. A detectable amount of HA-tagged protein was observed with all delivery methods tested through Western blotting. Detection with the HA antibody was specific to the HA tag sequence, confirmed through the use of multiple controls at each stage of the transfection/infection (Figure 3.4; Figure 3.5, Chapter 3). Intensity of detection increased over time following infection, indicating a higher amount of heterologous protein expression (Figure 3.6, Chapter 3). Banding patterns observed on the blots did not always coincide with the predicted 60 kDa molecular weight of the ORCT protein. Bands observed higher than 60 kDa could be the result of post-translational protein modification which could add roughly 12 kDa of weight from each N-linked glycosylation alone (Taylor and Drickamer, 2011). This could be confirmed through purification of the protein and digestion with N-glycanase. The protein can then be

visualized using SDS-PAGE and the protein motility observed (Lu *et al*., 1997). Bands observed lower than the predicted 60 kDa are most likely the result of protein degradation and protein turnover. Alternatively, multiple bands could indicate non-specific binding, or cross reactivity, of the secondary antibody. To test this alternate possibility a number of controls could be employed: 1) probe blots with an alternative secondary HA- antibody, 2) probe blots with the secondary antibody in the absence of the primary antibody, 3) optimize the amount of each antibody to apply with a dilution series. In the case of BV infection multiple banding could be the results of over production of the protein overwhelming intracellular protein processing systems, resulting in fragmented and unfinished protein (O'Reilly *et al*., 1994). Thus a more narrow time course with collection every 4-6 hpi would have to be conducted in order to determine an appropriate time post-infection to conduct functional assays so that expression levels are optimal.

Although, protein was detected with all delivery systems, protein was not detected at all time points tested post transfection. It has been suggested that the transfection process does not exactly match the infection process (Nie and Theilmann, 2010; Stewart *et al*., 2005). As a matter of methodology, time post transfection and time post infection is measured when either the transfection cocktail or BV respectively, is applied to the cells. However, this does not necessarily accurately represent the time when the bacmid or plasmid is incorporated into the cells. During an infection time course, uptake of the BV into the cells occurs almost immediately upon application, thus beginning the virus life cycle, whereas during a transfection time course, there may be a delay between application of the DNA and uptake into the cells and the beginning of transcription. Therefore differences observed through Western blotting between transfections with p*Ac*Bac and BV

infections, specifically the absence of detection at 24 hpt (Figure 3.5, Chapter 3), could be due to definitions of time and not actual events in the virus life cycle.

In this study, results of protein production detected by Western blotting were not, in all cases, mimicked in the Coomassie stained gels. It can be expected that staining a Coomassie gel for 24 hours allows detection of 0.1µg of protein in a visible band (Sambrook and Russell, 2001). A lack of visible bold bands observed through Coomassie staining, indicated a low amount of protein produced above background total protein levels from Sf9 cells. Infection with BV, 72 and 96 hpi yielded dark, visible bands on the Coomassie stained gel that corresponded to bands detected through Western blotting, indicating higher levels of protein production (Figure 3.6, Chapter3). However, the amount of non-specific banding in the Western due to previously discussed protein over production make these time points less than ideal for functional assays.

The research shown here laid the preliminary groundwork for expression of *D. melanogaster* OCT-like proteins in insect Sf9 cell lines. Stably expressing polyclonal Sf9 cells were produced with the p2ZOPe2 delivery vector through maintained antibiotic selection. Expression in these cells has yet to be confirmed through Western blotting, however, their creation gives future researchers the first step towards designing functional assays to characterize the ORCT protein. Functional assays are the next step in confirming Sf9 cells as an appropriate heterologous expression system for the study of these transporters. Simple uptake studies with C^{14}TEA or fluorescent labeled TEA would confirm a number of hypotheses: 1) That ORCT is able to transport TEA, 2) That the amount of ORCT protein produced in Sf9 cells is enough to allow detectable amounts of C^{14}TEA uptake, 3) The ORCT protein is functional and correctly inserted into the cell membrane, 4)

Sf9 cells have no background transport of TEA, or that background uptake of TEA is minimal in non transfected cells when compared to transfected cells.

4.4 Relative mRNA Expression of *orct* and *orct2*

Using a TEA ion-selective microelectrode, Rheault and O'Donnell (2004), demonstrated for the first time the transport of TEA across the epithelial cells of the main and lower segments of the MTs, the ureter and midgut of *D. melanogaster*. Calculation of the transport capacity of TEA in these tissues indicated that uptake was a carrier mediated, active process. The transport protein responsible for the movement of organic cations across these tissues has yet to be conclusively identified. Relative mRNA expression of the two putative OCTs, *orct* and *orct2*, was assessed across a number of *D. melanogaster* tissues using qPCR. Results indicated that *orct* was constitutively, highly expressed in the MTs relative to whole body under control conditions. This localization profile supports the previously mentioned physiological findings by Rheault and O'Donnell (2004). Although expression of *orct2* was constitutively low in the tissues tested relative to its own whole body expression, when compared to *orct*, whole body expression of *orct2* was nearly 5 fold higher. This indicates that although *orct2* expression in tested tissues was low, its expression profile could be stronger in other tissues (i.e. fat body, salivary glands).

When exposed to TEA concentrations reflecting larval LC_{50} and larval $1/2LC_{50}$ for TEA (Bijelic *et al*., 2005) for 1 and 15 generations, midgut expression increased for both *orct* and *orct2*. Rheault and O'Donnell (2004) calculated J_{MAX} for transport of TEA across the posterior midgut to be 3.7 pmol cm^{-2} s^{-1}. A value much lower than that calculated for transport kinetics of TEA across the lower MT (J_{MAX} = 17.8 pmol cm^{-2} s^{-1}). However, given the roughly 8-fold difference in surface area between the MT and midgut (Maddrell, 2009), I

propose that overall transport capacity of the midgut for TEA is higher than that of the paired MTs. Therefore any increase in gene expression of *orct* and *orct2* could, given no transcriptional regulation, play a significant part in the elimination of excess TEA from the insect across the midgut.

Rheault and O'Donnell (2004) calculated K_m values for TEA across the MTs and the midgut to be 0.13 and 0.22 respectively. K_m values could be thought of as a measure of tissue affinity for a substrate. Different K_m values in the MTs and midgut indicated that either different transporters were responsible for TEA uptake in these tissues, or that a number of transporters were differentially distributed between these tissues. The research presented in this thesis supported differential expression of *orct* and *orct2* across the Malpighian tubules and the midgut, with *orct* displaying higher expression in the MTs and *orct2* displaying higher expression in the midgut (Figure 2.19).

Increases in expression of *orct* in the MTs and ovary following 15 generations of exposure could indicate adaptation to environmental conditions. The possibility exists that changes in expression of *orct* and *orct2* could be due to a stress response, brought on by increased toxicity in the fly, due to the high amount of TEA in the media. This could be tested by studying the regulation of other stress induced genes (i.e. heat shock proteins) or by studying the expression of *orct* and *orct2* while the flies are exposed to other conditions of stress (i.e. prolonged high ambient temperature, anoxic conditions).

There was a trend observed in all tissues tested for expression to increase following 15 generations of exposure that appears to be independent of exposure concentration. Chahine and O'Donnell (2010), showed that *D. melanogaster* exposed to methotrexate, a prototypical organic anion, took over 10 generations of chronic exposure to register any observable change in gene expression. In contrast, more recent studies using *A. aegypti*,

another dipteran, have shown that increases in the expression of metal transporting, membrane bound proteins can be measured following only 24 hours of exposure (Bobyn, P. and Matier, B.J., University of British Columbia – Okanagan, unpublished data).

Expression of vertebrate OCT orthologs studied through Northern blots showed that all OCT isoforms are present in the kidney (Table 1.1, Chapter1), and most are present in the liver. This localization pattern is consistent with transporters responsible for the elimination of toxins. Presence of the *orct* and *orct2* transcripts in tissues of the insect alimentary and excretory system support the hypothesis that these transporters play at least a partial role in the elimination of organic cations from the insect.

4.5 Future Studies

Although several questions and future lines of study have been identified through this discussion, there are additional questions regarding the mechanism governing the elimination of OCs by the excretory system of *D. melanogaster* and specifically, the further characterization of ORCT and ORCT2:

1) Do the ORCT and ORCT2 proteins transport prototypical OCs such as TEA?

Characterization of the transport kinetics and substrate profiles of the ORCT and ORCT2 proteins is essential to understanding the mechanism of OC transport in *D. melanogaster* and other insects. A number of expression systems can be evaluated for the study of protein function and used to assess different qualities of the protein. Rheault and O'Donnell (2004) varied bathing concentration of TEA and observed uptake of a TEA over a series of time points to calculate K_m and J_{MAX} for flux across *D. melanogaster* tissues. Sf9 cell lines could be used for simple uptake assays that test time dependent and concentration

dependent uptake kinetics of C^{14}TEA. Cell lines can be used for competition studies using other type I and type II OCs to inhibit C^{14}TEA uptake. Expression of ORCT and ORCT2 in *X. laevis* oocytes could provide a useful model system to study the dependence on membrane voltage and the electrogenicity of the transport protein through voltage clamp studies. Rheault *et al*. (2005), varied saline concentrations of cations to mimic membrane depolarization and hyperpolarization of cells of MTs from *D. melanogaster*. Oocytes could be used in the same way, for uptake studies and inhibition studies by varying the amount of cations in the bathing saline and measuring C^{14}TEA uptake. A more recent technique that would allow similar functional assays comes from research that synthesized brush border membrane vesicles (Harvey *et al*., 2010). This technique has the benefit of using the insect's own membrane, containing its own native membrane proteins from chosen tissues to create small vesicles that can be exposed to substrates for uptake studies. The benefits of this technique are that brush border membrane vesicles do not rely on correct assembly of the protein of interest in a heterologous system and the technique allows researchers to assess transport capacity of certain tissues in isolation. The limitation is that researchers lose the ability to differentiate the contributions of individual transporters to net flux of a substrate. Instead, all transporters present on the native brush border membrane are represented in the vesicle.

2) Does protein expression mimic trends of mRNA expression and to what membrane are ORCT and ORCT2 localized?

This thesis examined mRNA expression in a few *D. melanogaster* tissues using qPCR, however, whole body localization studies using *in situ* hybridization or reverse transcription PCR would be useful in determining other tissues where the *orct* and *orct2*

transcripts are expressed. mRNA could be extracted from additional *D. melanogaster* tissues thought to be important in the elimination or sequestration of toxic compounds (i.e. hindgut, fat body, salivary gland) and analyzed for the presence of *orct* and/or *orct2* transcripts through reverse transcription PCR. If transcripts are found in certain tissues, qPCR could be used to quantify the expression within identified tissues. As a matter of practicality, as not all tissues are easily extracted in a large enough quantity for RNA extraction, whole mount *in situ* hybridization could be used as an alternative to probe for *orct* and *orct2* transcripts.

The ORCT and ORCT2 proteins could be localized to either the basolateral or apical membrane of the MTs through immunohistochemistry. mRNA expression supports the presence of these transporters in excretory tissues and based on previous studies, these transporters have been hypothesized as the basolateral membrane proteins responsible for the movement of type I OCs into epithelial cells of the MTs and midgut (Figure 1.5, Chapter1) (Rheault and O'Donnell, 2004; Rheault *et al*., 2005). It is possible therefore that one (or both) of these transporters is basolateral and that the other (or both) could act as an apical transporter. Immunohistochemistry would also allow researchers to correlate mRNA expression patters to protein expression patterns observed. It is possible that although mRNA expression increased with exposure to OCs, that this increase is not adaptive, and does not correlate to an increase in protein expression.

References

Altschul, S.F., Gish, W., Miller, W., Myers, E.W. and Lipman, D.J. (1990). Basic local alignment search tool. *J. Mol. Biol.* **215**, 403-410.

Bakos, E., Evers R., Sinko, E., Varadi, A., Borst, P. and Sarkadi, B. (2000). Interactions of the human multidrug resistance proteins MRP1 and MRP2 with organic anions. *Mol. Pharmacol.* **57**, 760-768.

Bertram, G., Schleithoff, L., Zimmermann, P. and Wessing, A. (1991). Bafilomycin A1 is a potent inhibitor of urine formation by Malpighian tubules of *Drosophila hydei*: Is a vacuolar-type ATPase involved in fluid secretion? *J. Insect Physiol.* **37**, 201-209.

Beyenbach, K.W. (2003). Transport mechanisms of diuresis in Malpighian tubules of insects. *J. Exp. Biol.* **206**, 3845-3856.

Bijelic, G., Kim, N.R. and O'Donnell, M.J. (2005). Effects of dietary or injected organic cations on larval *Drosophila melanogaster*: Mortality and elimination or tetraethylammonium from the hemolymph. *Arch. Insect Biochem. Physiol*. **59**, DOI: 10.1002/arch.20085.

Bijelic, G. and O'Donnell, M.J. (2005). Diuretic factors and second messengers stimulate secretion of the organic cation TEA by the Malpighian tubules of *Drosophila melanogaster*. *J. Insect Physiol*. **51**, 267-275.

Bohr-Gasse, (2007). "The Predictor". NMT- The MYR predictor. http://mendel.imp.ac.at/myristate/SUPLpredictor.htm (13 July, 2011).

Boom, S.A.P., Gribnau, F.W.J and Russel, F.G.M. (1992). Organic cation transport and cationic drug interactions in freshly isolated proximal tubular cells of the rat. *J. Pharmacol. Exp. Ther.* **263**, 445-450.

Bowman, E.J., Siebers, A. and Altendorf, K. (1988). Bafilomycins: A class of inhibitors of membrane ATPases from microorganisms, animal cells, and plant cells. *Proc. Natl. Acad. Sci. USA.* **85**, 7972-7976.

Brondyk, W. H. (2009). Selecting an appropriate method for expressing a recombinant protein. *Method. Enzymol.* **463,** 131-147.

Bubner, B., Gase, K. and Baldwin, I.T. (2004). Two-fold differences are the detection limit for determining transgene copy numbers in plants by real-time PCR. *BCM biotechnol.* **13**, 4-14.

Burg, M.B. and Weller, P.F. (1969). Iodopyracet transport by isolated perfused flounder renal proximal tubules. *Am. J. Physiol*. **217**, 1053-1056.

Busch, A.E., Quester, S., Ulzheimer, J.C., Waldegger, S., Gorboulev, V., Arndt, P., Lang, F. and Koepsell, H. (1996). Electrogenic properties and substrate specificity of the polyspecific rat cation transporter rOCT1. *J. Biol. Chem*. **271**, 32599-32604.

Buss, D.S. and Callaghan, A. (2008). Interaction of pesticides with p-glycoprotein and other ABC proteins: a survey of the possible importance to insecticide, herbicide and fungicide resistance. *Pestic. Biochem. Phys.* **90,** 141-153.

Bustin, S.A., Benes, V., Garson, J.A., Hellemans, J., Huggett, J., Kubista, M., Mueller, R., Nolan, T., Pfaffl, M.W., Shipley, G.L., Vandesompele, J. Wittwer, C. (2009). The MIQE guidelines – minimum information for publication of quantitative real-time PCR experiments. *Clin. Chem.* **55**, 611-622.

Chahine, S. and O'Donnell, M.J. (2009). Physiological and molecular characterization of methotrexate transport by Malpighian tubules of adult *Drosophila melanogaster*. *J. Insect Physiol.* **55**, 927-935.

Chahine, S. and O'Donnell, M.J. (2010). Effects of acute or chronic exposure to dietary organic anions on secretion of methotrexate and salicylate by Malpighian tubules of *Drosophila melanogaster* larvae. *Archiv. Insect Biochem. Physiol.* **73**, 128-147.

Dai, X., Willis, L.G., Palli, S.R. and Theilmann, D.A. (2005). Tight transcriptional regulation of foreign genes in insect cells using an ecdysone receptor based inducible system. *Protein Expres. Pruif.* **42**, 236-245.

Dantzler, W.H. (1989). Organic acid (or anion) and organic base (or cation) transport by renal tubules of nonmammalian vertebrates. *J. Exp. Zool*. **249**, 247-257.

Dantzler, W.H., Wright, S.H. and Brokl, O. (1991). Tetraethylammonium transport by snake renal brush-border membrane vesicles. *Pflügers Arch*. **418**, 325-332.

Dow, J.A.T. (2009). Insights into the Malpighian tubule from functional genomics. *J. Exp. Biol*. **212**, 435-445.

Dow, J.A.T. and Davies, S.A. (2001). The *Drosophila melanogaster* Malpighian tubule, a genetic model for insect epithelia. *Adv. Insect Physiol.* **28,** 1-83.

Dow, J.A., Maddrell, S.H.P., Gortz, A., Skaer, N.J.V., Brogan, S. and Kaiser, K. (1994). The Malpighian tubules of *Drosophila melanogaster*: a novel phenotype for studies of fluid secretion and its control. *J. Exp. Biol*. **197**, 421-428.

Dresser, M.J., Leabman, M. and Giacomini, K.M. (2001). Transporters involved in the elimination of drugs in the kidney: Organic anion transporters and organic cation transporters. *J. Pharm. Sci*. **90**, 397-421.

Dresser, M., Zhang, L. and Giacomini, K. (1999). Molecular and functional characteristics of cloned human organic cation transporters, in Amidon and Sadee. eds., *Membrane Transporters as Drug Targets*, Kluwer Academic/Plenum Publishers, New York. 441-469.

Drummond, A.J., Ashton, B., Buxton, S., Cheung, M., Cooper, A., Duran, C., Field, M., Heled, J., Kearse, M., Markowitz, S., Moir, R., Stones-Havas, S., Sturrock, S., Thierer,T. and Wilson, A. (2010) Geneious v5.3, Available from http://www.geneious.com/

Eraly, S.A., Monte, J.C. and Nigam, S.K. (2004). Novel slc22 transporter homologs in fly, worm, and human clarify the phylogeny of organic anion and cation transporters. *Physiol. Genomics.* **18**, 12-24.

Eraly, S.A. and Nigam, S.K. (2002). Novel human cDNAs homologous to *Drosophila Orct* and mammalian carnitine transporters. *Biochem. Biophys. Res, Commun*. **297**, 1159-1166.

Evans, J. M., Allan, A. K., Davies, S. A. and Dow, J. A. T. (2005). Sulphonylurea sensitivity and enriched expression implicate inward rectifier K+ channels in *Drosophila melanogaster* renal function. *J. Exp. Biol.* **208**, 3771-3783.

Gaertner, L.S. and Morris, C.E. (1999). Accumulation of daunomycin and fluorescent dyes by drug transporting Malpighian tubule cells of the tobacco hornworm, *Manduca sexta*. *Tissue & Cell*. **31**, 185-194.

Gaertner, L.S., Murray, C.L., and Morris, C.E. (1998). Transepithelial transport of nicotine and vinblastine in isolated Malpighian tubules of the tobacco hornworm (*Manduca sexta*) suggests a p-glycoprotein-like mechanism. *J. Exp. Biol.* **201,** 2637-2645.

Gasteiger E., Gattiker A., Hoogland C., Ivanyi I., Appel R.D., Bairoch A. (2003). ExPASy: the proteomics server for in-depth protein knowledge and analysis. *Nucleic Acids Res*. **31**, 3784-3788.

GraphPad Prism. (2011). *GraphPad Software*, La Joll, CA. USA. V. 5.04 for Windows. www.graphpad.com

Gründemann, D., Valentin, G., Gambaryan, S., Veyhl, M. and Koepsell, H. (1994). Drug excretion mediated by a new prototype of polyspecific transporter. *Nature*, **372**, 549-552.

Harvey, W.R., Cioffi, M. and Wolfersberger, M.G. (1983). Chemiosmotic potassium ion pump of insect epithelia. *Am. J. Physiol.* **244,** R163-R175.

Harvey, W.R., Okech, B.A., Linser, P.J., Becnel, J.J., Ahearn, G.A. Sterling, K.M. (2010). H+ V-ATPase-Energized transporters in brush border membrane vesicles from whole larvae of *Aedes aegypti*. *J. Insect Physiol.* **56**, 1377-1389.

Hawk, C.T. and Dantzler, W.H. (1984). Tetraethylammonium transport by isolated perfused snake renal tubules. *Am. J. Physiol*. **246**, F476-F487.

Hegedus, D. D., Pfeifer, T. A., Hendry, J., Theilmann, D. A. and Grigliatti, T. A. (1998). A series of broad host range shuttle vectors for constitutive and inducible expression of heterologous proteins in insect cell lines. *Gene.* **207,** 241-249.

Hegedus, D. D., Pfeifer, T. A., Theilmann, D. A., Kennard, M. L., Gabathuler, R., Jefferies, W. A. and Grigliatt, T. A. (1999). Differences in the expression and localization of human melanotransferrin in lepidopteran and dipteran insect cell lines. *Protein Expres. Purifi.* **15,** 296-307.

Hellemans, J., Mortier, G., De Paepe, A., Speleman, F. and Vandesompele, J. (2007). qBase relative quantification framework and software for management and automated analysis of real-time quantitative PCR data. *Genome Biol.* **8**, R19.

Hofmann, K. and Stoffel, W. (1993). TMbase- a database of membrane spanning proteins segments. *Biol. Chem.* **347**, 166.

Hoskins, R.A., Carlson, J.W., Kennedy, C., Acevedo, D., Evans-Holm, M., Frise, E., Wan, K.H., Park, S., Mendez-Lago, M., Rossi, F., Villasante, A., Dimitri, P., Karpen, G.H.

and Celniker, S.E. (2007). Sequence finishing and mapping of *Drosophila melanogaster* heterochromatin. *Science*. **316**, 1625-1628.

Ianowski, J.P. and O'Donnell, M.J. (2004). Basolateral ion transport mechanisms during fluid secretion by *Drosophila* Malpighian tubules: Na+:K+:2Cl- cotransport and Cl- conductance. *J.Exp.Biol*. **207**, 2599-2609.

Integrated DNA Technologies Inc. (2011). www.idtdna.com

Invitrogen. (2010). InsectSelect™ System: For the stable expression of heterologous proteins in lepidopteran insect cell lines using pIZ/V5-His. **Version H**.

Jehle, J. A., Blissard, G. W., Bonning, B. C., Cory, J. S., Herniou, E. A., Rohrmann, G. F., Theilmann, D. A., Thiem, S. M. and Vlak, J. M. (2006). On the classification and nomenclature of baculoviruses: A proposal for revision. *Arch. Virol*. **151**, 1257-1266.

Kekuda, R., Prasad, P., Wu, X., Wang, H., Fei, Y., Leibach, F. and Ganapathy, V. (1998). Cloning and functional characterization of a potential-sensitive polyspecific organic cation transporter (OCT3) most abundantly expressed in placenta. *J. Biol. Chem.* **273**, 1571-1579.

Leader, J.P. and O'Donnell, M.J. (2005).Transepithelial transport of fluorescent p-glycoprotein and MRP2 substrates by insect Malpighian tubules: Confocal microscopic analysis of secreted fluid droplets. *J. Exp. Biol.* **208**, 4363-4376.

Li, X., Schuler, M.A. and Berembaum, M.R. (2002). Jasmonate and salicylate induce expression of herbivore cytochrome P450 genes. *Nature*. **419**, 712–715.

Li, X., Schuler, M.A. and Berenbaum, M.R. (2007). Molecular mechanism of metabolic resistance to synthetic and natural xenobiotics. *Annu. Rev. Entomol.* **52**, 231–253.

Linton, S.M. and O'Donnell, M.J. (1999). Contributions of K+:Cl- cotransport and Na+/K+-ATPase to basolateral ion transport in Malpighian tubules of *Drosophila melanogaster*. *J.Exp.Biol*.. **202**, 1561-1570.

Livak, K.J. and Schmittgen, T.D. (2001). Analysis of relative gene expression data using real-time quantitative PCR and the 2(-Delta Delta C(T)) method. *Methods.* **25**, 402-408.

Lison, L. (1938). Études histophysiologiques sur les tubes de Malpighi des Insects. III. L'élimination des colorants basiques chez les Orthoptères. *Z. Zellforsch. Mikrosk. Anat.* **28**,179-209.

Lu, D., Xie, R.L., Rydzewski, A. Long G.L. (1997). The effect of N-linked glycosylation on molecular weight, thrombin cleavage, and functional activity of human protein S. *Thromn. Haemost.* **77**, 1156-1163.

Luckow, V. A., Lee, S. C., Barry, G. F. and Olins, P. O. (1993). Efficient generation of infectious recombinant baculoviruses by site-specific transposon-mediated insertion of foreign genes into a baculovirus genome propagated in *Escherichia coli*. *J. Virol.* **67,** 4566-4579.

Luckow, V.A. and Summers, M.D. (1988). Signals important for high-level expression of foreign genes in *Autographica californica* nuclear polyhedrosis virus expression vectors. *Virology*. **167**, 56-71.

Maddrell, S.H.P. (1981). The functional design of the insect excretory system. *J. Exp. Biol*. **90**, 1-15.

Maddrell, S.H.P. (1991). The fastest fluid-secreting cell known- the upper Malpighian tubule cell of *Rhodnius*. *Bioessays*. **13**, 357-362.

Maddrell, S.H.P. (2009). Insect homeostasis: past and future. *J. Exp. Biol.* **212**, 446-451.

Maddrell, S.H.P. and Gardiner, B.O.C. (1976). Excretion of alkaloids by Malpighian tubules of insects. *J. Exp. Biol.* **64**, 267-281.

Marusalin, J., Matier, B., Rheault, M.R. and Donini, A. (2011). Aquaporin homologs in the gut, Malpighian tubules and anal papillae of the larval mosquito, *Aedes aegypti*. *J. Comp. Physiol. B.* Submitted.

Maseuda, S., Terada, T., Yonezawa, A., Tanihara, Y., Kishimoto, K., Katsura, T., Ogawa, O. and Inui, K. (2006). Identification and functional characterization of a new human kidney-specific H+/organic cation antiporter, kidney-specific multidrug and toxin extrusion 2. *J. Am. Soc. Nephrol.* **17**, 2127-2135.

McKinney, T.D. (1984)**.** Further studies of organic base secretion by rabbit proximal tubules. *Am. J. Physiol*. **246**, F282-F289.

McKinney, T.D. and Kunnemann, M.E. (1985). Procainamide transport in rabbit renal cortical brush border membrane vesicles. *Am. J. Physiol*. **249**, F532-F541.

McKinney, T.D., Myers, P. and Speeg, K.V. (1981). Cimetidine secretion by rabbit renal tubules in vitro. *Am. J. Physiol.* **241**, F69-F76.

Meijer, D.K.F., Mol, W.E., Müller, M. and Kurz G. (1990). Carrier-mediated transport in the hepatic distribution and elimination of drugs, with special reference to the category of organic cations. *J. Pharmacokinetic Biopharm.* **18**, 35-70.

Midgett, C. R. and Madden, D. R. (2007). Breaking the bottleneck: eukaryotic membrane protein expression for high-resolution structural studies. *J. Struct. Biol.* **160,** 265-274.

Miller, D.S. (1995). Daunomycin secretion by killifish renal proximal tubules. *Am. J. Physiol.* **269**, R370-R379.

Miller, D.S., Ficker, G. and Drewe, J. (1997). P-glycoprotein-mediated transport of a

fluorescent rapamycin derivative in renal proximal tubule. *J. Pharmacol. Exp. Ther*. **282**, 440-444.

Miller, D.S. and Holliday, C.W. (1987). Organic cation secretion by *Cancer borealis* urinary bladder. *Am. J. Physiol. Regulatory Integrative and Comp. Physiol*. **252**, R153-R159.

Miller, D.S. and Holohan, P.D. (1987). Organic cation secretion in flounder renal tissue. *Am. J. Physiol.* **253**, R861-R867.

Miller, L. K. (1988). Baculoviruses as Gene Expression Vectors. *Annu. Rev. Microbiol.* **42,** 177-199.

Miller, L. K., Ed. (1997). The Baculoviruses. The Viruses. Edited by H. F.-C. a. R. R. Wagner. New York: Plenum Press.

Nawata, C.M. and Wood, C.M. (2008). The effects of CO2 and external buffering on ammonia excretion and Rhesus glycoprotein mRNA expression in rainbow trout. *J. Exp. Biol.* **211**, 3226-3236.

Nie, Y. and Theilmann, D.A. (2010). Deletion of AcMNPV AC16 and AC17 results in delayed viral gene expression in budded virus infected cells but not transfected cells. *Virology*. **404**, 168-179.

Nijhout, H.F. (1975). Excretory role of the midgut in larvae of the tobacco hornworm, *Manduca sexta* (L.). *J. Exp. Biol.* **62**, 221-230.

O'Donnell, M.J., Dow, J.A.T., Huesmann, G.R., Tublitz, N.J. and Maddrell S.P.H. (1996). Separate control of anion and cation transport in Malpighian tubules of *Drosophila melanogaster*. *J. Exp. Biol*. **199**, 1163-1175.

O'Donnell, M.J., Ianowski, J.P., Linton, S.M. and Rheault, M.R. (2003). Inorganic and organic anion transport by insect renal epithelia. *Biochim. Biophys. Acta.* **1618**, 194-206.

O'Donnell, M.J. and Maddrell, S.H.P. (1983). Paracellular and transcellular routes for water and solute movements across insect epithelia. *J. Exp. Biol.* **106**, 231-253.

O'Donnell, M.J., Rheault, M.R., Davies, S., Rosay, P., Harvey, B., Maddrell, S.H.P., Kaiser, K. and Dow, J. A. T. (1998). Hormonally controlled chloride movement across *Drosophila* tubules is via ion channels in stellate cells. *Am. J. Physiol. Regul. Integr. Comp. Physiol*. **274**, 1039-1049.

O'Donnell, M.J. and Spring, J.H. (2000). Modes of control of insect Malpighian tubules: synergism, antagonism, cooperation and autonomous regulation. *J. Insect Physiol.* **46**, 107-117.

Okabe, M., Unno, M., Harigae, H., Kaku, M., Okitsu, Y., Sasaki, T., Mizoi, T., Shiliba, K., Takanaga, H., Terasaki, T., Matsuno, S., Sasaki, I., Ito, S. and Abe, T. (2005). Characterization of the organic cation transporter SLC22A16: a doxorubicin importer. *Biochem. Biophys. Res. Commun.* **333**, 754-762.

Okuda, M., Saito, H., Urakami, Y., Takano, M. and Inui, K. (1996). cDNA cloning and functional expression of a novel rat kidney organic cation transporter, OCT2. *Biochem. Bioph. Res. Co.* **224**, 500-507.

O'Reilly, D.R., Miller, L.K. and Luckow, V.A. (1994). Post-translational modification. Baculovirus Expression Vectors: A Laboratory Manual. *Oxford University Press Inc*. Oxford. 216-236.

Otsuka, M., Matsumoto, T., Morimoto, R., Arioka, S., Omote, H. and Moriyama, Y. (2005). A human transporter protein that mediates the final excretion step for toxic organic cations. *Proc. Natl. Acad. Sci. USA.* **13**, 17923-17928.

Ott, R.J., Hui, A.C., Hsyu, P.H. and Giacomini, K.M. (1991). Organic cation transport in human renal brush-border membrane vesicles. *Am. J. Physiol*. **261**, F443-F451.

Ozvegy, C., Litman, T., Szakacs, G., Nagy, Z., Bates, S., Varadi, A. and Sarkadi, B. (2001). Functional characterization of the human multidrug transporter, ABCG2, expressed in insect cells. *Biochem. Bioph. Res. Co.* **258**, 111-117.

Pannabecker, T.L., Hayes, T.K. and Beyenbach, K.W. (1993). Regulation of epithelial shunt conductance by the peptide leucokinin. *J. Memb. Biol*. **132**, 63-76.

Pelis, R.M., Suhre, W.M. and Wright, S.H. (2006). Functional influence of N-glycosylation in OCT2-mediated tetraethylammonium transport. *Am. J. Physiol. Renal Physiol.* **290**, F1118-F1126.

Pfaffl, M.W. (2001). A new mathematical model for relative quantification in real-time RT-PCR. *Nucleic Acidc Res.* **29**, e45.

Pritchard, J.B. and Miller, D.S. (1993). Mechanisms mediating renal secretion of organic anions and cations. *Physiol. Rev*. **73**, 765-796.

Pfeifer, T. A., Guarna, M. M., Kwan, E. M., Lesnicki, G., Theilmann, D. A., Grigliatti, T. A. and Kilburn, D. G. (2001). Expression analysis of a modified factor X in stably transformed insect cell lines. *Protein Expres. Purifi.* **23,** 233-241.

Pfeifer, T., Hegedus, D., Wang, Y.-J., Zhao, Y., Meredith, J., Brock, H.W., Phillips, J.E., Grigliatti, T.A. and Theilmann, D.A. (1999). Analysis of an insect neuropeptide (ITP), expressed in insect cell systems. *Arch. Insect Biochem.* **42**, 245-252.

Phillips, J. (1981). Comparative physiology of insect renal function. *Am. J. Physiol. Regul. Integr. Comp. Physiol*. **241**, R241-257.

Rennick, B.R. (1981). Renal tubule transport of organic cations. *Am. J. Physiol. Renal Fluid*

Electrolyte Physiol. **240**, F83-F89.

Rennick, B.R., Moe, G.K., Lyone, R.H., Hoobler, S.W. and Neligh, R. (1947). Absorption and renal excretion of the tetraethylammonium ion. *J. Pharmacol. Exp. Ther.* **91**, 210-217.

Rheault, M.R., Debicki, D.M.D. and O'Donnell, M.J. (2005). Characterization of tetraethylammonium uptake across the basolateral membrane of the *Drosophila* Malpighian (renal) tubule. *Am. J. Physiol. Regul. Integr. Comp. Physiol.* **289**, R495-R504.

Rheault, M.R. and O'Donnell, M.J. (2004). Organic cation transport by Malpighian tubules of *Drosophila melanogaster*: application of two novel electrophysiological methods. *J.Exp.Biol*. **207**, 2173-2184.

Rheault, M.R., Plaumann, J.S. and O'Donnell, M.J. (2006). Tetraethylammonium and nicotine transport by the Malpighian tubules of insects. *J. Insect Physiol*. **52**, 487-498.

Rohrmann, G. F. (1986). Polyhderin Structure. *J. Gen. Virol.* **67,** 1499-1513.

Rohrmann, G. F. (2008). Baculovirus Molecular Biology. NCBI bookshelf.

Rozen, S. and Skaletsky, H.J. (2000). Primer3 on the WWW for general users and for biologist programmers. In: Krawetz, S. and Misener, S. (eds.) Bioinformatics Methods and Protocols: Methods in Molecular Biology. *Humana Press*, Totowa, NJ. 365-386.

Saier, M.H. (2000). A functional-phylogenetic classification system for transmembrane solute transporters. *Microbiol. Mol. Biol. Rev.* **64**, 354-411.

Salkind, S.J. (1930). Farbstoffansscheidung iin den Malpigischen Gefässen der Insedtenlarven. *Z. Zellforsch mikrosk Anat.* **10**, 53-72.

Sambrook, J. and Russell, D. (2001). Molecular Cloning: A Laboratory Manual. Cold Spring Harbor Laboratory Press. Cold Spring Harbor, New York. 3rd Ed.

Sarkadi, B., Price, E., Boucher, R., Germann, U. and Scarborough, G. (1992). Expression of the human multidrug resistance cDNA in insect cells generates a high activity drug-stimulated membrane ATPase. *J. Biol. Chem.* **267**, 4854-4858.

Schomig, E., Spitzenberger, F., Engelhardt, M., Martel, F., Orging, N. Grundemann, D. (1998). Molecular cloning and characterization of two novel transport proteins from rat kidney. *FEBS Lett.* **425**, 79-86.

Schramm, U., Fricker, G., Wenger, R. and Miller, D.S. (1995). P-glycoprotein-mediated secretion of a fluorescent cyclosporine analogue by teleost renal proximal tubules. *Am. J. Physiol*. **268**, F46-F52.

Schultz, J., Milpetz, F., Bork, P. and Ponting, C.P. (1999). SMART, a simple modular architecture research tool: Identification of signaling domains. *Proc. Natl. Acad. Sci.* **95**, 5857-5864.

Schweikl, H., Klein, U., Schindlbeck, M. and Wieczorek, H. (1989). A vacuolar-type ATPase, partially purified from potassium transporting plasma membranes of tobacco hornworm midgut. *J. Biol. Chem.* **264**, 11136-11142.

Sharma, R. C. and Schimke, R. T. (1996). Preparation of electro-competent *E. Coli* using saltfree growth medium. *Biotechniques.* **20,** 44-46.

Sigrist, C.J.S., Cerutti, L., de Castro, E., Langendijk-Genevaux, P.S., Bulliard, V., Bairoch, A. and Hulo, N. (2010). PROSITE, a protein domain database for functional characterization and annotation. *Nucleic Acids Res.* **38**, 161-166.

Smith, G. E., Fraser, M. J. and Summers, M. D. (1983). Molecular engineering of the *Autographica californica* nuclear polyhedrosis virus genome: deletion mutations within

the polyhedrin gene. *J. Virol.* **46,** 584-593.

Smith, P.M., Pritchard, J.B. and Miller, D.S. (1988). Membrane potential drives organic cation transport into teleost renal proximal tubules. *Am. J. Physiol*. **255**, R492-R499.

Sperber, I. (1947). The mechanism of renal excretion of some detoxification products in the chicken. *Proc. Int. Congr. Physiol.* 17th, Oxford. 217-218.

Stewart, T.M., Huijskens, I., Willis, L.G. and Theilmann, D.A. (2005). The *Autographa californica* multiple nucleopolyhedrovirus *ie0-ie1* gene complex is essential for wild-type virus replication, but either IE0 or IE1 can support virus growth. *J. Virol.* **79**, 4619-4629.

Sweet, D.H. and Pritchard, J.B. (1999). The molecular biology of renal organic anion and organic cation transporters. *Cell Biochem. Biophys.* **31**, 89-118.

Tamai, I., Yabuuchi, H., Nexu, J., Sai, Y., Oku, A., Shimane, M. and Tsuji, A. (1997). Cloning and characterization of a novel human pH-dependant organic cation transporter, OCTN1. *FEBS Lett.* **419**, 107-111.

Taylor, M.E. and Drickamer, K. (2011). Introduction to Glycobiology. *Oxford University Press*. Oxford. 3rd Ed.

Taylor, C., Stanley, K. and Shirras, A. (1997). The *orct* gene of *Drosophila melanogaster* codes for a putative organic cation transporter with six or 12 transmembrane domains. *Gene*. **201**, 69-74.

Theilmann, D.A. and Stewart, S. (1992). Molecular analysis of the trans-activating IE-2 gene of *Orgyia pseudotsugata* multicapsid nuclear polyhedrosis virus. *Virology*. **187**, 84-96.

Vermeulen, J., Pattyn, F., De Preter, K., Vercruysse, L., Derveaux, S., Mestdagh, P.,

Lefever, S., Hellemans, J., Speleman, F. and Vandesompele, J. (2009). External oligonucleotide standards enable cross laboratory comparison and exchange of real-time quantitative PCR data. *Nucleic Acids Res.* **37**, e138.

Vialard, J., Lalumiere, M., Vernet, T., Briedis, D., Alkhatib, G., Henning, D., Levin, D. and Richardson, C. (1990). Synthesis of the membrane fusion and hemagglutinin proteins of measles virus, Using a novel baculovirus vector containing the β-galactosidase gene. *J. Virol.* **64**, 37-50.

Wieczorek, H., Putzenlechner, M., Zeiske, W. and Klein, U. (1991). A vacuolar-type proton pump energizes K+/H+ antiport in an animal plasma-membrane. *J. Biol. Chem.* **266**, 15340-15347.

Wieczorek, H., Wolfersberger, M.G., Cioffi, M. and Harvey, W.R. (1986). Cation-stimulated ATPase activity in purified plasma membranes from tobacco hornworm midgut. *Biochim Biophys Acta*. **857**, 271-281.

Wright, S.H. (2005). Role of organic cation transporters in the renal handling of therapeutic agents and xenobiotics. *Toxicol. Appl. Pharmacol*. **204**, 309-319.

Wright, S.H. and Dantzler, W.H. (2004). Molecular and cellular physiology of renal organic cation and anion transport. *Physiol. Rev*. **84**, 987-1049.

Wright, S.H., Evans, K.K., Zhang, Z., Cherrington, N.J., Sitar, D.S. and Dantzler, W.H. (2004). Functional map of TEA transport activity in isolated rabbit renal proximal tubules. *Am. J. Physiol.* **287**, F442-F451.

Zhang, X., Cherrington, N.J. and Wright, S.H. (2007). Molecular identification and functional characterization of rabbit MATE1 and MATE2-K. *Am. J. Physiol. Renal Physiol.* **293**, F360-F370.

Zuker, M. (2003). Mfold web server for nucleic acid folding and hybridization prediction.

Nucleic Acids Res. **31**, 3406-3415.

Zuidema, D., Schouten, A., Usmany, M., Maule, A. J., Belsham, G. J., Roosien, J., Klinge-Roode, E. C., van Lent, J. W. M. and Vlak, J. (1990). Expression of cauliflower mosaic virus gene I in insect cells using a novel polyhedrin-based baculovirus expression vector. *J. Gen. Virol.* **71,** 2201-2209.

Appendix 1: qPCR Normalization Using Multiple Reference Genes

Livak and Schmittgen (2001) were the first to demonstrate a conversion of Cq values (then Ct values) to normalized relative quantities (NRQs). Their model assumes 100% reaction efficiency and uses only a single reference gene.

$$NRQ = 2^{\Delta\Delta Cq} \qquad \text{Eq. 2.2}$$

It is now known that not all primers work at 100% efficiency to exponentially double the reaction following each cycle (n^2). Pfaffl (2001) improved upon the original model by adjusting for individual primer efficiencies; however the model still relies on only one reference gene for normalization.

$$NRQ = \frac{E_{goi}^{\Delta Ct,goi}}{E_{ref}^{\Delta Ct,ref}} \qquad \text{Eq. 2.3}$$

Here the difference in cycle threshold value (Ct) of the gene of interest (goi) is modified to consider the efficiency (E) of the goi. This is then compared to the same normalized Ct value for the reference gene (ref). For improved normalization, it is now possible to use the geometric mean of multiple reference genes as a baseline for changes in expression of a gene of interest. The Pfaffl model was adjusted by Hellemans *et al.* (2007) to normalize to multiple reference genes.

$$NRQ = \frac{E_{goi}^{\Delta Ct,goi}}{\sqrt[f]{\prod_{o}^{f} E_{ref_o}^{\Delta Ct,ref_o}}} \qquad \text{Eq. 2.4}$$

The expression of the goi is now compared to the root of the number of total reference genes (f) to the geometric mean of the number of reference genes, while still adjusting for varying efficiencies of the different primer pairs.